Universidade de Aveiro Secção Autónoma de Ciências da Saúde
2011

Joana Fernandes da Rocha

Caracterização da diferenciação neuronal dependente de PPA

Understanding APP-dependent neuronal differentiation

Universidade de Aveiro Secção Autónoma de Ciências da Saúde
2011

Joana Fernandes da Rocha

Caracterização da diferenciação neuronal dependente de PPA

Understanding APP-dependent neuronal differentiation

Dissertação apresentada à Universidade de Aveiro para cumprimento dos requisitos necessários à obtenção do grau de Mestre em Biomedicina Molecular realizada sob a orientação científica da Professora Doutora Sandra Vieira, Professora Auxiliar Convidada da Secção Autónoma de Ciências da Saúde da Universidade de Aveiro, e co-orientação da Professora Doutora Odete da Cruz e Silva, Professora Auxiliar da Secção Autónoma de Ciências da Saúde.

Este trabalho contou com o apoio do Centro de Biologia Celular (CBC) da Universidade de Aveiro, e é financiado por fundos FEDER através do Programa Operacional Factores de Competitividade – COMPETE e por Fundos Nacionais da FCT – Fundação para a Ciência e a Tecnologia no âmbito do projecto PTDC/SAU-NMC/111980/2009.

Dedicada ao meu avô, Joaquim Fernandes.

Dedicada aos meus pais, sem o apoio dos quais teria sido impossível concretizar esta etapa da minha vida.

o júri

presidente

Professor Doutor José Ignacio Guinaldo Martin
Prof. Auxiliar Convidado, Secção Autónoma de Ciências da Saúde, Universidade de Aveiro

Professora Doutora Sandra Isabel Moreira Pinto Vieira
Prof. Auxiliar Convidada, Secção Autónoma de Ciências da Saúde, Universidade de Aveiro

Professora Doutora Odete Abreu Beirão da Cruz e Silva
Prof. Auxiliar, Secção Autónoma de Ciências da Saúde, Universidade de Aveiro

Professora Doutora Isabel dos Santos Cardoso
Professora Equiparada a Assistente, Departamento de Anatomia Patológica, Escola Superior de Tecnologia da Saúde do Porto-ESTSP

agradecimentos

À minha orientadora, Sandra Vieira, porque "o professor medíocre ensina, o bom explica, o muito bom demonstra, e o excepcional inspira". Obrigada por toda a inspiração.

À professora Odete da Cruz e Silva, pela oportunidade de realizar este trabalho no laboratório de neurociências do CBC e pela co-orientação desta dissertação.

Aos meus pais e aos meus irmãos, Pedro e Ana, por tornarem o ambiente familiar tão confortável e um aconchego face às adversidades do trabalho.

À minha Madrinha.

À Joana Oliveira, à Filipa Martins e à Sara Soares. Porque enriqueceram esta experiência com os prazeres de uma boa amizade.

À Rita e à Catarina por todo o apoio e atenção apesar da distância.

Às minhas amigas Ana Graça, Andreia Joana, Beatriz, Joana, La-Salete, e Sofia. Porque o triunfo de qualquer conquista reside na possibilidade de a partilhar. Obrigada pelo apoio incondicional e por acreditarem em mim.

À Joana Vieira e à Margarida Resende, por mais um ano das Joanas e Guida.

A todos os meus colegas e amigos de Ciências Biomédicas, em especial ao Igor, ao Miguel, ao Edgar, à Carina, ao João Figueiredo e ao João Terrível.

À Mariana por toda a ajuda prestada ao longo deste ano.

A todos os meus colegas do CBC. À Gabi, à Sandra Rebelo, à Margarida, à Sofia, à Sara Esteves, à Sara Domingues, à Mónica.

À FCT pelo financiamento do projecto PTDC/SAU-NMC/111980/2009.

palavras-chave

Proteína Precursora de Amilóde de Alzheimer (PPA), fosforilação, diferenciação neuronal, neurite, Ácido Retinóico, células SH-SY5Y, Domínio Intracelular da PPA (DIP)

resumo

A Proteína Precursora de Amilóide de Alzheimer (PPA) é uma proteína membranar tipo 1 sujeita a processamento proteolítico que tem sido associada a funções como adesão celular, sobrevivência, migração e diferenciação. Apesar de lhe terem sido atribuídas funções na neuritogénese, os dados experimentais obtidos até à data que envolveram modulação dos níveis da PPA revelam-se contraditórios. De facto, enquanto a adição do fragmento PPA secretado (PPAs) ao meio celular favorece a neuritogénese, a quantidade de PPA celular e de outros fragmentos da PPA poderão já não constituir um benefício para este processo. Adicionalmente, dados preliminares do laboratório de Neurociências do Centro de Biologia Celular sugerem que a PPAp (PPA fosforilada na S655) poderá ser fundamental na diferenciação neuronal mediada pela PPA, nomeadamente por aumentar a proteólise da PPA a PPAs ou a ligação da PPA a sinais de transdução específicos.

No presente trabalho, avaliou-se a capacidade da PPA e PPAp em mediar o período inicial de diferenciação neuronal induzida por ácido retinóico. Para tal recorreu-se a células de neuroblastoma SH-SY5Y, um modelo celular do tipo neuronal bem estabelecido para estudos de diferenciação. Adicionalmente, várias ferramentas moleculares, como PPA-GFP selvagem e fosfomutantes foram usadas. A avaliação da diferenciação incluiu a análise de vários parâmetros neuritogénicos por microscopia de luz (de campo claro e de fluorescência), nomeadamente monitorização de células diferenciadas e análises morfométricas das células transfectadas e da população geral. Os níveis de PPA e PPAs, e de proteínas relacionadas com citosqueleto e suas modificações pós-traducionais (MAP2, Tubulina Acetilada e Actina) também foram quantificados. Além do mais, a influência do DIP na diferenciação neuronal dependente de PPA foi avaliada usando um composto farmacológico para inibir a sua produção.

De um modo geral, os resultados obtidos demonstram que a PPA, PPAs e DIP modulam a neuritogénese de um modo complexo e ordenado. Enquanto a indução de níveis altos de expressão de PPA (48h) podem ser detrimentais para a diferenciação tipo-neuronal, de uma forma dependente de DIP, induções mais breves (24h) beneficiam este processo de um modo dependente da fosforilação na S655, potencialmente envolvendo a secreção de PPA e rearranjos específicos do citosqueleto.

keywords

Alzheimer's Amyloid Precursor Protein (APP), phosphorylation, neuronal differentiation, neurite, Retinoic Acid, SH-SY5Y cells, APP Intracellular Domain (AICD)

abstract

Amyloid Precursor Protein (APP) is a type 1 membrane protein that suffers proteolytic cleavages and has been implicated in roles such as cell adherence, survival, migration and differentiation. Although a role in neuritogenesis has been attributed to APP, some contradictory results have been reported regarding the benefits of knocking-down or overexpressing APP. Further, while the addition of the APP proteolytic sAPP (secreted APP) fragment to the cell medium enhances neuritogenesis, the amount of cellular APP and other APP fragments may be deleterious for this process. Further, preliminary work from the Neuroscience laboratory of the Center for Cell Biology indicated that pAPP (APP phosphorylated at the S655 residue) can potentially be crucial in APP-mediated neuronal differentiation, for example by increasing APP cleavage to its biological fragment sAPP or APP binding to specific signal transducers.

In this work, the capacity of APP and pAPP to mediate neuronal differentiation was tested, in the initial period of retinoic acid (RA)-induced SH-SY5Y cells differentiation. These neuroblastoma cells are a well documented neuronal-like cell model used in neuronal differentiation studies. Several molecular tools were used, including wild-type and phosphomutants APP-GFP. The evaluation of differentiation included neuritogenic output analysis by bright field and epifluorescence microscopy, using various approaches. Namely scoring the number of differentiated cells and performing morphometric analyses of transfected cells and of the all cellular population. The levels of APP and medium secreted sAPP, and of cytoskeleton-related proteins and post-translational modifications, such as MAP2, Acetylated Tubulin and Actin were also quantified by Western blot analysis, and related to the morphological parameters. Additionally, the potential role of AICD in APP-mediated neuronal differentiation was inferred from pharmacologic assays, where its generation is inhibited.

Together the results obtained show that APP, sAPP and AICD modulate neuritogenesis in a complex and well-ordered manner. While long-term increases in APP can be detrimental to neuronal-like differentiation, in an AICD-dependent manner, short-term increases benefit this process in an APP S655 phosphorylation dependent manner, potentially involving sAPP secretion and specific cytoskeleton rearrangements.

INDEX

Abbreviations

Aβ	Amyloid β-peptide
ADAM	A disintegrin and metalloproteinase
AICD	APP intracellular domain
APC	Adenomatous polyposis coli
APH-1	Anterior pharynx-defective 1
APLP	Amyloid precursor-like protein
APP	Amyloid- β Precursor Protein
ARH	Autosomal-recessive hypercholesterolemia
Arp	Actin-related proteins
ATP	Adenosine-5'-triphosphate
BACE	β-site APP-cleavage enzyme
BCA	Bicinchoninic acid
BDNF	Brain-derived neurotrophic factor
bFGF	Basic fibroblast growth factor
BMPs	Bone morphogenetic proteins
BSA	Bovine serum albumin
Ca^{2+}	Calcium
CaMKII	Calmodulin-dependent protein kinase II
CaP	Coprecipitates of calcium phosphate and DNA
CapZ	Capping protein
Cdc 42	Cell division control protein 42
cDNA	Complementary deoxyribonucleic acid
CLASP2	Cytoplasmic linker associated protein 2
CRMP-2	Collapsin-response mediator protein-2
CTF	Carboxy-terminal fragment
Dab	Disabled
DAPI	4',6-diamidino-2-phenylindole
DNA	Deoxyribonucleic acid
EB1	End-binding protein 1
ECL	Enhanced chemiluminescence
Ena	Enabled

ER	Endoplasmic reticulum
ERK	Extracellular signal-regulated kinases
FBS	Foetal bovine serum
GAP-43	Growth-associated protein-43
GDP	Guanosine diphosphate
GSK-3	Glycogen synthase kinase 3
GTP	Guanosine triphosphate
HEPES	4-(2-hydroxyethyl)-1-piperazineethanesulfonic acid
HSPGs	Heparin sulfate proteoglycans
ICH	Immunocytochemistry
IGF	Insulin-like growth factor-1
ILK	Integrin linked kinase
Jip	c-Jun N-terminal kinase interaction
KPI	Kunitz proteinase inhibitor
MAPs	Microtubule-associated proteins
MARK	Microtubule affinity-regulated kinase
MDC-9	ADAM9/meltrin gamma
MEK	Mitogen-activated protein kinase/extracellular signal-regulated kinase kinase
MFs	Microfilaments
MLC	Myosin light chain
mRNA	Messenger Ribonucleic acid
MTs	Microtubules
NFs	Neurofilaments
NgCAM	Neuron-glia cell adhesion molecule
NGF	Nerve growth factor
NT	Neurotrophin
Op18	Oncoprotein 18
PAK	p21-activated protein kinase
pAPP	APP phosphorylated
PBS	Phosphate buffered saline
PEN-2	Presenilin enhancer 2
PI3-kinase	Phosphatidylinositol-3 kinase

PIP3	Phosphatidylinositol (3,4,5)-triphosphate
PKA	cAMP-dependent protein kinase
PKC	Protein kinase C
PTEN	Phosphatase and tensin homolog deleted on chromosome 10
RA	Retinoic acid
Rac 1	Ras-related C3 botulinum toxin substrate 1
Rho	Ras homolog
ROK	Rho-kinase
RT	Room temperature
SAD	Synapses of amphids defective
sAPP	Secreted APP
SDS	Sodium dodecylsulfate
Sema 3A	Semaphorin 3A
SM	Sec1/Munc18
SNAREs	Soluble NSF Attachment Protein Receptor
sorLA	Sorting protein-related receptor containing LDLR class A repeats
TBS	Tris-Buffered Saline
TBS-T	Tris-Buffered Saline Tween
TGN	Trans-Golgi network
Tiam 1	T-cell lymphoma invasion and metastasis-inducing protein 1
Trk	Tyrosine kinases
VASP	Vasodilator-stimulated phosphoprotein
VPS	Vacuolar protein sorting
WASP	Wiskott-Aldrich Syndrome Protein
WAVE	WASP-family verprolin-homologous protein
WB	Western blotting
Wt	Wild-type

1. Introduction

1.1. The Neuron

The Human brain consists of over 10^{11} neurons, specialized cells that exhibit great variability in their size (cell bodies range from 5 to 100 µm diameter) and shapes[1].

The basic cellular organization of neurons resembles that of other cells; however, they are clearly distinguished by their specialization for intercellular communication. They usually have a rounded or polygonal cell body (perikaryon or soma) from which long, branched extensions (the neurites), normally arise (See Figure 1). This extensive branching is the most distinct feature of these cells specialization in communication[2], and include two morphological and molecular distinct type of processes, axons and dendrites.

Figure 1. Schematic representation of the typical branching structure of a neuron. In this figure we can visualize the multiple dendrites and a longer axon arising from the cell body. The axon terminals, specialized endings of the axon, are also represented. Adapted from http://www.3dscience.com/3D_Models/Biology/Cells/Neuron.php (December, 2010)

Axons are typically long, thin, and relatively uniform in diameter, and they branch at right angles. On the other hand, dendrites are relatively short and thick as they emerge from the cell body, but their calibre decreases with distance from the cell body, and they branch in a Y-shaped pattern[3]. Besides their length, the two types of processes differ from each other in morphology, in capacity for protein synthesis, in some molecular constituents of their cytoskeletons and plasma membranes, and in synaptic polarity [4]. Table 1 summarizes the main differences existing between the different regions of a neuron. The axon originates from a specialized region, the axon hillock, located either in the soma or in the proximal segment of a dendrite. These structures usually conduct information away from the cell body, possessing specialized endings – axon terminals – which come in close connection with the membrane of the target cell. In other hand,

dendrites primary function is to receive and integrate information from other neurons and the complexity of each dendritic arbour varies accordingly to neuron type and the number of inputs that a particular neuron receives. Thus, dendrites represent the afferent system of the neuron, and synapses occur either on small projections called dendritic spines or on the smooth dendritic surface[5].

Table 1. Neurons structure and ultra-structure. Neurons have 3 specialized regions that have different organelle composition and molecular cytoskeleton constituents: the cell body or soma, the axon, and the dendrites[5-6].

	Main organelles				Neuronal Cytoskeleton		
	Nucleus	**Reticulum and ribosomes**	**Golgi complex**	**Mitochondria**	**Neurofilaments (NFs)**	**Microtubules (MTs)**	**Microfilaments (MFs)**
Soma	Large, round and euchromatic; One or more prominent nucleoli.	Rich in smooth endoplasmic reticulum and free polyribosomes – presence of Nissl bodies.	Close to the nucleus.	Presence of large numbers;	NFs, namely NF60 and NF65, are less abundant than in the axon; but contain proportionally more NF60 than the axons.	Random dispersed.	Short oligomers of actin organized into a meshwork most apparent near the plasma membrane and in the vicinity of axonal MTs
Axon		Absent. The axon hillock is free of Nissl bodies.	Opposite (and only) the axon hillock.	Greater density in the axon hillock, at nodes, and in presynaptic endings.	Mature axons: heavily phosphorylated; Growing axons: express calmodulin-binding membrane-associated phosphoprotein, growth-associated protein-43 (GAP-43), and poorly phosphorylated NFs.	Have intrinsic polarity with rapidly growing ends away from the soma; Tau is the most abundant microtubule-associated protein.	Special concentrated at the axon hillock and in presynaptic terminals
Dendrites		Contain smooth endoplasmic reticulum (and ribosomes)	Near the bases of the main dendrites	Present; however rarely in filopodia and simple spines.	Contain few or no NFs. NFs proteins poorly phosphorylated	MTs exhibit mixed polarities. Express the microtubule-associated protein (MAP-2)	Particularly concentrated in dendritic spines and growth cones; growth cones contain many longer MFs, with bundles of MFs in the filopodia and lamellipodia.

1.2.Neuronal growth, polarization and differentiation

Structurally, the neuron is a complex cell containing 3 distinct regions with specific functions: the cell body, the main site of synthesis of neuronal proteins and membranes; an axon, specialized for the conduction of action potential, and multiple dendrites, which are specialized to receive chemical signals from the axon termini of other neurons. A single axon in the central nervous system can synapse with many neurons and induce responses in all of them simultaneously; on the other hand, neurons have extremely long dendrites with complexes branches that allow them to form synapses with and receive signals from a large number of other neurons, possibly up to a thousand. Give such complexity, the central challenge of neuronal development is to explain how the cell polarize into three different highly organized regions, namely how the axons and dendrites grow out, find the right target cells, and synapse with them selectively in order to create a functional network.

The nervous system in the vertebrates develops chiefly from two sets of cells of the ectoderm: the neural tube (the origin of the central nervous system) and the neural crest (gives rise to the peripheral nervous system). The early neural epithelium consists of a homogeneous population of pluripotent cells in different phases of the proliferative cycle which is reflected in miscellaneous appearances[5]. At some point in development, stem cells—the dividing cells that populate the proliferative zones of the developing brain—undergo asymmetrical divisions that produce both another stem cell and a neuronal precursor (called a neuroblast) that will never again undergo cell division, instead it will suffer a series of events leading to neuronal polarization and the development of a mature neuron. Therefore, for each neuron it can be assigned a “birthday” and neurons of a given type generally have the same birthdays which occur within a strictly limited period of development[2]. The state of the art in neuronal development and differentiation, points to a clear existence of an intrinsic program that is activated during the early stages of neuronal differentiation and controls the polarization of neurons. However, this intrinsic “polarity program” is subject to modification by environmental signals and cell injury[7].

1.2.1. Developmental stages of neurons

Neuronal polarization can be divided into several specific steps, either in vivo or in vitro dissociated neuronal cultures.

In vivo, before differentiate, the immature neuron or its precursor commonly migrates from its birthplace and settles in some other location. As a rule, the axon and the dendrites begin to grow out from the nerve cell body during migration. While migrating, postmitotic neurons endure extensive stereotypical changes and acquire their polarity from the emergence of a leading process and a trailing process, each becoming the axon or the dendrite. This is true for neuronal subpopulations undergoing long-range migration as cerebellar granule neurons, cortical (Figure 2) and hippocampal pyramidal neurons. However, in the case of retinal ganglion cells and bipolar retinal cells, for example, the postmitotic neurons can inherit their axon and dendrite polarity directly from the apico-basal polarity of their progenitors[8-9].

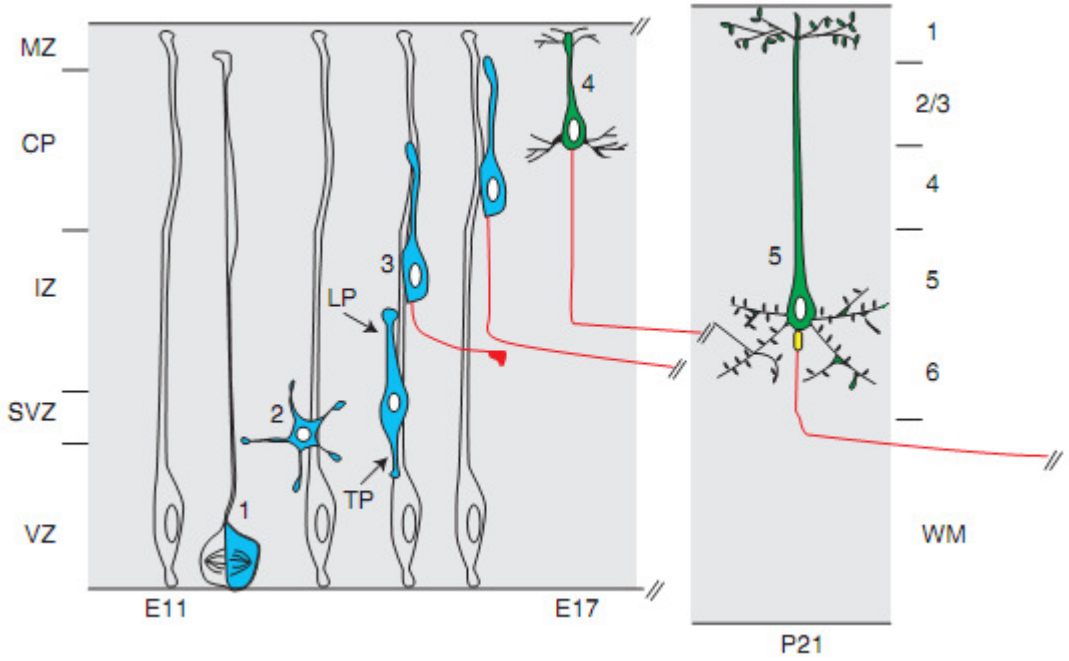

Figure 2. Polarization of cortical neurons in vivo. Neurons are generated between E11 and E17 by radial glial progenitors in the ventricular zone (VZ) of the neocortex. Upon cell cycle exit through asymmetric cell division, the postmitotic neuron (blue) begins to rapidly extend multiple neurites. Then, one major process forms in the radial direction and becomes the leading process (LP). At this point, the neuron initiates radial translocation along a radial glial process and leaves behind a trailing process (TP), which elongates tangentially in the intermediate zone (IZ) (red). The cell body continues to translocate toward the top of the cortical plate (CP), its final destination, while the axon rapidly elongates. The leading process gives rise to the apical dendrite (green), which initiates local branching in the marginal zone (MZ). During the first postnatal weeks of development, pyramidal neurons acquire other key features of their terminal polarity such as the axon initiation segment (AIS; yellow cartridge) and dendritic spines (gray protusions). Adapted from reference [8].

Dissociated rodent hippocampal neurons are a typical and well establish model system for studying neuronal polarization. Embryonic hippocampal neurons in culture acquire their characteristic polarized morphology during five distinct stages (illustrated in Figure 3), as first described by Dotti et al (1988). The events range from stage 1, cells bearing immature neurites, to stage 5, functional differentiated neurons harbouring dendritic spines and synapses. In their report, the authors note that, whereas the events of stages 1-4 appear to be part of an endogenously determined program of neuronal development, cell interactions play an important role in modulating the maturation of hippocampal neurons since the distinction between stages 4 and 5 represent a change in the control of the development.

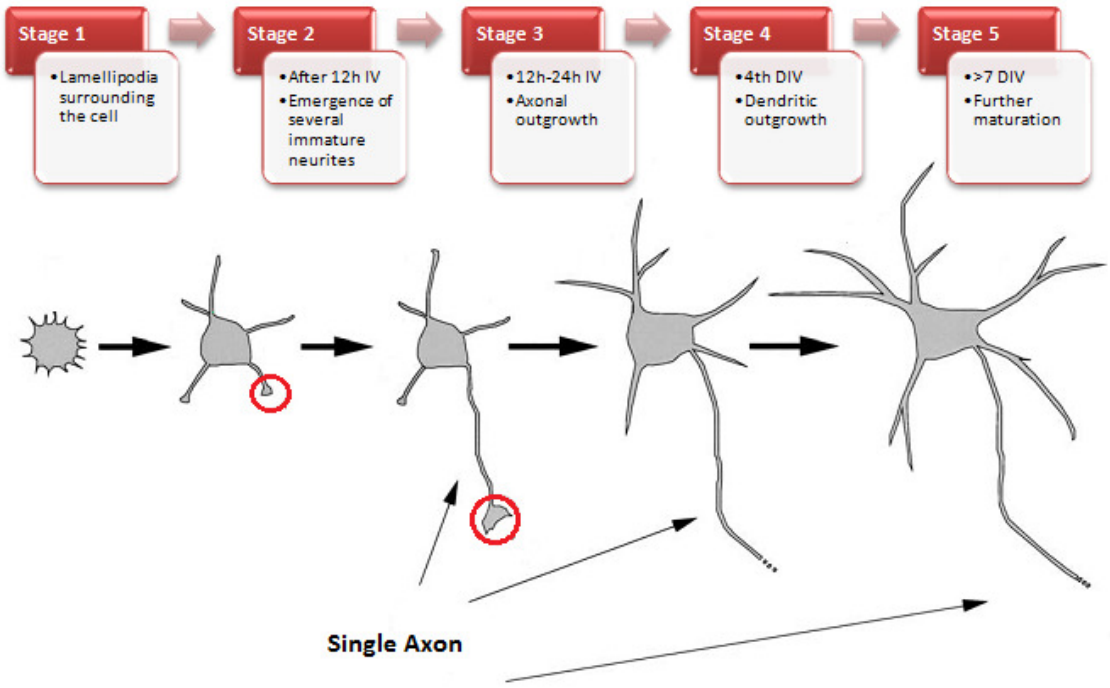

Figure 3. Stages of development of hippocampal neurons in culture. The red circle indicates growth cones. IV: *in vitro;* DIV: *days in vitro.* Adapted from reference[3].

The main event in stage 1 hippocampal neurons is the formation of lamellipodia which develop around the periphery of the cell soon after the cells attach to the substrate. Changes in these structures were correlated to the formation of neurites, as lamellipodia break up into discrete motile patches that will become the neuritic growth cones. In stage 2 the lamellipodia are transformed into minor processes that extend to a length of 15-25 µm – the neurites. Once they reach this length, they stop net elongation, although continue to extend and retract for short distances. The stage 3 is marked by the formation and growth of the axon. One of the minor

processes begins to grow at a much more rapid rate (about 5-10 times greater than the other processes) and becomes the future axon, while the other neurites remain quiescent. As a result, stage 3 neurons have a single axon and several short neurites, which implies that the cell has become polarized. Although stage 3 neurons present an actively growing neurite that will become the axon, axon formation is still very flexible at this stage. Indeed, cutting the axon to the length of the minor neurites makes the process of axon specification random as initially. However, if the cut axon is still 10 μm longer than the other processes, the same cut one will re-grow as axon[10]. Stage 4 comprehends the growth of dendrites that similar to axon develop from the minor processes that appear during the first day in culture. Besides starting later than the axon growth, dendrites grow more slowly than axons. Additionally, unlike axons, several dendrites grow at the same time. Eventually, after seven days in culture, neurons form synaptic contacts and spontaneous electrical activity propagates throughout the neuronal network[4, 11].

Summarizing, and accordingly to Bradke and Dotti (2000), neuronal polarization occurs in three different, succeeding steps: initially polarization seems to be solely morphological, then a molecular polarization occurs with segregation of axonal and dendritic proteins, upon the segregation of the cytoskeleton proteins and the maturation of the sorting and transport machinery for membrane proteins. Finally, the cell reaches a state of functional polarization when the molecular segregation creates different domains in a cell, accordingly to the different functions a neuron fulfills[10].

It is worth pointing out that axon-dendrite polarization was first postulated to be an outgrowth of the soma by His (1886) and Cajal (1890), a theory posteriorly validated by the experiments of Ross Harrison in 1907[2]. Nowadays, the events leading to the emergence of the dendrite and the axon are collectively called as “symmetry-breaking” events[8], as neurons start out as simple symmetric spheres, gradually adopting its complex polarize morphology.

1.2.2. Alterations in cytoskeleton dynamics and membrane trafficking

Differentiated neurons contain several compartments with distinct membrane and cytoskeleton proteins. This highly organized structure is imperative for unidirectional signal propagation in neurons[12]. The cytoskeleton both establishes and maintains polarity in neurons. The rearrangements of actin and microtubules cytoskeletons are crucial for the initial establishment of polarity. Of central importance for axon formation and neuronal polarity is the growth cone which is a highly motile cellular compartment at the tips of growing axons that has

the ability to sense extracellular cues and transducing those signals to the cytoskeleton. The growth cone is a broad flat expansion, with many long microspikes or filopodia that are protrusions of F-actin, and some veil-like sheets of branched actin, the lamellipodia (see Figure 4). The filopodia attach to the substrate and exert a force that pulls the rest of the cell forward, allowing it to move by elongation[1-2].

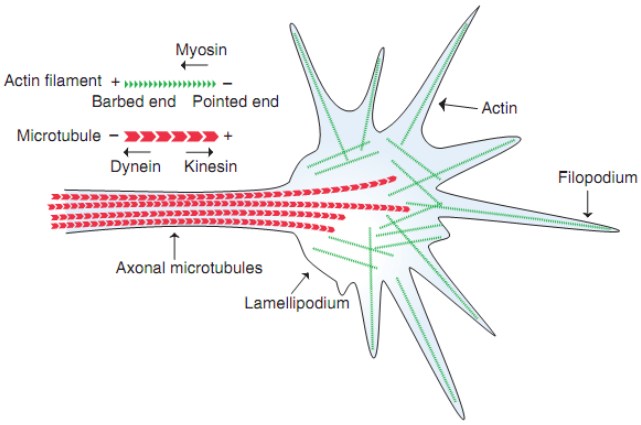

Figure 4. Schematic representation of the growth cone structure. The microtubules are distributed along the axonal shaft and protrude into the central region of the growth cone. Actin is found mainly within the peripheral region of the growth cone enclosing filopodia and lamellipodia. Reproduced from the reference[13].

First (stage 2 neurons), the future axon shows enhanced growth cone dynamics and, thereby, actin turnover, whereas the future dendrites, quiescent at that moment, have a static growth cone with a rigid actin cytoskeleton[13]. Such local actin instability may cause reduced obstruction of microtubule protrusion and, consequently, of neurite outgrowth. Figure 5 illustrates these cytoskeleton rearrangements in neuronal polarization.

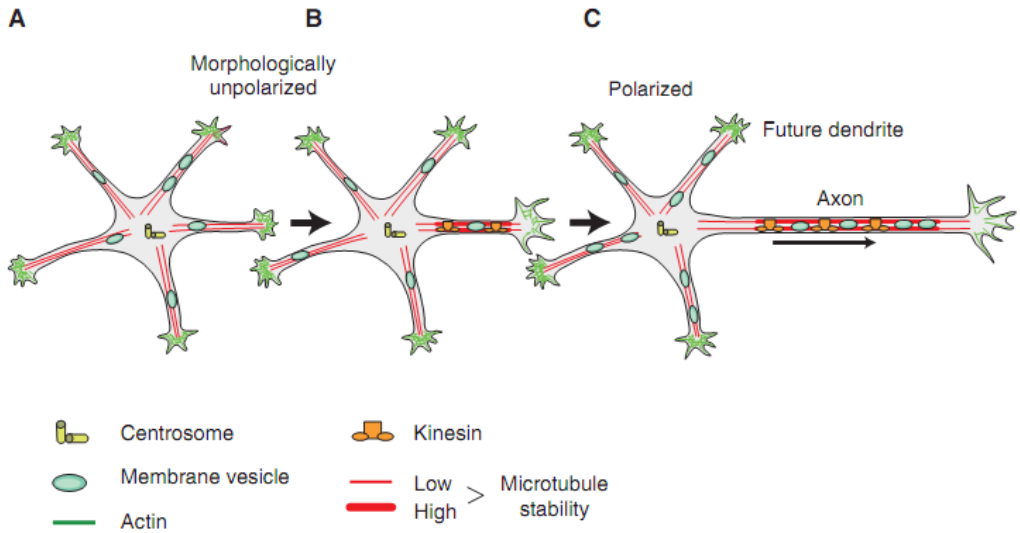

Figure 5. Cytoskeleton rearrangements in neuronal polarization. **A**. Unpolarized neurons with several equal neurites. **B**. In the future axon starts to occur changes in the cytoskeleton dynamics, namely, actin instability and increased microtubule stability. Stable microtubules are recognized by particular kinesin motors that induced unidirectional membrane trafficking toward the axon. **C**. This neurite starts elongating rapidly and a morphologically polarized neuron bearing an axon is formed. Reproduced from the reference[12].

Actin dynamics are regulated by actin nucleating, severing, branching, and bundling proteins[13]. The basis of the actin cytoskeleton is the polymerization of ATP-bound globular actin (G-actin) in helical actin filaments (F-actin). Cofilin has the ability to increase actin dynamics by filament severing and depolymerization. The released G-actin is sequestered, for example, by profilin, since elongation of existing or newly nucleated filaments demands local release of G-actin from profilin. Nucleation-promoting factors, such as WASP, have the ability to release G-actin. Capping proteins such as CapZ prevent filament elongation. In the other hand, anti-capping proteins as Ena/VASP family prevent the binding of capping proteins, allowing filament elongation. Furthermore, branching of the actin filaments can be initiated by the Arp2/3 complex and bundling is mediate by fascin[12].

Axonal microtubules show increased stability with neuronal polarization. Stabilization of microtubules can be achieved by active stabilization of existing microtubules, increased polymerization, a reduction of microtubule destabilization and possibly microtubule bundling. Structural MAPs, MAP2 and tau, are highly expressed in the nervous system and regulate neurite formation, both of which acting as microtubule stabilizing proteins. MAP2 is one of the most conspicuous in the mammalian brain and its intracellular location has been shown to follow a developmentally specified program involving the main MAP2 isoforms. Namely, the low molecular weight isoform (65-70 kDa), MAP2c, a juvenile isoform that is downregulated after the early stages of neuronal development; and the high molecular weight isoforms (280 kDa), of which MAP2b is expressed both during development and adulthood, while MAP2a becomes expressed when MAP2c levels are falling and is not detected uniformly in all mature neurons. MAP2 has been extensively implicated in neuronal development and neurite outgrowth, not only due to its microtubule-stabilizing activity, but also due to its ability to bind F-actin and alter actin dynamics[14].

Microtubule destabilizing proteins such as Op18/Stathmin has also been pointed has having a role in neuronal polarity[13]. Microtubule elongation is favoured by factors that bind α/β-tubulin heterodimers and increase polymerization, as for example CRMP-2, or by plus-end binding proteins (including APC, EB1, and EB3) that stabilize the dynamic plus-end. The inhibition of the microtubule destabilizer Stathmin via DOCK7, also increases microtubule stability[12].

The polarization of neurons involves a large incremental increase in surface area and volume, and thus membrane trafficking is required to support the development of polarity and neurite growth[3]. Furthermore, stage 3 axons contain synaptic vesicles and other axonal membrane associated proteins, indicating that organelles and other cytoplasmic components are

preferentially directed toward the nascent axon[10]. Results from Burack et al (2000) suggest that there are at least two mechanisms for polarized protein sorting: one is the direct transport of the proteins to the appropriate membrane, the other is the nonspecific transport of proteins within the cell, with some post-transport mechanisms acting to exclude or insert the transported proteins ate the plasma membrane[3].

1.2.3. Extracellular cues in differentiation

Several lines of evidence suggest that extracellular cues can direct the polarized emergence of the axon and the dendrites both in vitro and in vivo[9]. Figure 6 points up the main extracellular cues mentioned in the literature.

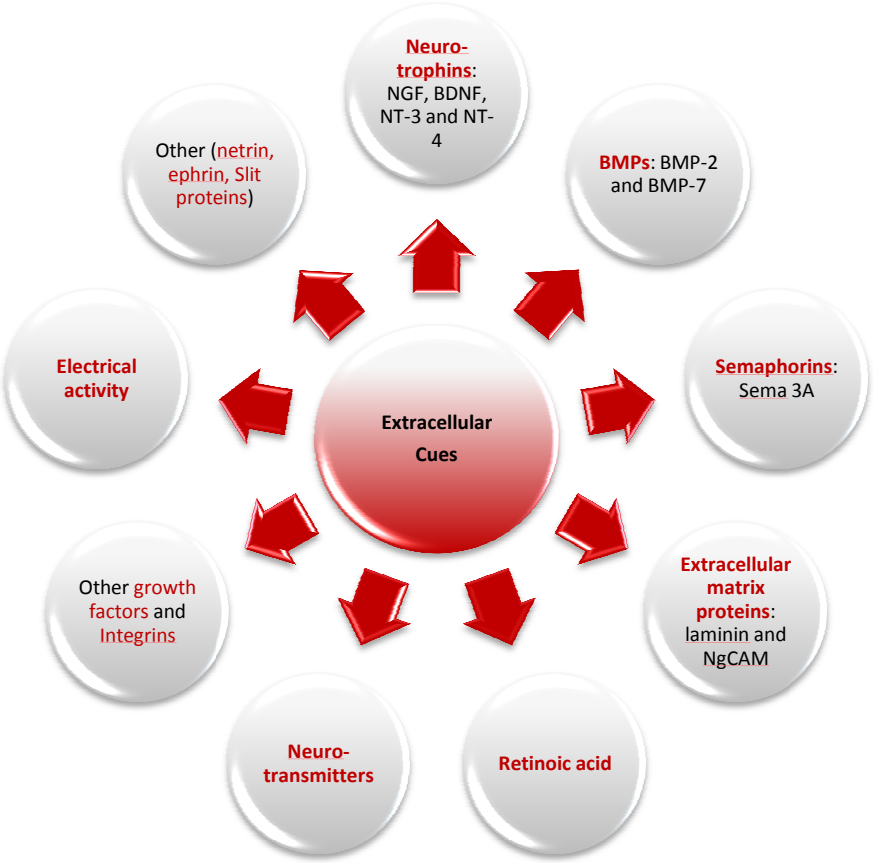

Figure 6. Extracellular cues involved in neuronal polarization.

In vivo, the "symmetry-breaking" events that lead to the emergence of neurites require the ability of postmitotic neurons to sense gradients of extracellular cues leading to the asymmetric activation of signalling pathways underlying the emergence of the axon[8]. This ability

of neurons is, as mentioned above, attributed to the growth cone. The numerous extracellular ligands act through distinct receptors existing in the growth cone, promoting localized changes in filamentous actin in the growth cone which, in turn, direct microtubule dynamics and thereby the direction of axonal elongation[15]. Candidate proteins that have been shown to influence axonal and dendritic development include mainly neurotrophins, bone morphogenetic proteins (BMPs) and morphogens such as retinoic acid, semaphorins, and other more.

Neurotrophins are an important family of neurotrophic factors that have complex influences on neuronal development[16]. This family is composed by the nerve growth factor (NGF), the brain-derived neurotrophic factor (BDNF), the neurotrophin-3 (NT-3), and the NT-4. Neurotrophins mediate their effects by binding to two types of cell surface receptors, the Trk tyrosine kinases (NGF binds to TrkA, BDNF and NT-4 bind to TrkB, and NT-3 binds to TrkC) and the p75 neurotrophin receptor (p75NTR). Interestingly, while Trk receptors transmit positive signals, p75NTR transmits both positive and negative signals and the signals generated by the two neurotrophin receptors can either augment or oppose each other[16-17].

In general, neurotrophins increase the dendritic complexity of pyramidal neurons by increasing total dendritic length, the number of branchpoints, and/or the number of primary dendrites[18]. BDNF was also shown to play an instructive role in axon specification, being this effect dependent on the activation of cAMP-dependent protein kinase (PKA) and phosphorylation of LKB1 by PKA[8-9]. NGF most studied effects, first established by Levi-Montalcini's pioneering work, are its influence in neuronal survival and maintenance of growth cones for neurite extension, on sensory and sympathetic neurons. This NGF effect on growth cones is local, direct, rapid, and independent of communication with the cell body [2, 16]. Other growth factors have been shown to be involved somehow in neuronal polarization. This is the case of the basic fibroblast growth factor (bFGF), which accelerates the outgrowth of both axons and dendrites in hippocampal neurons[7], and insulin-like growth factor-1 (IGF-1) that functions as a neurotrophic factor regulating neurite growth in developing brain[3] and affects dendritic growth and branching of post-natal layer 2 cortical neurons[18].

Regarding BMPs, their mechanisms are varied and the various BMPs have differential effects on developing neurons. It was demonstrated that dendrite outgrowth in sympathetic neurons in culture requires the presence of BMP-2 or BMP-7, and possible the physiological source of BMPs may be the Schwann cells[19].

Semaphorin 3A (Sema 3A), is involved in the regulation of asymmetric growth of cortical neurons by acting as a chemorepellant for axons and as chemoattractant for apical cortical dendrites[3, 8-9, 13].

Extracellular matrix proteins and adhesion molecules may also serve as extracellular signals, namely laminin or NgCAM. In fact, in dissociated cultures of hippocampal pyramidal neurons, the first immature neurite contacting a substrate interface of laminin or NgCAM is specified to become the axon. These results suggest that immature neurites can detect changes in the nature of the extracellular substrate regardless of the nature of the novel substrate they are encountering[3, 8].

Retinoic acid (RA) is a potent morphogen that functions as a locally synthesized differentiation factor for the developing nervous system[20]. It works by binding to nuclear receptors (hRAR), enhancing the interaction of these receptors with specific response elements (RAREs) located in the regulatory region of target genes, which culminates in the regulation of gene expression[21]. Because RA activates the early events of cell differentiation, which then induce context-specific differentiation programs, RA is considered a major differentiation factor[20].

Growing evidences suggest that for specific subtypes of neurons the actions of some extracellular cues are remarkably slow, but may be profoundly potentiated by physiological levels of electrical activity[8]. Additionally, the outgrowth of axons and dendrites can also be differentially regulated by neurotransmitters; namely, glutamate has the ability to suppress dendrite elongation in cultured embryonic hippocampal neurons. On contrary, activation of GABA receptors can counteract the glutamate negative effect on dendritic outgrowth[7]. Integrins have also been implicated as extracellular cues relevant for neuronal polarization in hippocampal neurons[22].

1.2.4. Signaling networks in differentiation

A multitude of neuronal polarity-regulating molecules have been revealed in the last few years. Various signaling molecules were proved to influence neuronal differentiation and polarization (further on summarized in Table 2). In the following text these signaling pathways are explained and contextualized in neuronal polarization. Noteworthy, many signaling networks operating in differentiation culminate in the regulation of actin and/or microtubule dynamics.

Rho-family of small GTPases: both Ras- and Rho-family small GTPases have been shown to be involved in axon specification and growth. At least ten types of Rho GTPases have been found in mammals, but the most extensively characterized comprises RhoA, Rac1 and Cdc42. The results of studies of Rho GTPases in neurons suggest that Rac1 and Cdc42 positively regulate axon growth thought the promotion of lamellipodia and filopodia formation in growth cones, while Rho acts as a negative regulator of neurite/axonal growth. So, it has been hypothesised that polarity-inducing signals switch Rac/Cdc42 to their GTP-bound active states in the future axon (stage 2 neurons), whereas Rho remains in its GDP-bound inactive state. In parallel, the other growth cones remain with GDP-bound inactive Cdc42/Rac, where the relatively high content of GTP-bound active Rho inhibit those neurites elongation[15].

The best characterized Rho effector is the Rho-kinase (ROK). ROK phosphorylates myosin phosphatase impeding it of dephosphorylating myosin light chain (MLC) of myosin II. Myosin II is then activated, thereby leading to contraction of actomyosin filaments, which promotes neurite retraction. Cdc42 is critical for axon formation, acting through N-WASP/Arp2/3 and p21-activated protein kinase (PAK) to regulate actin networks in the growth cone. The PAK pathway signals to the actin cytoskeleton via cofilin. The two main effector pathways involved in actin dynamics downstream of Rac1 are PAK and WAVE. Rac also inhibits the microtubule destabilizer Stathmin/Op18. Additionally, a Rac-specific guanine nucleotide exchange factor expressed in the nervous system, Tiam 1, has been show to regulate neurite growth[3, 13].

PI3-Kinase/Akt/GSK-3β pathway: several groups reported that local activation of PI3-kinase, and the accumulation of phosphatidylinositol (3,4,5)-triphosphate (PIP3) at the tip of one of the immature neurites, is important for axon specification and elongation. PI3-kinase generates localized membranar sites enriched in PIP3, and such enrichment recruits the protein kinase Akt (also named protein kinase B) via its PH domain. Upon translocation, Akt is activated by dual phosphorylation on T308 and S473 by membrane-targeted protein kinase PKD1 and PKD2, respectively. Additionally, Integrin linked kinase (ILK) is also capable of increasing Akt activity by phosphorylation on S473. Activated forms of Akt are found enriched in growth cones of polarized neurons, and activated Akt and ILK phosphorylate constitutively active glycogen synthase kinase 3 (GSK-3β), inactivating it. The decreased activity of GSK-3β is required for neuronal polarization. GSK-3 has multiple substrates that have the potential to regulate tubulin polymerization and microtubule stability, namely the microtubule plus-end binding proteins APC and CLASP2, CRMP-2, which localizes to axon tips, and the microtubule associated proteins MAP1B and tau[8, 23].

PTEN: the phosphatase and tensin homolog (PTEN) is a lipid and protein phosphatase that antagonizes PI3K signaling pathway, as PTEN dephosphorylates PIP3 into PIP2. Thus, increasing levels of PTEN leads to a loss of axon formation, whereas its reduction leads to a multiple axon phenotype. PTEN most likely works together with the PI3-kinase pathway to maintain the delicate balance of phospholipid composition at the membrane to ensure proper neuronal polarization and axon formation[8].

LKB1, SAD-A/B, and MARKs: LKB1 translocates from the nucleus and is activated by binding to its necessary coactivator Strad and by being phosphorylated by PKA and p90RSK kinase. Once activated, LKB1 phosphorylates SAD-A/B kinases and potentially the microtubule affinity-regulated kinases, MARK1-4. SAD (and MARK kinases), in turn, target and phosphorylate several MAPs, reducing their microtubule binding affinity[8].

RAS/RAF/MEK/ERK pathway: several studies in vitro support an important promoting function of this pathway in axon growth. This pathway seems to regulate axonal cytoskeleton via phosphorylation of several MAPS, and also regulates a broad range of transcription factors, including SRF[8].

CRMP-2: Experimental research in hippocampal neurons shown that CRMP-2 is involved in the regulation of axon formation during neuronal polarization, in addition to its role as a mediator of semaphorin-induced growth cone collapse. Apparently, CRMP-2 regulates microtubule dynamics by binding to tubulin heterodimers, and given the enriched localization of this protein in the growing axon, it can be speculated that CRMP-2/tubulin complexes locally change the rate of microtubule assembly, and thereby contribute to axonal growth[3, 23].

Calcium: Calcium (Ca^{2+}) is a second messenger and a well established key mediator of neurite outgrowth regulation, in almost all types of neurons. It can act directly, or through the activation of various calcium-binding proteins to modulate the state of polymerization of actin filaments and microtubules, and thus differentially regulate growth cone motility (filopodia behaviour) and neurite elongation. A calcium-sensitive phosphatase, calcineurin, has also been implicated in the establishment of neuronal polarity. Furthermore, Ca^{2+} can activate the protein gelsolin that can cleave actin filaments[7]. Supporting all these findings, in vivo imaging studies have provided direct evidence for a negative relationship between the frequency of spontaneous Ca^{2+} transients and the rate of axon outgrowth[8]

Table 2. Signaling molecules with a role in neuronal polarization[3, 7-9, 13].

Signalling Molecule	Methodology Applied	Effect on Neuronal Polarization	Ref.
Rho GTPases	Treatment of neurons with *Clostridium difficile* toxin B.	Induction of multiple axons, shows fewer filopodia and lamellipodia.	[24]
Rho A	Constitutively active form of RhoA and overexpression of RhoA proteins.	Inhibits neuritogenesis.	[25-27]
	Dominant-negative form.	Enhances neurite outgrowth.	[26]
Cdc42	Hippocampal Cdc42-knockout neurons.	Defects in actin cytoskeleton, fail to form filopodia, and lack axons.	[28]
	Dominant-active or dominant-negative Cdc42 ectopic expression in *Drosophila* sensory neurons.	Inhibits the growth of both axon and dendrites.	
Rac 1	Dominant-active or dominant-negative Rac 1 ectopic expression in *Drosophila* sensory neurons.	Inhibits axonal growth but it does not affect dendritic development.	[28-31]
	Dominant-active Rac in mouse Purkinje cells.	Specifically affects axonal growth but not dendritic growth.	[28]
	Specific ablation from the cortex.	Does not influence axon growth, rather influence axon guidance	[32-34]
	siRNA knockout of mammalian Rac1.	Does no affect axon identity.	[34]
	Constitutively active version of Rac1 in cultured neurons.	Does not affect axon specification.	[26]
Rho-kinase	Dominant-negative ROK.	Inhibits the LPA-induced neurite retraction.	[35]
	Dominant-active ROK.	Induces neurite retraction.	
N-WASP	Dominant-negative N-WASP in PC12 cells.	Inhibits the NGF-induced neurite formation.	[36]
Tiam1	Overexpression in hippocampal neurons.	Induces multiple axons.	[37]
	Antisense oligonucleotides.	Inhibits axon formation.	
PI3K	Pharmacologic inhibition using LY294002 or Wortmannin.	Prevents axon formation.	[38-41]
	Overexpression of the constitutively active catalytic subunit of PI3K (p110α).	Leads to the formation of multiple axons.	[41]
Akt or PKB	Overexpression of myristoylated Akt.	Multiple axons.	[41]
	RNAi or pharmacologic inhibition.	Failure of axon formation.	
PTEN	Increased levels of PTEN expression.	Loss of axon formation.	[38-39]
	RNAi-mediated knockdown.	Multiple axon phenotype.	[38]
GSK-3	Use of several types of GSK-3 inhibitors.	Formation of multiple axons.	[38, 42-44]

Signalling Molecule	Methodology Applied	Effect on Neuronal Polarization	Ref.
	Double knockin-mice bearing single point mutations in GSK-3β (S9A) and GSK-3α (S21A).	No obvious deficits in neuronal morphogenesis in vivo and in vitro.	[43]
CRMP-2	Overexpression.	Multiple axons.	[45]
	Expression of truncated forms.	Impair axon formation.	
APC	Expression of truncated forms	Inhibit axon formation.	[46-47]
LKB1	Genetic deletion in cortical pyramidal neurons.	Prevents axon formation.	[48-50]
	Overexpression.	Multiple axons.	
SAD kinases	RNAi knockdown.	Partially abrogates the ability of LKB1 overactivation to induce the formation of multiple axons in cortical neurons.	[49]
	Double knockout mice for SAD-A and SAD-B.	Neurons incapable of forming axons in vivo.	[51]
	Overexpression of SAD-A/B.	Induces a modest but significant increase in multiple axon formation.	[52]
MARK2	RNAi-mediated knockdown.	Induces supernumerary axons	[53]
	Overexpression.	Inhibits axon formation.	
MEK	Use of pharmacological inhibitors: PD98059 and U0126.	Striking inhibition of axon growth.	[54]
RAS/RAF/MEK/ERK pathway	Studies of gain and loss of function.	Strong axon promoting function.	[55]
Calcium	Exposure of neurons to Ca^{2+} ionophore.	The neurons don't form an axon and only form minor processes.	[56]
	Focal application of Ca^{2+} channel blocker nifedipine to a minor process.	Greatly increase the probability of that process becoming the axon.	
	Focal application of Cytochalasin D to a minor process.	Induced that process to become the axon.	

1.3.The Amyloid-β Precursor Protein (APP)

Amyloid Precursor Protein (APP) is an ubiquitously expressed type 1 membrane protein that suffers proteolytic cleavages and, as its name implies, is the precursor protein of the amyloid β-peptide (Aβ), the main component of brain senile plaques, characteristic of Alzheimer disease.

APP is widely expressed on the cell surface, particularly in neurons, and has been implicated in roles such as cell adherence, survival, migration and differentiation. Recently, it is being established as a neuromodulator of developing and mature nervous system. APP phosphorylation might be important in APP-mediated neuronal differentiation, possible by altering APP traffic, by increasing APP cleavage to its physiological fragments, and/or by increasing the binding of APP to specific signal transducers.

1.3.1. APP characterization and gene family

In 1986 the gene encoding APP was identified [57-60], and found to be located on the Down´s syndrome region of the chromosome 21 (21q21.2-3)[57]. The human APP gene contains 19 exons and is expressed in many cell and tissue types including endothelial, glia and neurons of the brain[61]. *APP* is one of 3 members of a small gene family that, in humans, includes *APLP1* and *APLP2*. All encode type 1 integral membrane glycoproteins with a large extracellular domain and a short cytoplasmic region. These three functional and structurally related proteins are well conserved in evolution and share similar functions, but only APP contains the Aβ domain, encoded by parts of exons 16 and 17 [62-63].

1.3.2. APP isoforms and functional domains

APP has eight isoforms derived from alternative splicing of its 19-exon gene, which are expressed in a cell-type specific manner and differ only in the size of their extracellular sequence. The three major isoforms are: APP 695, APP 751, and APP 770 (illustrated in

Figure 7). All of these transcripts encode multidomain proteins with a single membrane-spanning region. APP 751 and APP 770 contain the exon 7, which encodes a serine protease inhibitor (also called Kunitz proteinase inhibitor (KPI)) domain, missing in APP 695[64].

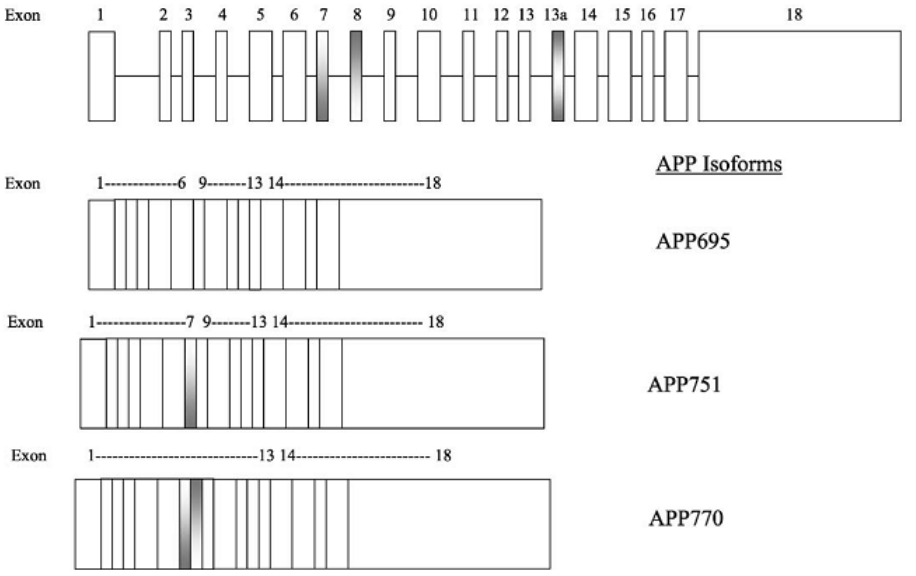

Figure 7. Schematic representation of the 19-exon APP gene and its three major isoforms produced by alternative splicing. Reproduced from the reference[63].

In neurons, APP 695 is the predominantly expressed isoform (APP 770:751:695 mRNA ratio is 1:10:20 in cortex[65]). The other isoforms are expressed mainly in non-neuronal cells, but are also in brain glial cells[64]. Other alternatively generated splice variants involve exon 15, and are found in peripheral leukocytes and in microglia cells. Two other APP variants miss exon 14 through 18, meaning they lack the β-amyloid sequence and the transmembrane region, thus are nonamyloidogenic[66].

APP possesses a large extracellular amino-terminal domain, a single transmembrane spanning domain, and a small intracellular cytoplasmic domain. In Figure 8 is depicted the overall structure of APP and the relative position of some of its functional domains.

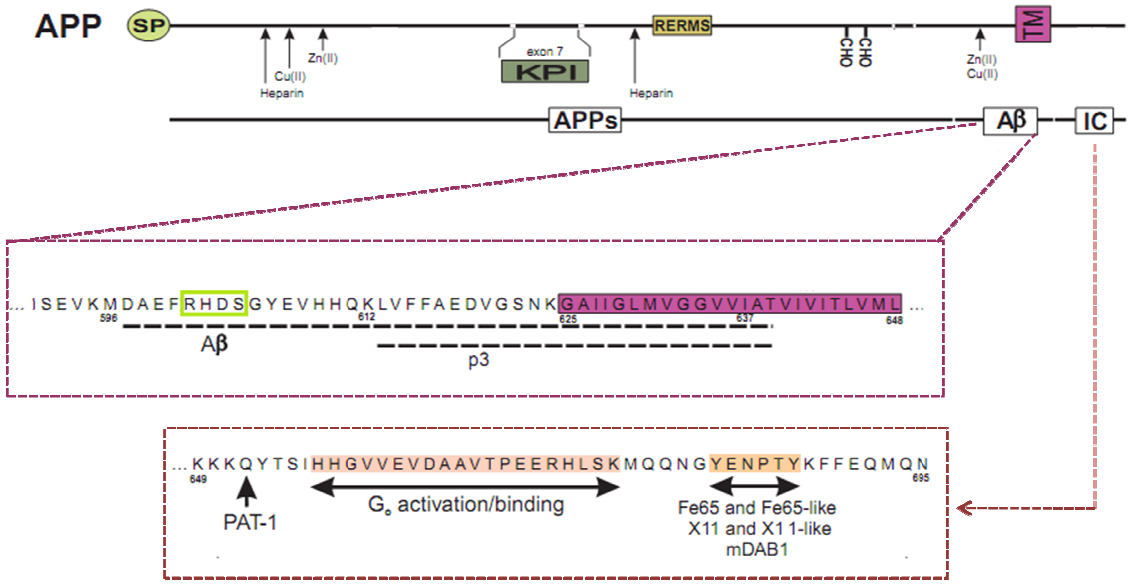

Figure 8. APP functional domains. The first panel depicts the overall structure of APP and its main functional domains and subdomains, including the signal peptide (SP), the relative positions of the heparin, metal-binding and glycosylation sites (CHO), the KPI domain present in the isoforms 770 and 751, the RERMS motif, and the transmembrane region (TM). In the below structure is represented the relative positions of the soluble APP (sAPP), of the amyloid β-peptide (Aβ), and of the intracellular domain (IC). The middle panel refers to the amino acid sequence of the Aβ sequence; the RHDS motif and the TM portion (purple) are depicted; p3 refers to the smaller peptide resulting from the proteolytic process of APP within the Aβ sequence. The last panel refers to the sequence of the IC domain; proteins that bind to the YENPTY sequence are indicated; the binding site to G_o is shown in light pink; a tyrosine residue critical for basolateral sorting of APP and for binding of PAT-1 is also shown. Adapted from reference [67].

The extracellular domain starts with a 17-residue signal peptide, followed by a cysteine-rich domain, and an acidic domain. The cysteine-rich domain contains two heparin-, a copper-, and a zinc-binding domain. This ion-metal binding to APP was shown to modify its conformation and to interfere with APP binding to constituents of the extracellular matrix. The isoforms 770 and 751 contain a 56-amino acid KPI domain that inhibits proteases, and isoform 770 has an additional 19-amino acid domain homolog to the MRC OX-2 antigen, found on the surface of neurons and

thymocytes (OX-2 domain). More or less in the middle of the extracellular domain lies a putative growth-promoting motif called “RERMS” (residues 403-407 of APP 770), followed by a gelateinase A inhibitor (residues 407-417), a collagen binding site (residues 523-540), and the Aβ sequence. The Aβ domain comprises the 28 residues just outside the membrane plus the first 12-14 residues of the transmembrane domain (amino acids 700-723). The Aβ sequence contains additionally zinc, cooper and heparin binding sites, and a RHDS motif (amino acids 5-8 of Aβ) that appears to promote cell adhesion[64, 68-69]. Furthermore, the cytoplasmic region of APP contains a ^{681}GYENPTY^{687} motif containing an NPXpY internalization signal for membrane proteins[70].

1.3.3. APP cellular localization and intracellular trafficking

APP is an transmembranar protein that is dynamically sorted through the membranes of intracellular organelles and the plasma membrane[71]. The major pathways of APP and its proteolytic derivates include anterograde, retrograde and transcytotic transports (Figure 9)[72].

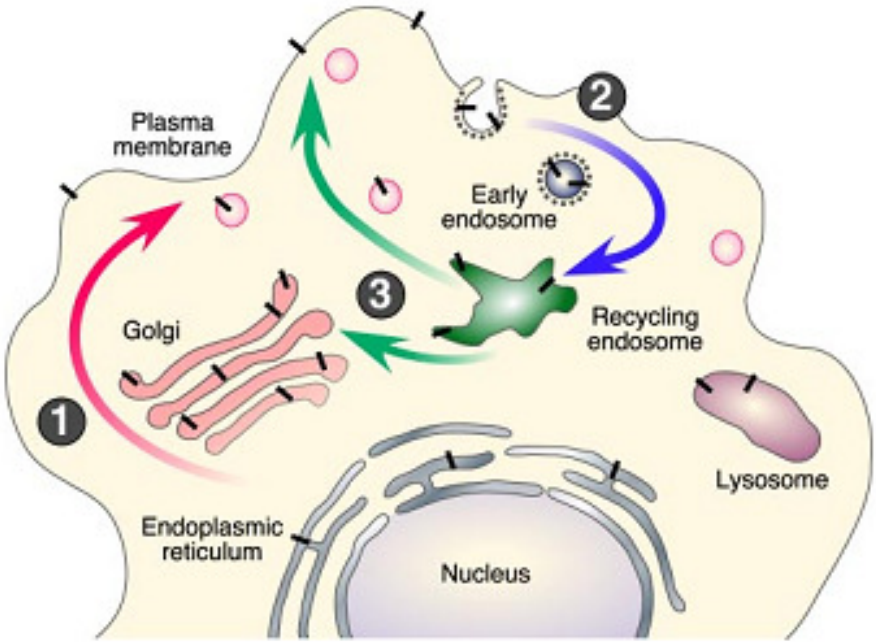

Figure 9. **Intracellular trafficking of APP. 1.** Constitutive secretory pathway: nascent APP molecules reach the cell surface; **2.** Internalization; **3.** Trafficking through endocytic and recycling compartments back to the cell surface or degraded in lysosome. Reproduced from reference [73].

APP is cotranslationally translocated into the endoplasmic reticulum via its signal peptide, and then post-translationally modified (“matured”) through the secretory pathway. Its acquisition of *N*- and *O*-linked sugars occurs rapidly after biosynthesis, and its half-life is relatively brief. Both during and after its trafficking through the secretory pathway, APP can undergo a variety of

proteolytic cleavages, specified in the subsequent topic[64]. In neurons, APP is subjected to the constitutive secretory pathway and undergoes fast axonal transport to presynaptic terminals. After arrival at the cell surface, APP suffers internalization, via its YENPTY motif, being delivered to the endosomes (retrograde transport). From the late endosomes, APP is either transported to lysosomes, or recycled by transport vesicles to the trans-Golgi network (TGN) and to the cell surface[72].

APP is transported via the clathrin coat complex, which are involved in two main sorting routes: the endocytic pathway, connecting the cell surface to the endosome, and the pathway connecting the TGN to the endosome. APP contains the NPXY amino acid motif, which governs the targeting of cargo to clathrin-coated vesicles. A number of families of clathrin adaptor proteins have been found to mediate the binding of the APP's NPXY motif to clathrin coats and therefore serve as regulators of APP endocytosis: autosomal-recessive hypercholesterolemia (ARH) protein, disable family member (Dab) 1, c-Jun N-terminal kinase interaction (Jip1b) protein, members of the Fe65 and of the X11 families, in particular X11a (Figure 8, bottom panel)[71].

The retromer is the second coat complex implicated in the transport of APP and its β-secretase BACE. It is a coat complex composed of vacuolar protein sorting (VPS) 35, VPS26, VPS29, VSP5, and VPS17. VPS35 represents the core of the retromer complex, binding to other retromer elements, and also binding the cytoplasmic tail of the transmembrane protein cargo that is being sorted. sorLA is a type-1 transmembrane molecule that is sorted by the neuronal retromer. As it binds APP and BACE, sorLA might function as the equivalent of an adaptor protein, binding the retromer complex to cargo proteins such as APP[71].

The fusion of transport vesicles to the membrane of the targeted organelle completes the process of transmembrane protein sorting. The fusion event is governed by three main families of proteins: the SNAREs, Rab, and Sec1/Munc18. The SNAREs expressed in the membrane of the transport vesicle interact with a single SNARE protein in the membrane of the organelle, with Rab and SM mediating this interaction[71].

1.3.4. APP proteolytic processing

As described above, part of the newly synthesized APP undergoes fast axonal transport in the secretory pathway, being targeted as a full-length protein into axons. A fraction of the full-length APP reaches the plasma membrane, is incorporated in endocytic vesicles, re-enters the cell and undergoes endoproteolytic cleavages by proteases, releasing biologically active peptides. Two main proteolytic cleavage sites have been identified close to the membranar domain, and one site

occurs within the transmembranar domain. Starting from the amino terminus of the protein, these are termed β (between residues 596 and 597 of APP695), α (between residues 596 and 597 of APP695) and γ (711-712 or 713-714) cleavage sites. Each cleavage is catalyzed by separate enzymes: β-, α- and γ-secretases, respectively[68]. The cellular distribution of APP secretases seems to be restricted to specific cellular compartments.

The α- and β-cleavages are mutually exclusive events, with APP undergoing two post-translational processing pathways. In the non-amyloidogenic pathway, APP is cleaved within the Aβ region by the α-secretase, liberating a large soluble extracellular N-terminal fragment - sAPPα. The carboxy-terminal fragment (CTF), named C83, remains tethered to the membrane, and is subsequently subjected to a transmembrane cleavage by γ-secretase, producing a non-pathogenic p3 peptide and the cytoplasmic APP intracellular C-terminal domain, AICD. In the alternative, amyloidogenic pathway, APP is first cleaved by β-secretase, generating the large soluble sAPPβ peptide and the CTF C99. This is subsequently processed by γ-secretase, producing the Aβ peptide associated with Alzheimer's disease (that has two predominant forms differing in their C-terminals length, Aβ40 and Aβ42), and the intracellular AICD fragment [63]. Figure 10 is a schematic representation of the APP cleavage sites and its principal proteolytic products.

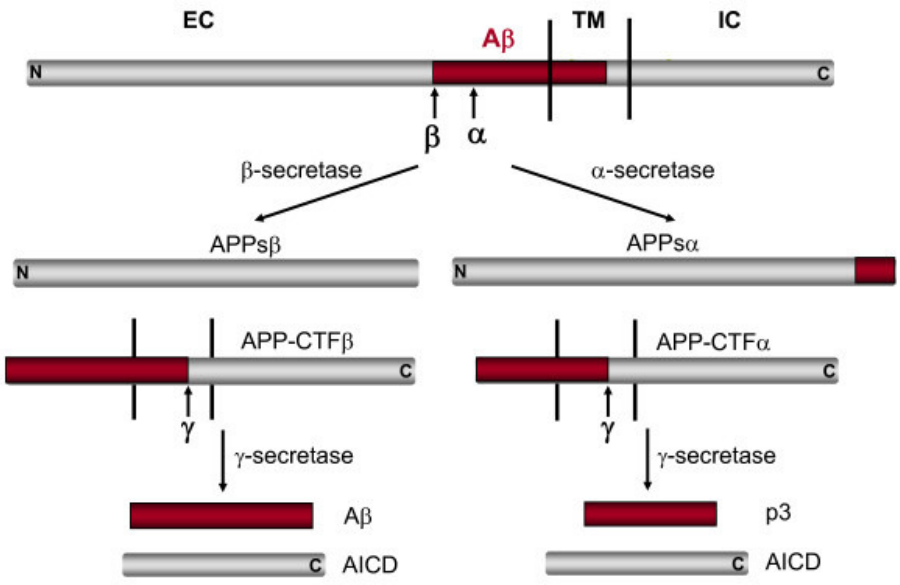

Figure 10.Schematic diagram of APP proteolytic processing. Cleavage by α-secretase enables the secretion of sAPPα into the medium and the preservation of the C83 fragment in the membrane. The C83 fragment can undergo cleavage by γ-secretase to release the p3 peptides and AICD (right side). Alternatively, proteolytic cleavage by β-secretase results in the secretion of the slightly truncated sAPPβ molecule and the retention of the C99 fragment. The C99 fragment can also undergo cleavage by γ-secretase to release the Aβ peptides and AICD (on the left). Reproduced from reference[74].

α-secretases: several membrane-bound disintregrin and zinc metalloproteinases including ADAM17 (or TACE), ADAM10, ADAM9 and MDC-9 have been identified has having α-secretase-like activity. Cleavage of APP by activation of α-secretase is a constitutive, relatively major and ubiquitous pathway of APP metabolism in most cells, and precludes the generation of intact Aβ[63, 73]. These proteins are synthesized as preproproteins, and to become active their prodomain is cleaved in the late Golgi by proprotein convertases (PPCs)[68]. The aspartyl protease β-site APP-cleavage enzyme (BACE) 2 has also been identified has a α-secretase, as it can cleave APP in the middle of the Aβ domain, between Phe19 and Phe20. Importantly, activation of PKC by phorbol esters upregulates the α-cleavage pathway, and the same occurs with estrogen, testosterone, various neurotransmitters and growth factors [63, 73].

β-secretases: β-cleavage is attributed to two enzymes, named the β-site APP-cleavage enzymes BACE1 and BACE2. Both enzymes are expressed in neural tissues, but experiments using BACE1 knockout mice strongly indicate that BACE1 is the major β-secretase in the brain. BACE1 is produced as a pro-enzyme in the ER and the in the nuclear envelop, and its prodomain is cleaved by furin or other PPCs just before trafficking through the Golgi[63, 68]. Mature BACE is mainly found in the endosome, and in lower levels in the cell surface and TGN, with virtually no mature BACE being found in the lysosome or endoplasmic reticulum. Thus, β-cleavage may occur in any of the cellular sites where mature BACE1 is found, but since the endocytic pathway is the most acidic, it is thought to be the best suitable subcellular location for BACE activity[71]. Supporting this, studies of BACE-APP interaction using FRET analysis showed that APP binds BACE with greatest efficiency in the endosome, less in the cell surface, and to a negligible degree in the TGN and secretory pathway[75].

γ-secretases: γ-secretase is a multimeric complex, made of four essential subunits: Presenilin-1 or -2, Nicastrin, APH-1, and PEN-2[76]. Each subunit has been found necessary for the enzymatic activity of the complex, which is dramatically impaired when any of the components are deficient[77]. Aph-1 and Nicastrin initially form a subcomplex to bind and stabilize Presenilin, and Pen-2 confers the gamma-secretase activity by facilitating Presenilin endoproteolysis[76]. Besides being consider a scaffolding protein within the γ-secretase complex, Nicastrin has been shown to act as γ-secretase receptor as it binds APP (and Notch) through its ectodmain[78].

Strong evidence suggests that the γ-secretase complex cleavages APP mainly in the TGN and early endosomal locations[79]. The complex acts in multiple sites within the APP transmembrane domain, cleaving the remaining APP CTFs inside the membrane. APP αCTF (or

CTF83) cleavage yields AICD and p3 fragment production, and βCTFs (CTF99 or 89) processing results in different Aβ forms and AICD[80]. The γ-secretase complex acts through a mechanism known as regulated intramembrane proteolysis (RIP), that besides a proteolytic process, comprises a transcriptional regulation event following translocation to the nucleus[80]. Very interestingly, it has been suggested that the origin of APP CTFs, either from the β- or α-secretase processings, may determine the affinity of γ-secretase to the CTFs[80]. Of note, in addition to cleaving APP CTFs, γ-secretase cleaves other several functionally important membrane proteins, like Notch, cadherin, tyrosinase, ErbB4, CD44, etc[77].

1.3.5. Phosphorylation of APP

Direct phosphorylation of the APP molecule may have important roles in the regulation of APP binding, traffic and processing. Indeed, APP is a phosphoprotein with several putative phosphorylation sites. Two of that residues shown to be phosphorylated, Ser^{198} and Ser^{206}, are localized in the APP ectodomain. In addition, the APP cytoplasmic tail comprises three Tyr residues and five Ser/Thr putative phosphorylation sites: Thr^{654}, Tyr^{653}, Ser^{655}, Thr^{668}, Ser^{675}, Tyr^{682}, Thr^{686} and Tyr^{687}, most of which are located within three functional motifs: ^{653}YTSI^{656}, ^{667}VTPEER^{672}, and ^{682}YENPTY^{687} [81-82]. However, there is still some controversy concerning which residues are actually phosphorylated in vivo [81-82].

Phosphorylation of Ser^{655}, that has been observed to occur in mature APP molecules in vitro and in vivo [83-85], may be a pivotal regulatory process for APP trafficking and proteolysis, since this residue is located in the basolateral sorting motif, ^{653}YTSI^{656}, and it is the only APP Ser/Thr residue phosphorylated by PKC. Additionally, NMR analysis showed that APP phosphorylation at S655 induces significant local conformational changes in the APP C-terminus at and downstream the ^{653}YTSI^{656} motif[86]. Besides PKC, Ser^{655} maybe be phosphorylated by calmodulin-dependent protein kinase II (CaMKII)[87], and by APP kinase I[88].

Preliminary work from the Neuroscience laboratory of the Center for Cell Biology research unit suggest that APP phosphorylated at S655 is an active molecule, crucial in the regulation of the APP subcellular trafficking. Though the use of APP S655 phosphomutants **-** serine 655 to alanine (S655A), and serine 655 to glutamate (S655E), mimicking unphosphorylated and phosphorylated APP, respectively – evidence was gather that S655 phosphorylation of mature APP molecules is a signal for APP traffic via the secretory pathway, facilitating its incorporation into TGN vesicles and Golgi exit**.** S655A is thus highly retained at the Golgi, exhibits delayed incorporation into secretory post-TGN vesicles, and delayed sAPPα medium secretion. In contrast,

S655E appear to have facilitated Golgi exit, enhanced traffic between the Golgi and PM as well as a higher rate of sAPPα secretion. Furthermore, another study from the Neuroscience laboratory showed that S655 phosphorylation enhances mature APP half-life by increasing APP binding to the retromer complex and the subsequent retromer-mediated APP retrieval to the TGN, thus increasing APP recycling[89]. These raises the hypothesis that part of the mature APP population is phosphorylated at S655 when it is necessary to target APP for a more dynamic TGN-to-PM trafficking, and sAPPα generation, what may occur through the catalytic action of PKC[90].

1.4.Potential role for the Amyloid-β Precursor Protein as a modulator of neuronal differentiation

APP is a very complex molecule that is now proved to be determinant for neural function, as either in its full-length configuration, or in its resulting proteolytic fragments. Furthermore, it has been proposed that not only the accumulation of Aβ, but also reductions in the level or activity of certain APP fragments play a critical role in the cognitive dysfunction characteristic of Alzheimer´s Disease.

Various studies currently address the physiological roles of APP and its fragments, gathering growing evidence of its implication in development and cell growth, intercellular communication, signal transduction, nuclear signaling, and structural and functional plasticity. Three APP products have received particular attention, the sAPPα, Aβ and the AICD. Secreted APPα is neuroprotective, neurotrophic, and regulates cell excitability, calcium homeostasis, and synaptic plasticity, therefore potentially regulating learning and memory, while Aβ appears to exert opposing effects[91]. The intracellular carboxyterminal fragments of APP also deserve attention due to their ability to bind several proteins, most of which being adaptor proteins that can bind other components to exert their effects. Particularly, AICD possesses transcriptional regulatory activity when in complexes with other proteins, such as the ternary complex composed by AICD, the adaptor protein Fe65 and acetyl-transferase TIP60. Noteworthy, that is little consensus and several conflicting findings regarding the AICD-dependent regulated genes, with candidate target genes being: APP itself, KAI1, a tumor suppressor and antimetastasis gene; neprilysin, a neutral endopeptidase with Aβ-degrading activity; LRP1; the EGF receptor; GSK-3β, a kinase involved in tau phosphorylation; Transgelin, an actin cross-linking protein. Furthermore, AICD has been shown to contribute to apoptosis, development, synaptic plasticity and cytoskeletal dynamics[80].

Despite its numerous potential roles in neural functions, here we will mainly focus the potential role of APP in neurite outgrowth and neuronal differentiation.

APP preferential localizes at nerve terminals, where it is supposed to play a role in establishing or maintaining cell-cell contacts[92]. During early development, APP is present in growing neurites of neonatal rat brain[93], and developing neurons undergo increased APP expression, with this protein being preferentially localized in the neuritic growth cones [94].

The first evidences that APP was involved in neurite outgrowth came from the findings that antibodies against APP specifically diminished the effects of NGF on neurite length and branching in pheochromocytoma PC12 cells, indicating that APP mediates neuritic outgrowth promotion by NGF [95], and from a study using human neuroblastoma La-N-1 cells stably expressing an antisense APP mRNA, which exhibited a 30% reduction in cell proliferation, reduced cell adhesion, and 2-4 fold increases in neurite-bearing cells[96]. Noteworthy, the cell adhesion- and neurite outgrowth-promoting roles of APP appear to be correlated, what is not surprising as neuronal migration, neurite outgrowth, and even synaptogenesis involve substrate adhesion[73].

The expression of APP695, the major APP neuronal isoform, is developmentally regulated during the differentiation of hippocampal neurons and neuronal-like cell lines in vitro. Interestingly, despite the fetal neuronal cells express higher levels of APP, they show little secretory processing into its soluble derivative, suggesting that the principal functional role in central nervous system development is responsibility of APP membrane-bound holoprotein[97]. Consistent with that were the results obtained by Qui et al (1995) when using a system in which developing neurons were grown on transfected non-neuronal cells expressing various isoforms of APP, to be able to distinguish the functional properties of cell surface APP from those of soluble APP and Aβ peptides. Results demonstrated that neurite outgrowth from hippocampal neurons was promoted by increased surface-expressed APP but not by increased sAPP and other secreted derivatives in the medium. In addition, they were able to prove that surface-expressed APP770 and APP751 isoforms (APP isoforms containing the KPI domain) promote neurite outgrowth more vigorously than APP695, most probably due to their higher roles in cell adhesion, mediated by the APP ectodomain [98]. In this same year, Alliquant et al. reported that a 6, 18, and 24h block in APP expression using antisense oligonucleotides was sufficient to produce significant inhibitory effects on neurite growth of primary cortical neurons. APP antisense-induced inhibition of neurite growth affected all neurites, both axonal and dendritic, without changing size or pattern of cell bodies spreading on the substratum, suggesting that the effects on neurite growth were not caused by a global change in cell-substratum adhesion[99]. A previous study had demonstrated that the

binding of APP to specific proteoglycan species of heparin sulfate proteoglycans (HSPGs), a component of the extracellular matrix, is an important step in the regulation of neurite outgrowth. Moreover, the study established that APP must be substrate-bound in vitro to exert its physiological effects, since when added to the cultures in soluble form, APP did no stimulate neurite outgrowth as efficiently. Noteworthy, APP appeared to inhibit the action of laminin on neurite outgrowth, suggesting a dynamic role in altering the general adhesiveness of the environment[100].

A couple years later, an experience was performed exploiting the differences in neuron survival and development between hippocampal neurons deriving from wild-type and APP-deficient mice. These were co-cultured with astrocytes from wild-type or APP-deficient mice, to allowed determining the effects of APP secretory products. The APP-deficient neurons showed markedly shorter axons at 1 day in vitro (DIV), but the APP-deficient neurons grown with wild-type astrocytes ultimately developed axons equal in length to those of wild-type neurons, implying that APP primarily contributes to the onset of axon formation. Moreover, wild-type neurons always had more branched neurites and ultimately had more minor processes than did APP-deficient hippocampal neurons. By 3 DIV, wild-type and APP-deficient neurons co-cultured with wild-type astrocytes had significantly shorter axons than neurons co-cultured with APP-deficient astrocytes, while the number of minor processes and the number of branch points were significantly greater. Data indicated that both cell-associated APP and secreted APP products appear to be important for normal neuronal development, with cell-associated APP enhancing neuron survival, the timely initiation of axon growth, and axon arborization, whereas APP secreted products appear to modulate neuronal polarization limiting the growth of axons and enhancing dendritic growth[101].

More recent data suggests that full-length APP acts in a cell autonomous manner to promote neurite outgrowth, both in vitro and in vivo. sAPPα addition to neurons was known to stimulate neurite outgrowth, but only recently it was shown that sAPPα does not stimulate neurite outgrowth in the absence of cell surface APP. Furthermore, and corroborating several previous evidences suggesting a functional interaction between APP and integrins to mediate neurite outgrowth, this study showed that sAPPα competes with full-length APP for binding to integrin β1 (Itgβ1), in this way inhibiting the ability of APP to regulate Itgβ1-induced neurite outgrowth, and explaining why APP-deficient neurons had longer neurites that could not be further elongated by sAPP addition. APP and Itgβ1 appear to directly interact via APP ectodomain, but can also indirectly interact via Fe65, to which both proteins bind [102]. Indeed, a study where

interaction-deficient FE65 was introduced via adenovirus into cultured hippocampal neurons, showed that a complex including APP, FE65 and an additional protein (most probably MENA, the mammalian homolog of the *Drosophila* enabled protein) is involved in neurite outgrowth at early stages of neuronal development. Although the FE65 mutants did not affect total neurite output, they decreased axon segment length and slowing of axonal growth cones, apparently by altering the local formation of the complex [103].

In addition to NGF and HSPGs, induction of APP expression by RA has been described in a number of cell lines of neuronal and non neuronal origin [104]. Furthermore, all members of the APP family are up-regulated in parallel with neurite extension upon differentiation of human neuroblastoma SH-SY5Y cells with RA (further discussed in the following subtopic). A synergistic effect on neurite generation between RA, BDNF and APP synthesis has also been reported[105].

Regarding the effects of APP phosphorylation (pAPP) in neuronal differentiation, Ando et al (1999) explored the function of Thr668 pAPP in PC12 cells differentiation. They demonstrated that APP is phosphorylated at Thr668 when cells start to elaborate processes, and increases with neuronal differentiation, being mainly localized in growth cones. In the same study, they also reported that this role in neurite extension was independent of sAPP generation[106].

Besides full-length APP and sAPPα, AICD was also related to neuronal differentiation. Most recently, some authors correlated increased AICD levels with suppression of NGF-induced PC12 differentiation[107]. It appears that AICD interferes with Ntrk1 receptor signalling, and that elevated AICDs signalling to the nucleus downregulates p53 and cyclinD and suppresses STAT3 phosphorylation (an activator of transcription), potentially enhancing cell proliferation and inhibiting neuronal differentiation[107]. Such results corroborate with previous studies in an *in vivo* mouse model using TAG1, a functional ligand of APP that increases AICD production and simultaneously leads to low neurogenesis[108]. Mechanistically, the role of AICD in neurite development may involve its binding to the actin regulatory protein MENA (the mammalian homolog of the *Drosophila* enabled protein), mediated by Fe65, potential influencing actin remodelling and cytoskeleton dynamics[109].

1.4.1. Expression and processing of Amyloid-β Precursor Protein in retinoic acid-differentiated human SH-SY5Y cell line

Besides PC12 cells and primary neurons, several studies focusing APP role in differentiation have been performed in the neuroblastoma SH-SY5Y cell line. Nonetheless, data concerning the differentiation days at which APP protein levels increase in the RA-differentiated

SH-SY5Y cells are contradictory. König and colleagues (1990) were the first to study the expression of the *APP* gene in neuronal differentiation using 10 μM RA-induced SH-SY5Y differentiated cells, reporting a marked increase in total APP mRNA that peaked at differentiation day 4. Furthermore, they observed alterations in the spliced pattern of the APP transcripts, in favour of the APP695 mRNA, associated with an increase of total APP gene expression[110]. Contrarily, Beckman and Iverfeldt (1997), reported a smaller fold induction of the APP mRNA expression even after 6 days of differentiation, under the same differentiation conditions[111]. Later, Ruiz-León and Pascual (2003), accomplish morphologic differentiation of SH-SY5Y cells and a strong reduction of the cellular proliferation after 4 days of treatment with only 1 μM RA. In this study, a similar increase of APP-mRNA levels was observed after 4-6 days of treatment with 1 μM RA as by Beckman and Iverfeldf using 10 μM RA. In addition, the authors did not observe any alterations in the isoforms pattern, but reported a generalized and significant increase of both full-length and secreted APP [104]. Very intriguing were the results published by Murray and Igwe (2003), which induced SH-SY5Y neuronal phenotype with different RA concentrations and found no statistically significant changes in total APP mRNA and protein expression. However, when analyzing the different APP transcripts, they observed an increase in the expression of the APP_{695} mRNA transcript with increased RA concentration, and suggested that it is this increased APP_{695} transcript that supports a neuronal phenotype in RA-treated SH-SY5Y cells[112]. In one last study by Holback and colleagues (2005), a 3-fold increase was obtained for APP in SH-SY5Y cells after 6 days of incubation with 10 μM RA (in agreement with Beckman and Iverfeldt results), and increased sAPPα and AICD levels [105].

Table 3. Alterations in APP expression and APP proteolysis to sAPP and AICD in RA-differentiated SH-SY5Y cells. Dif: differentiation. PAD: gene coding for the APP; Signif: significantly.

Treatment		APP mRNA			APP prot	sAPPα	AICD	C99	Morphological changes
		Total	695	751/770					
RA 1 µM	4 d	↑ ≈ 2-fold[104]; No change (but a change in profile)[112].	↑ from 20% to 34% of total APP mRNA[112].	No change[112].	General ↑ of intracellular APP [104]; No change[112].	General ↑ [104].			↓↓ cell proliferation and morphologic dif ≈ 10µM RA [104]; Elongated and slender cell bodies, and enhanced neuritogenesis [112].
RA 10 µM	3d	↑≈2-fold [111].							Intense neurite extension and proliferation arrest [111].
	4 d	↑ 10.2-fold [110]; No quantitative change (but a slight increase)[112].	↑ 10-fold [110]; ↑ from 20% to ≈40% of total APP mRNA[112].	APP_{751} ↑ 9.5-fold and APP_{770} ↑ 12-fold [110]; No change[112].	No change[112].				Neuronal-like phenotype[110]; ≈ 1µM but to a much greater extense[112].
	6 d	↑ 3-fold [111].			↑ 3-fold [105].	↑ 4-fold [105].	↑4-fold [105].	No change [105].	Marked dif with longer neuritis[110].
	8 d		↑ from 54% to 70% of total PAD transcripts [110].	APP_{751} ↑ 6-fold(↓ from 37,5% to 26,5 of total APP mRNA) and APP_{770}: ↑ 3.4-fold (↓ from 8.5% to 3,5% of total APP mRNA)[110];					More slender and longer bipolar morphology[110];
	9 d				No signif ↑ [105].	↑ 7-fold [105].	No further ↑[105].	↓ ≈50% [105].	
	6d + BDNF				No signif ↑[105]	↑ 1.7-fold over 6d[105].		↓≈75% [105].	
	9d + BDNF				Signif ↑[105].		↑ 1.7-fold over 9d[105].		

2. Aims

In the present work it will be addressed the ability of APP and APP phosphorylated at S655 to mediate neuronal differentiation, namely morphogenic and neuritogenic processes. To this end, the well documented cell model of SH-SY5Y neuroblastoma cells will be used, under RA-differentiation conditions or undifferentiated, together with several molecular tools.

2.1.General Aims

i. To evaluate the effects of APP overexpression in retinoic acid (RA)-induced neuronal-like differentiation;

ii. To study the effect of APP phosphorylation at S655 (mimicked by APP S655 phosphomutants) in RA-induced neuronal-like differentiation;

iii. To determine if APP alone can induce morphologic alterations related to neuronal-like differentiation, and the influence of APP S655 phosphorylation in this process;

iv. To determine the role of AICD in regulating mechanisms underlying neuronal-like differentiation;

2.2.Specific Aims.

i. To optimize SH-SY5Y cells transfection with Wt, S655A and S655E APP-GFP cDNA constructs. These mutants mimic, to some extent, APP dephosphorylated and phosphorylated state at the S655 cytoplasmic residue, respectively;

ii. To optimize conditions of differentiation of SH-SY5Y non-transfected and transfected cells;

iii. To test if APP overexpression influences RA-mediated SH-SY5Y differentiation, by transfecting cells with Wt APP-GFP cDNA at the second day of RA-induced differentiation;

iv. To test if the APP S655 phosphomutants can differentially affect SH-SY5Y differentiation, by transfecting cells with S655A and S655E APP-GFP cDNAs at the second day of retinoic acid (RA)-induced differentiation;

v. To record morphologic and neuritogenic alterations in non-differentiated SH-SY5Y cells transfected with Wt, S655A, and S655E APP-GFP cDNAs for 24 and 48h, and to analyze the role of AICD in these mechanisms, by incubating cells with a drug inhibitor of AICD production in the last 24h of the 48h time point.

3. Methods

3.1.Culture, growth and maintenance of SH-SY5Y cell line

SH-SY5Y human neuroblastoma cells are originally derived from the cell line SK-N-SH, established from a bone marrow biopsy of a neuroblastoma patient. The SH-SY5Y cell line is maintained in 10% foetal bovine serum (FBS) minimal essential medium (MEM):F12 (1:1), with 2 mM L-glutamine and 100 U/mL penicillin and 100 mg/mL streptomycin [10 mL Streptomycin/Penicilin/Amphotericin solution, Gibco], in a 5% CO2 humidified incubator at 37°C. Cells were split when at 70-80% confluent.

3.2.Trypan Blue assay for initial cell plating

In order to plate a defined number of living cells, a dye exclusion assay was used, in which living cells with an intact cytoplasmic membrane exclude the reagent, while dead cells stain blue due to dye incorporation through permeabilized damaged cytoplasmic membranes. To an aliquot (90 µL) of cells suspension, 10 µL of 0,4% Trypan Blue were added and incubated for 1 minute at room temperature. The unstained (viable) cells were counted in a hemacytometer, and cell concentration calculated for further cell plating.

3.3.Transient transfection of the cell lines with APP-GFP cDNAs

In order to study the role of APP and APP phosphorylation in differentiation, Wt, S655A and S655E APP695-GFP cDNAs were used. S655A and S655E mimic an APP S655 constitutive dephosphorylated and phosphorylated states, respectively. To optimize SH-SY5Y cells transfection with the Wt and S655 APP-GFP cDNAs, two different transfection methods were initially tested, the Calcium phosphate and the TurboFect^{TM} lipid-mediated methods.

3.3.1.Transfection of coprecipitates of calcium phosphate and DNA (CaP) followed by a glycerol shock

Calcium phosphate-mediated transfection is a widely used method, and its efficiency can be increased by incorporating a glycerol shock in its procedure. Three hours before transfection the appropriate medium was replaced, and for each monolayer of cells to transfect two tubes were prepared. A first tube containing 1 µg of the respective DNA and 6,2 µL of 2M $CaCl_2$ was

prepared and final volume adjusted to 50 µL with sterilized H_2O; a second tube containing 50 µL of HEPES-buffered saline (HBS) 2x was also prepared, to which the DNA solution was added dropwise with gentle mixing. The mixture was incubated for 20-30 minutes at room temperature, after what it is vortexed and immediately transferred, dropwise, into the medium above the cell monolayer, with gentle rock of the six-well plate. Transfected cells were incubated for 12 hours at 37ºC in a humidified incubator in an atmosphere of 5% CO_2, after which were subjected to glycerol treatment. Briefly, growth medium was removed by aspiration, and 1,5 mL of 15% glycerol in 1x HBS added to the monolayer. Cells were incubated for 30 seconds, the glycerol removed by aspiration, and the monolayers washed twice with PBS. New medium was added, and the cells further incubated for 36 hours, after which cells and cell medium were collected in 1% SDS and 10% SDS, respectively, for Western blotting (WB).

3.3.2. Transfection by the TurboFect™ reagent

Transfections were carried out according to the manufacter´s instructions (Fermentas Life Sciences). Briefly, for each monolayer of cells grown in 6-well plates, 2 µg of DNA were diluted in 100 µL of serum-free growth medium. After being briefly vortexed, 2 µL of TurboFect™ were added to the diluted DNA. Of note, the amounts of DNA and TurboFect™ were scaled-up based on preliminary optimization assays. The mixture was vortexed and incubated for 15-20 minutes at room temperature, after what this mixture was added dropwise, to each well, with gentle rocking of the plate to achieve even distribution. Cells were further incubated for 5-48h at 37º C in a CO_2 incubator. This time period was further optimized to no more than 12h of incubation after which medium had to be changed, and transfection was left to occur for a total of 24 or 48h. This was the transfection method selected for the experimental assays (see Results).

3.4. Wt and S655 Phosphomutants APP-GFP cDNAs

APP isoformAPP isoform 695 (APP695) cDNA was used as template to generate S655 cDNA point mutations, namely Serine 655 to Alanine (S655A) or to Glutamate (S655E), using site-directed mutagenesis[90, 113] . These two amino acids, due to their size and charge, mimic a constitutively dephosphorylated and phosphorylated S655 residue, respectively. To engineer the APP695-GFP cDNA constructs (APP-GFP), the stop codons of Wt and S655 phosphomutants APP695 cDNAs were removed by PCR using specifically designed primers. The resultant fragments were digested with endonucleases (AgeI and NruI) and subcloned into the AgeI/SmaI restriction

sites of the GFP-encoding mammalian expression vector (pEGFP-N1, Clontech) as N-terminal APP-GFP translational fusions. The nucleotide sequences of the APP695 phosphorylation cDNA point mutants and the open reading frames were confirmed by DNA sequencing (ABI PRISM 310 genetic Analyser, Applied Biosystems).

3.5.Differentiation of the SH-SY5Y cell line

For the differentiation optimization assays, SH-SY5Y cells were differentiated by incubation with 1/10 µM RA in 1/10% FBS medium for four days, with RA being added every other day, and cell medium replaced at that time. The initial cell density plated was assigned after a previous optimization, accordingly to the FBS/RA combination. When differentiation was carried out on 10% FBS, initial cell density used was $1,0x10^4$ cell/cm^2, independently of the RA concentration used. For a combination of 1% FBS/1 µM RA, or 1% FBS/10 µM RA, cells were seeded at a density of $3,0x10^4$ cell/cm^2, or $6,0x10^4$ cell/cm^2, respectively. For the experimental assay, the 10 µM RA/10% FBS combination was used, and cells were plated at $1,0x10^4$ cell/cm^2.

3.6.Cells treatment with N-[N-(3,5-Difluorophenacetyl-L-alanyl)]-S-phenylglycine t-Butyl Ester (DAPT)

Non-differentiated SH-SY5Y cells were incubated with 1 µM DAPT[114] (InSolution™ γ-Secretase Inhibitor IX, Calbiochem), in the previous 24h before being harvested. In summary, 0,5 µL of DAPT were diluted in 12 µL DMEM, serum and antibiotics/antimycotics-free. From this first solution, 6 µL were transferred and diluted in 6 mL of complete medium in order to prepare the work solution, which was added to the cells for 24h at 2 mL/six-well.

3.7.Cell collection and quantification of protein content (BCA)

Cells' conditioned medium was collected with 1/10 v/v 10% boiling SDS, cells washed with PBS, and further harvested with 1% boiling SDS. Cell and media lysates were boiled for 10 min, and cell lysates sonicated for 30 sec. Total protein measurements were performed in an aliquot of the cell lysates using Pierce's BCA protein assay kit, following the manufacturer's instructions. This method combines the reduction of Cu^{2+} to Cu^{+} by protein in an alkaline medium with a sensitive colorimetric detection of the Cu^{+} cation using a reagent containing bicinchoninic acid. The first reaction step is the biuret reaction in which peptides containing three or more amino acid residues form a colored chelate complex with cupric ions in an alkaline environment containing

sodium potassium tartrate; BCA addition is the second step. Chelation of two molecules of BCA with one Cu^{+} ion gives origin to a purple-coloured reaction product, a water-soluble complex with a strong absorbance at 562 nm that is linear with increasing protein concentration over a working range of 20-2000 µg/ml. Total protein concentration of each sample was determined through a standard curve prepared by plotting BSA absorbance vs. BSA standard concentration. Briefly, microtubes with standard protein concentrations were prepared as in Table 4.

Table 4. Standards used in the BCA protein assay method. BSA, Bovine serum albumin solution (2 mg/ml).

Standard	BSA (µl)	10% SDS (µl)	H_2O (µl)	Protein mass (µg)	W.R. (ml)
P_0	-	5	45	0	1
P_1	1	5	44	2	1
P_2	2	5	43	4	1
P_3	5	5	40	10	1
P_4	10	5	35	20	1
P_5	20	5	25	40	1

A microtube was prepared per sample, to be assayed with 5 µl of each sample plus 45 µl of the solution in which the sample was collected (1% SDS). 1 ml of working reagent (W.R.; mixture of BCA reagent A with BCA reagent B in the proportion of 50:1) was rapidly added to all microtubes (standards and samples) and these incubated at 37 ºC exactly for 30 min. Tubes were coolled to RT and their absorbance at 562 nm was immediately measured.

3.8.Antibodies

The primary antibodies used in this study were the antibody 22C11 (Chemicon) directed against APP N-terminus, recognizing full-length APP and secreted APP (sAPP), and the antibody CT695 that recognizes APP C-terminal (detection of APP full length and APP C-terminal peptides), for APP and APP-GFP detection. To evaluate neuritogenic-related cytoskeleton alterations, the monoclonal anti-acetylated α-tubulin (Sigma), the polyclonal anti-actin N-terminal antibody (Sigma) that recognizes epitope(s) in the N-terminal domain of actin reacting with all actin isoforms, the monoclonal anti-MAP-2 antibody clone HM2 (Sigma) directed against all known MAP-2 isoforms. To investigate possible AICD transactivated genes the following antibodies were used: polyclonal anti-Glycogen Synthase Kinase-3 (GSK-3) that recognizes the alpha (~51 KDa) and beta (~46 KDa) isoforms; the polyclonal anti-KAI 1 (C-16, Santa Cruz Biotechnology) directed

against the human KAI1 C-terminus, and the polyclonal anti-Transgelin (H-75, Santa Cruz Biotechnology) raised against a region near the N-terminus of human Transgelin (H-75, Santa Cruz Biotechnology). As potential internal standards for Western blot assays, the monoclonal antibodies anti-β-Tubulin, that binds the two major and a minor β-tubulin isotypes, and anti-Glyceraldehyde-3-Phosphate Dehydrogenase (GAPDH) clone 6C5 (Ambion) that detects this ubiquitous glycolytic enzyme, were used. A list of all the antibodies used with their respective dilutions and secondary antibodies is depicted in Table 5.

Table 5. Antibodies used in the Immunoblots, respective target proteins and specific dilutions used. All the secondary antibodies are from Amersham Pharmacia.

Target Protein/Epitope	Primary Antibody	Secondary Antibody
Acetylated Tubulin	**Anti-Acetylated Tubulin clone 6-11B-1** (Sigma)	Horseradish Peroxidase conjugated α-Mouse IgG Dilution: 1:5000
Actin	**Anti-Actin N-terminal** (Sigma) Dilution: 1:1000	Horseradish Peroxidase conjugated α-Rabbit IgG Dilution: 1:5000
APP N-terminal	**22C11** (Chemicon) Dilution: 1:250	Horseradish Peroxidase conjugated α-Mouse IgG Dilution: 1:5000
APP C-terminal	**CT695** (Invitrogen) Dilution: 1:500	Horseradish Peroxidase conjugated α-Rabbit IgG Dilution: 1:5000
GAPDH	**Anti-GAPDH clone 6C5** (Ambion) Dilution:	Horseradish Peroxidase conjugated α-Mouse IgG Dilution: 1:5000
GSK-3 β	**Anti-GSK-3 total** (Chemicon) Dilution: 1:500	Horseradish Peroxidase conjugated α-Rabbit IgG Dilution: 1:5000
EGFP	**JL.8** (Clontech) Dilution: 1:1000	Horseradish Peroxidase conjugated α-Mouse IgG Dilution: 1:5000
KAI-1	**Anti-KAI 1 (C-16)** (Santa Cruz Biotechnology) Dilution: 1:500	Horseradish Peroxidase conjugated α-Rabbit IgG Dilution: 1:5000
MAP-2	**Anti-MAP-2 clone HM2** (Sigma) Dilution: 1:1000	Horseradish Peroxidase conjugated α-Mouse IgG Dilution: 1:5000
Transgelin	**Anti-transgelin (H-75)** (Santa Cruz Biotechnology) Dilution: 1:200	Horseradish Peroxidase conjugated α-Rabbit IgG Dilution: 1:5000
β-Tubulin	**2-28-33** (Invitrogen) Dilution: 1:2000	Horseradish Peroxidase conjugated α-Mouse IgG Dilution: 1:5000

3.9.Western Blot Assay

Mass-normalized cell aliquots were subjected to electrophoresis on a 7,5/10% (optimization assays) and 5-20% gradient (experimental assays) sodium dodecylsulfate (SDS) polyacrylamide gel, being subsequently transferred to nitrocellulose filters. After proteins electrotransfer, membranes were initially soaped in 1X TBS or 1x PBS for 10 min. Blocking of possible non-specific binding sites of the primary antibody was performed by immersing the membrane in 5% non-fat dry milk in 1X TBST solution for 1-2 h. Further incubation with primary antibody was carried out for a period of time accordingly to the manufactures instructions (ranging from 2 h to overnight incubation). After three washes with 1X TBS-T or 1X PBS-T, of 10 min each, the membrane was further incubated with the appropriate secondary antibody for 2 h with agitation. All primary and secondary antibodies used were diluted (specific dilutions in Table 5), accordingly to the manufactures instructions, in 1X TBS-T/3% non-fat dry milk, 1X TBS/1% BSA or 1X PSB-T/3% non-fat dry milk. Membranes were additional washed three times with 1X TBST or 1X PBS-T, before being submitted to the ECL™ (enhanced chemiluminescence; GE Healthcare) detection method, a light emitting non-radioactive method for detection of immobilised specific antigens, conjugated directly or indirectly with horseradish peroxidase-labelled antibodies. Washed membranes were incubated for 1 min at RT with the ECL detection solution or for 5 min with the ECL+ solution, freshly prepared fresh following the manufacturer's instructions. ECL/ECL+ detection solution in excess was drained. In a dark room, an autoradiography film was placed on the top of the membrane, inside a film cassette. The cassette was closed and the blot exposed for an appropriate period of time. The film was then removed and developed in a developing solution (Sigma Aldrich) washed in water, and fixed in a fixing solution (Sigma Aldrich). The blot was further washed in TBS-T and distilled water before drying, for better conservation.

3.10. F-actin detection, Fluorescence Microscopy and Morphological analyses

Cells grown on coverslips were fixed with a 4% paraformaldehyde PBS solution for 30 min (or with iced acetone when to analyse the cytoskeleton) and permeabilized with a 0,2% TRITON PBS solution (10 min). After three washes, coverslips were directly mounted on microscope slides with Fluoroguard Antifading Reagent (Bio-Rad).

In order to visualize F-actin, 2 µL Alexa Fluor 568 Phalloidin was diluted in 100 µL PBS 1% BSA and added to coverslips for two hours in the dark at 37 ºC. Coverslips were further washed

three times with PBS and one last time with distilled water, and then mounted with the antifading reagent on microscope glass slides for further epifluorescence microscopy analysis.

Epifluorescence microscopy was carried out using an Olympus IX-81 motorized inverted microscope equipped with a LCPlanFl 20x/0.40 objective lens. Cell counts and neurite length were measured using two image analyzer softwares: AnalySIS (Olympus) and ImageJ. Processes counting were divided in: all processes arising from a cell, counts of pre-neurites (processes longer than 20 μm), and counts of differentiated neurites (processes longer than two times the cell body length, 35 μm)[115]. Cells were considered differentiated when possessing at least one differentiated neurite.

3.11. Data analysis

Autoradiograms resulting from blots immunodetection were scanned in a GS-710 calibrated imaging densitometer (Bio-Rad) and protein bands quantified using the Quantity One densitometry software (Bio-Rad). Data are expressed as mean ± SEM (standard error of the mean) of three independent experiments. Statistical significance analysis was conducted by one way analysis of variance (ANOVA) followed by the Tukey test.

4. Results

4.1. Optimization of the transfection method

In order to optimize SH-SY5Y cells transfection, various transfection methods were tested. Cells were plated at a cell density of $1{,}75x10^5/cm^2$, and transfected for 24h with EGFP-N1 vector and Wt APP-GFP cDNAs, using the calcium-phosphate (Cap) method, either alone or followed by a glycerol shock, and the TurboFect™ reagent. The levels of APP-GFP transfection were evaluated by Immunoblot analysis using an anti-APP 22C11 antibody (Figure 11). Both the Cap-glycerol and the TurboFect™ methods yield efficient APP-GFP transfections (bands **a.**, immature and **b.**, mature forms, respectively). Although the Cap-glycerol method yielded the best efficient transfection rate, it was associated with an increase in cell death, as visually observed (data not shown). Therefore, in all subsequent assays, the TurboFect™ reagent method was used.

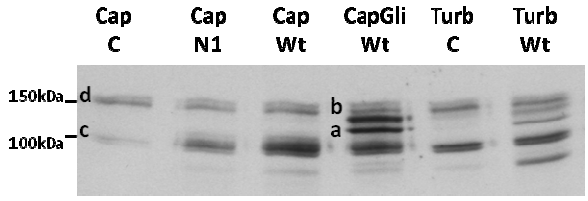

Figure 11. Immunoblot analysis of APP-GFP transfection in SH-SY5Y cells using different transfection methods. Cap: calcium-phosphate mediated transfection; Turb: TurboFect™ mediated transfection; C: control non-transfected cells; N1: cells transfected with vector EGFP-N1 only; Wt: Wt APP-GFP tranfected cells. The antibody 22C11 was used to detect a) APP-GFP 695 immature; b) APP-GFP 695 mature forms; c) Endogenous APP 751/770 immature; d) Endogenous APP 751/770 mature forms.

4.2.Establishment of SH-SY5Y differentiation conditions

Secondly, an experiment was delineated in order to optimize the best combination of foetal bovine serum/retinoic acid (FBS/RA) for SH-SY5Y cells differentiation, not only in non-transfected but also in transfected cells, since transfection itself can potentially be an insult for cells, and APP may induce cell death[115]. Cells were differentiated for four days using different FBS/RA conditions, being transfected at the second day with the EGFP-N1 vector and Wt APP-GFP. Since the levels of RA and FBS affect cell proliferation and cell death, conditions of 1/10 µM RA in

1/10% FBS medium were used in combination with different initial cell densities, previously optimized. When differentiation was carried out in 10% FBS, cells were plated at 1,0x104 cells/cm2 due to their higher proliferation. When using 1% FBS/1 μM RA, cells were seeded at 3,0x104 cells/cm2, and for 1% FBS/10 μM RA cells were seeded at 6,0x104 cells/cm2, due to increased cell death. Following four days of differentiation, transfection was visually observed in an epifluorescence microscope, and cells were harvested for immunoblot analyses. First, APP-GFP transfection was confirmed by immunoblot analyses (Figure 12).

APP-GFP transfection (bands a,b) was confirmed for all RA/FBS conditions, by immunoblot analysis either using the 22C11 antibody, against APP N-terminus, or the CT695 antibody, against the APP C-terminus (Figure 12). Of note, APP-GFP transfection appears to increase intracellular sAPP (22C11-positive and CT695-negative bands, marked with an asterisk). Further, as expected, the levels of endogenous APP generally increased in differentiated versus non-differentiated cells (compare NT lanes of Dif 1 and Dif2 with Cnd1; Dif 3 and Dif 4 with Cnd2). Only the APP levels of the Dif2 NT lane appear to be anomaly low, as it will be denoted to occur for other proteins, indicating that an experimental error probably occurred when loading this sample.

The protein levels of acetylated α-tubulin, a known parameter of differentiation that indirectly measures microtubules stabilization [115-117], were analysed to first evaluate cellular differentiation in the conditions tested. The levels of the putative housekeepings proteins β-Tubulin and GAPDH, potential internal standards for western blot analyses, were also monitored (Figure 12 lower panel). In this initial differentiation period (first 4 days), acetylated tubulin levels increased in 1 μM RA conditions (Dif1, Dif3), while maintaining in 10 μM RA conditions (Dif4; again in Dif2 NT lane it appears that an error occurred when loading the sample). Remarkably, in all conditions tested, acetylated α-tubulin always decreased with transfection, and more markedly for APP-GFP transfection. Further and somewhat expected, in all the RA/FBS conditions tested, β-Tubulin followed similar variations to the acetylated α-tubulin ones, and its levels increased with cellular differentiation but generally decreased with Wt APP-GFP transfection. Unexpectedly though, GAPDH levels suffered fluctuations with different RA/FBS differentiation conditions, but again decreasing with APP-GFP transfection in all conditions (compare Wt APP-GFP with N1 values at the same condition). In conclusion, nor β-Tubulin nor GAPDH can be used as control invariant proteins (β-Tubulin can even be used as a differentiation cytoskeleton-related marker), and we are currently still in the process of finding a good housekeeping protein to use in differentiation and transfection conditions.

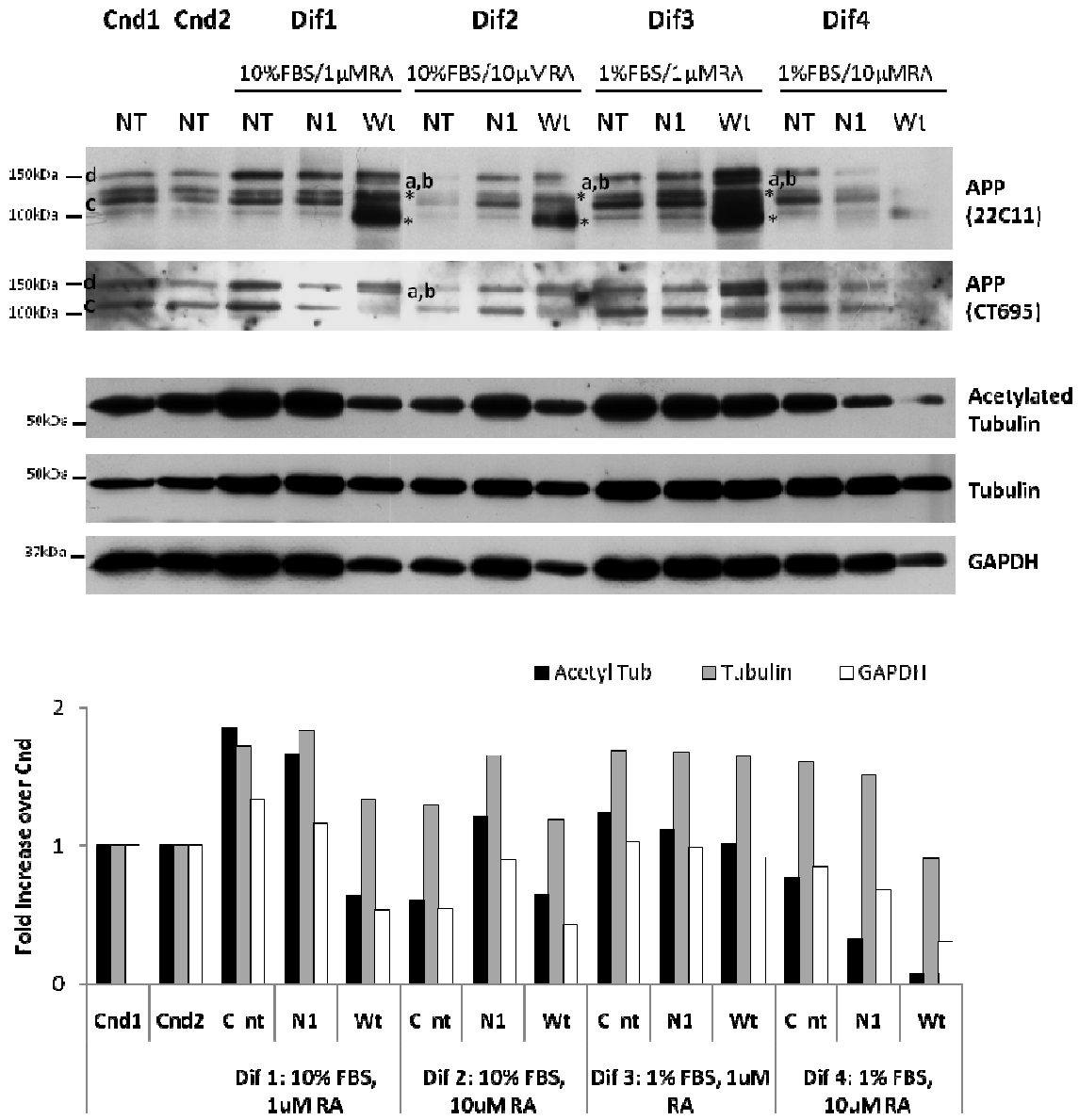

Figure 12. Evaluation of APP-GFP expression and of the variation of acetylated α-Tubulin, β-Tubulin and GAPDH with different differentiation conditions and APP-GFP transfection. Immunoblot analysis of SH-SY5Y cells differentiated for 4 days with different RA and serum conditions and transfected at the second day with wild type APP-GFP('Wt'). Cnd 1 and Cnd 2: control non-differentiated cells initially plated at 2,0x104/cm2 (control of Dif1 and Dif2) and 6,0x104/cm2 (control of Dif3 and Dif4), respectively; NT: non-transfected cells; N1: vector EGFP-N1 transfected cells. Upper panel: Confirmation of APP cDNA transfection using 22C11 and anti-APP C-terminus CT695 antibodies. a) APP-GFP 695 immature; b) APP-GFP 695 mature; c) and d), endogenous immature and mature APP 751/770, respectively; intracellular sAPP is marked with an asterisk. Lower panel and graph: Protein expression profiles of acetylated α-Tubulin, β-Tubulin and GAPDH with different RA/FBS differentiation conditions and Wt APP-GFP transfection. Tubulins and GAPDH quantitative data are presented as fold increases over control non-differentiated cells.

To evaluate the degree of SHSY-5Y differentiation under the different RA/FBS conditions tested, the neuritogenic output elicited by each FBS/RA combination was measured. The

percentage of differentiated cells (cells with a neurite longer than 35 µm) and the mean neuritic length were monitored in the general population or in the transfected population only (Figure 13).

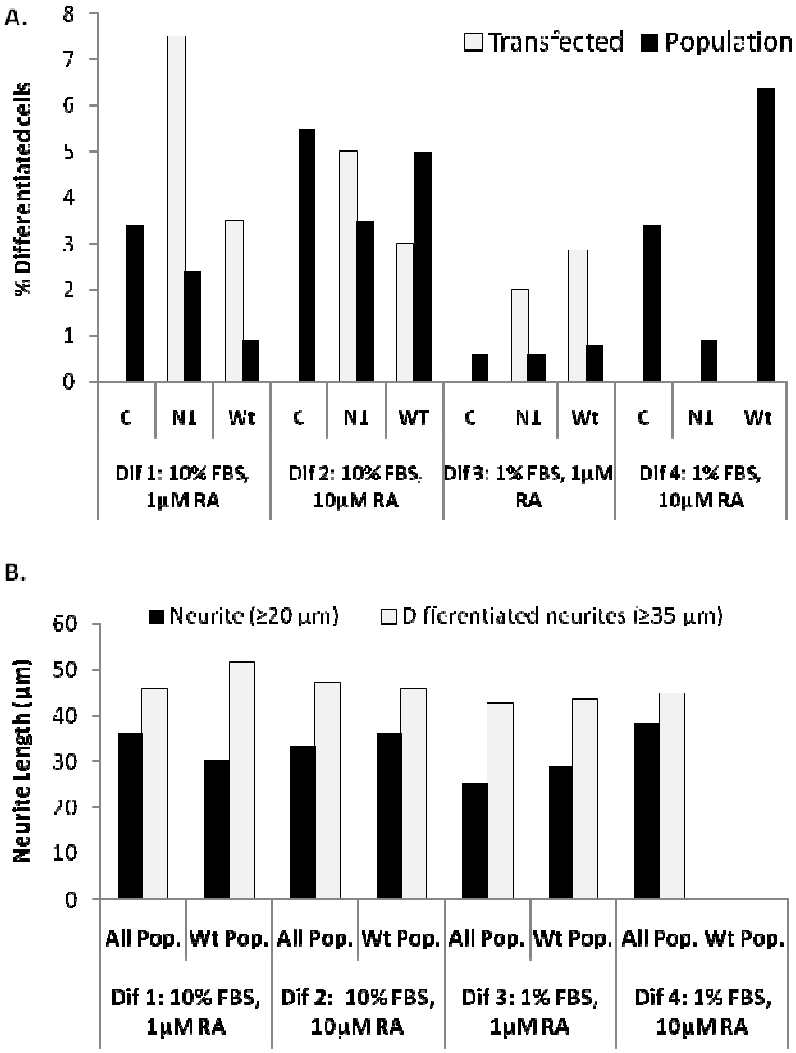

Figure 13. Morphological analysis of SHSY-5Y cells differentiated under different conditions. A. Percentage of differentiated cells**.** The percentage of cells bearing at least one neurite greater than 35 µm was determined for the general population ('Population'), and for vector EGFP-N1 or Wt APP-GFP transfected cells ('Transfected') only when applicable. **B.** Mean neurite length. The mean neurite length (all neurites greater than 20 µm were considered) and mean neurite length of differentiated cells (cells with neurites greater than the length of two cell bodies, 35 µm) were calculated for the general population ('All Pop.') and for Wt APP-GFP expressing cells alone ('Wt Pop.').

The percentage of differentiated cells was generally low at this time point of 4 days of differentiation (1-7% of all cells), and was sensitive to the differentiation conditions and to N1/APP-GFP transfections (Figure 13-A). Regarding the entire cell populations, the percentage of differentiated cells generally increased with both increases in RA and FBS concentrations (e.g.

compare conditions of equal RA concentration but increased FBS% - Dif 3 with Dif1). However, when only considering the population of N1 and APP-GFP expressing cells, cellular differentiation only increased with the FSB concentration (from Dif3 to Dif1; from Dif4 to Dif2). That is, increased RA concentration led to a decrease in the percentage of differentiated transfected cells and, remarkably, N1 and Wt APP-GFP expressing cells in condition Dif4 did not present any neurites. When considering both transfected and non-transfected populations, conditions of 10% FBS resulted in higher percentages of cellular differentiation, being condition Dif2 the one where this parameter is more homogeneous. In terms of neuritic length (Figure 13-B), at this early differentiation period the FBS/RA combination seems not to be very important, since the values did not suffer marked variations. The same occurred when expressing APP-GFP, which only induced a small increase in the length of longer neurites at condition Dif1.

In synthesis, the morphometric data suggests that 10% FBS conditions are preferable to study differentiation of transfected cells, since FBS appears to be protective at higher RA concentrations, where cells tend to die. The 10 μM RA/10% FBS combination led to high levels of differentiation and rendered the most homogeneous results in terms of transfected and non-transfected cells differentiation. Interestingly, both the immunoblot data and the morphometric data already indicated that Wt APP-GFP expression was not leading to higher SH-SY5Y differentiation, but rather doing the opposite, and this was further studied in more detail.

4.3.Effects of APP overexpression and APP S655 phosphorylation on RA-induced differentiation

Previous studies on APP in neuritogenesis, that used RA differentiated SH-SY5Y cells, all reported an increase in APP levels after 3-4 days of differentiation, indicating that APP is important in the early period of differentiation. The effects of APP overexpression, and of mimicking APP S655 dephosphorylation (S655A) and phosphorylation (S655E), were thus further evaluated in this early period of differentiation. For that, cells were differentiated for 4 days in 10% FBS/10 μM RA medium, being transfected with wild-type and S655 phosphomutant APP-GFP cDNAs (Wt, S655A, S655E) at the second day of differentiation. Transfection was conducted for 48h in order to allow morphological alterations dependent of genic transcription to occur.

APP-GFP transfection, APP and sAPP protein levels, and the protein levels of some neuritogenic cytoskeleton-related markers, were evaluated by immunoblot analyses.

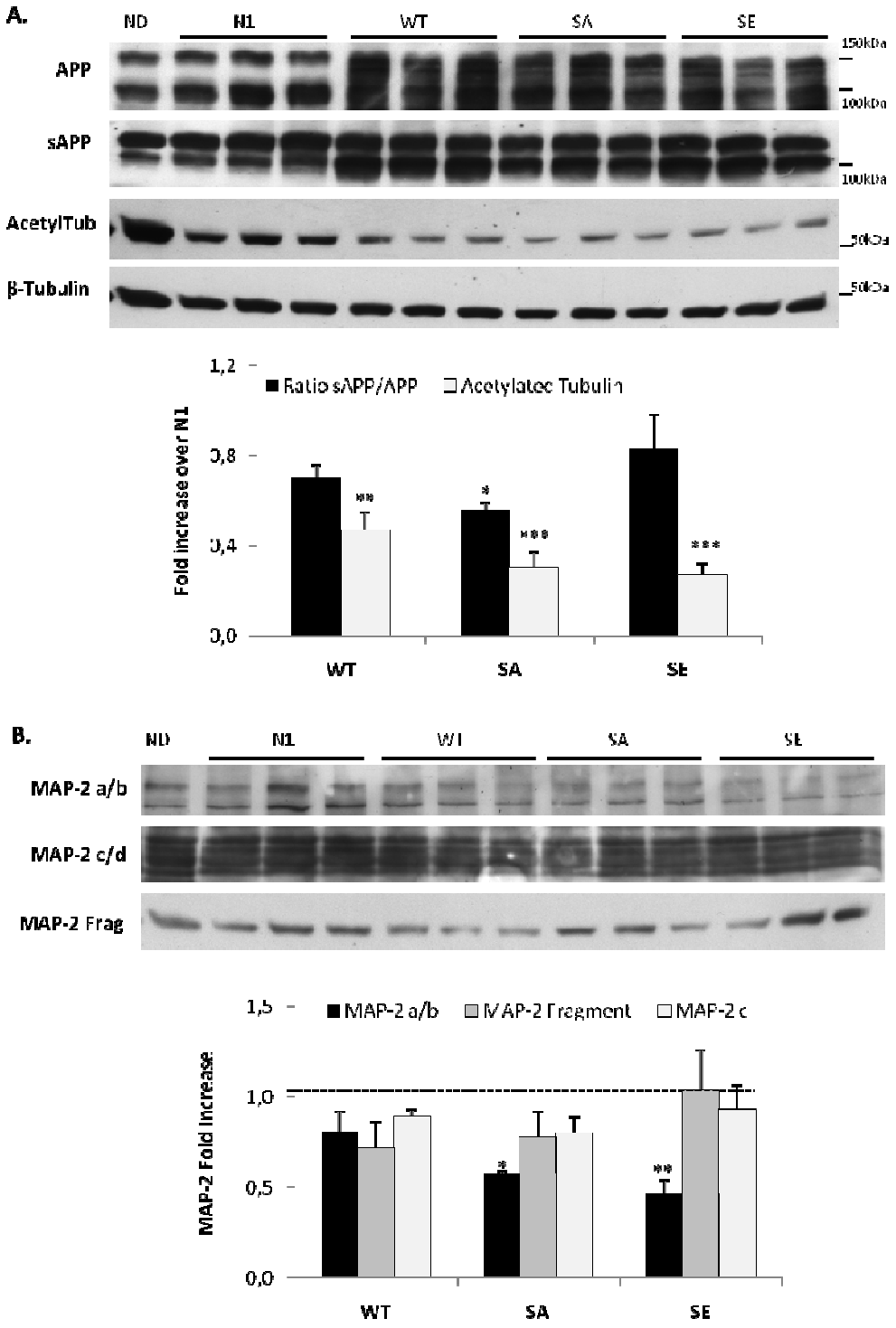

Figure 14. Effects of Wt, S655A and S655E APP-GFP transfection in sAPP/APP ratios and in microtubule-related neuritogenic markers. Immunoblot analysis of SH-SY5Y cells differentiated for 4 days in 10% FBS/10 µM RA medium and transfected at the second day with Wt, S655A and S655E APP-GFP cDNAs. **A.** Variation of sAPP/APP ratio and acetylated tubulin with APP-GFP transfection. Cellular APP and sAPP secreted into conditioned medium were detected with the 22C11 antibody. Bottom graph presents the sAPP/APP ratio and the acetylated tubulin fold increase over N1 transfected cells values. **B.** Variation of MAP-2 with APP-GFP transfection. A MAP-2 antibody was used that recognizes all MAP-2 isoforms. ND: Control non-differentiated cells; N1: vector EGFP-N1 transfected cells; Wt, SA and SE: wild-type, S655A and S655E APP-GFP tranfected cells, respectively. All data was normalized to Tubulin levels and to the APP-GFP proteins relative transfection rates. *p<0.05; **p<0.01; ***p<0.001. n= 3.

From the immunoblot results and graph quantifications (Figure 14) one can see that the sAPP/APP ratio decreases for Wt APP-GFP transfected cells (~0.7), in comparison with N1 transfection levels. This ratio was even lower for S655A transfected cells, but was higher for S655E cells (~N1 sAPP/APP ratio). Wt APP-GFP transfection also decreased α-tubulin acetylation by ~50%, in agreement with what was previously observed in the differentiation optimization assay. The APP S655 phosphomutants decreased even more acetylated tubulin levels (Figure 14-A) to around ~30% of N1 values. A second differentiation marker was tested, MAP-2, a microtubule-binding and stabilizing protein that has been described to participate in neuritic outgrowth [14, 116-117]. A decrease was also observed for the levels of the high molecular weight MAP-2a/b isoforms (Figure 14-B) with APP-GFP transfection, especially for the S655 phosphomutants. The levels of MAP-2c/d, the main MAP-2 isoforms in SHSY-5Y cells, only slightly decreased with Wt APP-GFP transfection, and suffered no significant alterations between the APP-GFP proteins. A similar variation pattern was observed for another MAP-2 positive band of ~50KDa, named 'MAP-2 fragment', which potentially results from MAP-2 degradation. Altogether these results show that Wt and especially both S655 APP phosphomutants decrease microtubules stability (lower levels of acetylated tubulin and of MAP-2 isoforms).

The morphometric parameters of the cellular population were also analysed, to characterize the effects of Wt and S655 phosphomutants APP-GFP transfection in SH-SY5Y differentiation. Since APP-GFP transfection and cells exposure to RA may result in cell death, as previously observed, the cellular viability was first evaluated by scoring the number of live and dead cells in microphotographs (Figure 15-A and B). Results show that APP-GFP transfection indeed decreased the number of cells, relatively to EGFP-N1 expressing cells. Such decrease was more pronounced for the APP phosphomutants, which appeared to be able to induce cell death also on neighbour non-transfected cells (Figure 15-B). Regarding the neuritogenic output, cells expressing Wt and S655A APP-GFP had a lower percentage of cells with processes and neurites than the N1 cells, resulting in lower percentage of differentiated cells (cells with at least one neurite longer than 35 μm). However, S655E APP-GFP transfection resulted in similar levels of cells with processes as for N1, and was able to induce higher percentages of differentiated cells, either in S655E transfected cells or in the general population (Figure 15-C). Of note, the observed higher cell death for the general population, upon S655A and S655E transfection, may contribute to their high levels of differentiated cells, simply by liberating more space for differentiation to occur.

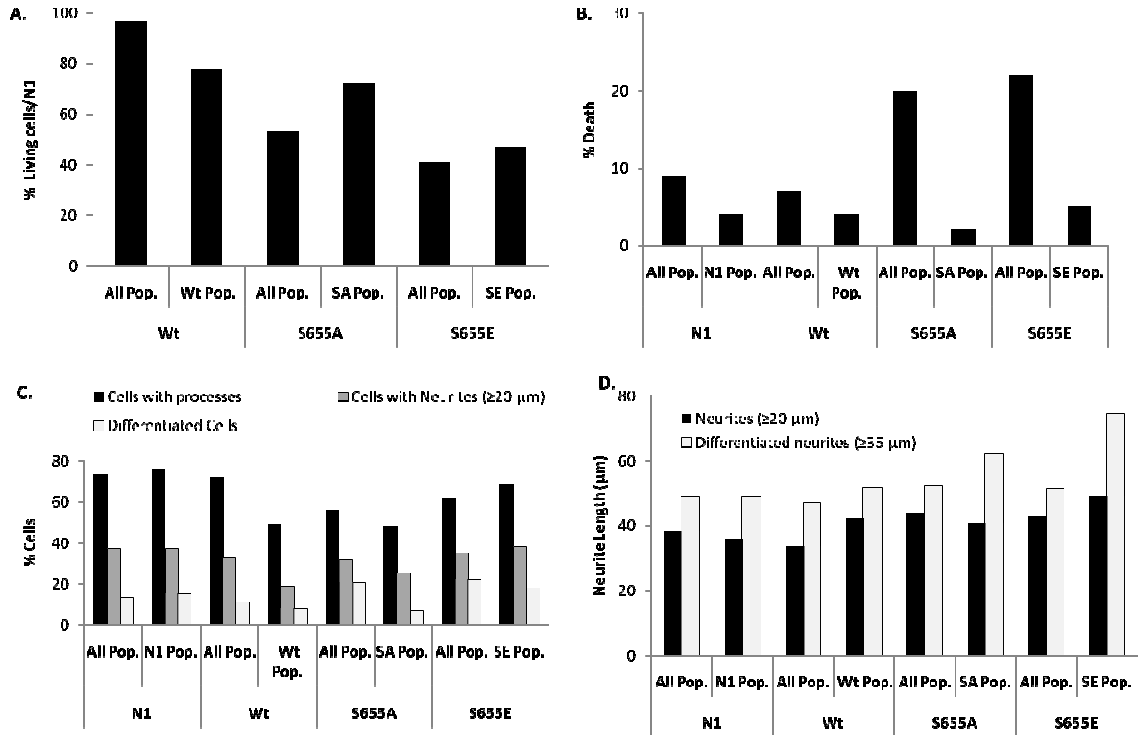

Figure 15. Morphological analysis of SHSY-5Y cells, differentiated for 4 days and transfected with N1, and the APP-GFP cDNAs. N1 pop: population of EGFP-N1 expressing cells; Wt, SA, SE pops: populations of cell expressing wild-type, S655A, and S655E APP-GFP. **A.** Percentage of living cells. The number of living cells was scored and presented as percentages of the number of cells in the EGFP-N1 sample (taken as 100%)**. B.** Percentage of cell death, calculated as the percentage of dead cells on the coverslips relatively to the number of living cells in the same sample. **C.** Percentage of cells with processes and neurites. Percentage of cells bearing protruding processes, processes >20 µm (pre-neurites and neurites), and > 35 µm (differentiated neurites). **D.** Neurite length. The neurite length of all pre-neurites (>20 µm) and neurites (>35 µm) was measured.

With respect to neuritic length, the phosphomimicking mutant also increased the length of the neurites in S655E expressing cells, and had a positive effect on the neuritic length of the non-transfected neighbour cells (Figure 15-D). S655A has a smaller positive effect, while the Wt had almost no effect on neuritic length, in accordance with the preliminary results (differentiation optimization assays). Thus, APP-GFP 48h transfection had in general negative (Wt and S655A) or neutral (S655E) effects on the number of processes (neuritogenesis), and only S655E had positive effects on neuritic length, probably the reason why it also increased cellular differentiation. Since neuritogenesis and neurite elongation are related to rearrangements on both microtubules and actin cytoskeletons, F-actin organization was studied in this experiment (Figure 16).

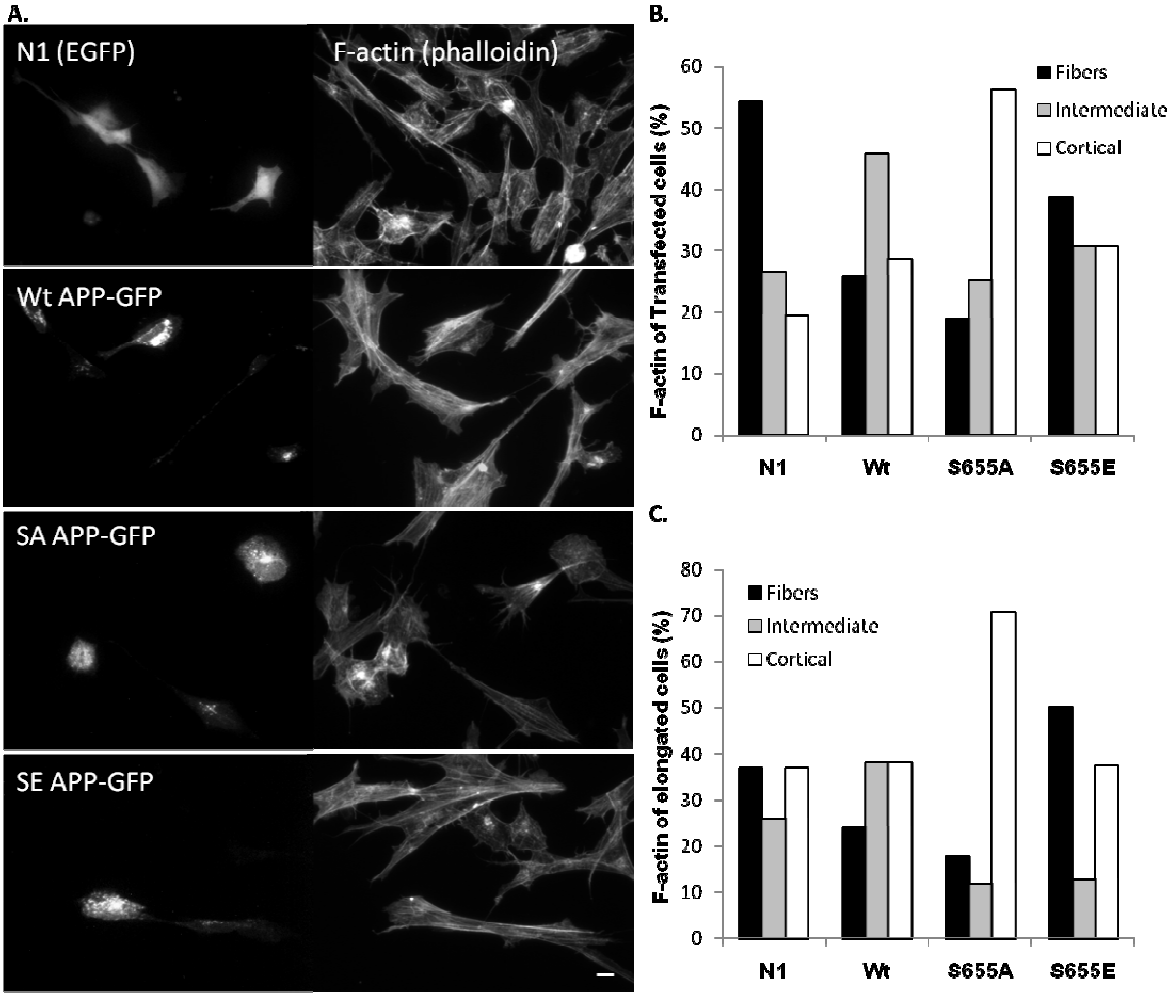

Figure 16. Analysis of F-Actin rearragments. F-actin distribution was evaluated using red fluorescent-labeled phalloidin, a drug that selectively labels actin filaments, in cells differentiated (10% FBS/10 µM RA) for 4 days and transfected with N1 EGFP and Wt, S655A, S655E APP-GFP at the second day of differentiation. Transfected cells were scored for F-actin stress fibers, cortical or intermediate phenotypes (not cortical but exhibiting stress fibers depolymerization and actin polymerization into F-actin spots). Data is presented in percentage of F-actin distribution in cells **A.** Epifluorescence microphotographs; **B**. F-actin analyses in all transfected cells. **C.** F-actin analyses only in transfect cells showing an elongated differentiated phenotype. Bar, 10 µm.

From the F-actin analysis, we distinguished three different phenotypes accordingly to the organization of the actin filaments, as previously reported[118]: a fibrous phenotype with cells that shown mainly long actin stress fibers that cross all cell ('Fibers', Figure 16); a cortical phenotype, where it is visible desorganization of actin fibers within the cell body and clumping of F-actin at the periphery, beneath the plasma membrane ('Cortical', Figure 16); and an intermediate phenotype, showing less stress fibers and some spots of F-actin polymerization within the cell body. Very interestingly, the three phenotypes showed different patterns of expression according with each transfectant. Thus, for Wt and S655A APP-GFP transfected cells,

stabilization of stress fibers was more affected, as these cells shown higher number of intermediate and cortical cells (Figure 16-B). S655E APP-GFP also affected stability of actin fibers but to a lower extent, presenting a lower decrease in the percentage of cells with stress fibers. The type of F-actin distribution was further analysed in the population of transfected cells that presented an elongated differentiated morphology (Figure 16-C). Results obtained suggest that initial depolimerization and further stabilization of stress fibers seem to be both important in neurite outgrowth, since these are the two major phenotypes found in elongated differentiated cells expressing S655E, the APP-GFP protein previously observed to induce increased neuritic length (Figure 15-B).

Altogether, these data led us to conclude that APP-GFP transfection for 48h, upon 2 days of RA-incubation, induced more detrimental than positive effects on differentiation, especially in terms of generation of protruding processes. This could be related to the overall destabilization of the microtubular and actin cytoskeletons. Nonetheless, mimicking S655 phosphorylation (S655E mutant) had a positive effect in neuritic length, most probably related to its higher sAPP/APP ratio and its ability to lead to more moderated F-actin fibers destabilization.

Several factors could contribute to these results. As previously observed in the optimization of differentiation assays, cells transfection appears to be detrimental to cells incubated with RA. Further, while APP positive effects on differentiation may be mediated by full-length APP and the sAPP fragment, negative effects could be mediated by the AICD fragment, who has been related to cytoskeleton dynamics[118]. Therefore we decided to further evaluate if APP itself could induce morphologic alterations relevant for the differentiation process, in the absence of any morphogen such as RA, and to better understand the role of APP phosphorylation at S655 in these alterations. In addition, by using pharmacologic tools we assessed the role played by the AICD fragment in these alterations.

4.4. Phosphorylation-dependent APP- and AICD-mediated morphological changes

In order to study the ability of APP to induce differentiation-related morphologic alterations, and to even trigger cell differentiation in the absence of a morphogen such as RA, non-differentiated SH-SY5Y cells were transfected with the N1-EGFP vector and with the Wt APP-GFP cDNA for 24 and 48h. The S655A and S655E APP-GFP cDNAs were transfected side-by-side with the Wt to address the influence of S655 phosphorylation in these changes. To specifically analyse the role of AICD in these mechanisms, cells were incubated with 1 µM DAPT, a gamma-secretase inhibitor that blocks AICD production, in the last 24h of the 48h time point.

Several morphological and morphometric analysis were performed to characterize each condition. The effects of APP-GFP transfection on cell density and cell death were first evaluated.

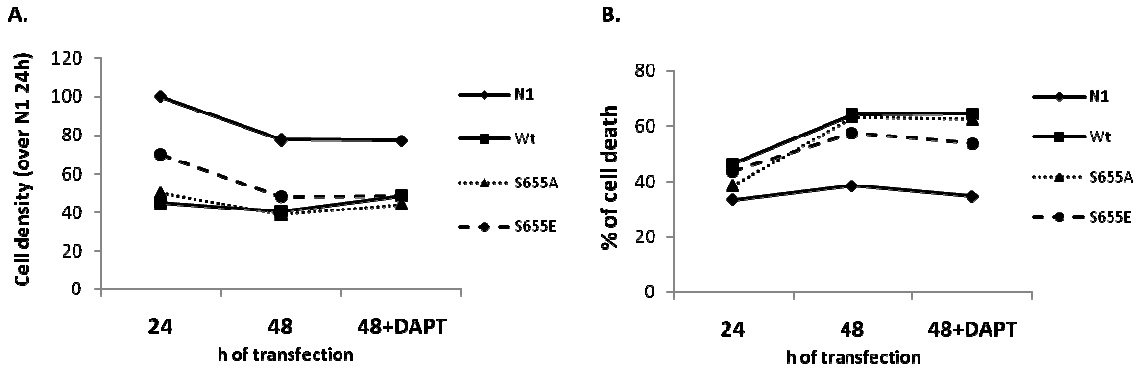

Figure 17. Quantification of cell density and cell death upon 24 and 48h of N1, Wt, S655A and S655E transfection and 1 µM DAPT incubation. A. Number of transfected living cells per mm^2, expressed as percentage over the N1 values at 24h (taken as 100%) **B.** Percentage of transfected dead cells in the transfected cells population. On average 100-200 transfected cells were score in epifluorescence microphotographs, for each condition.

All APP-GFP proteins decreased cell density by ~30-50% (24h) in comparison with N1 values, and cell density generally decreased with time for all transfectants, not being reverted by DAPT. In comparison, the percentage of transfected dead cells was only ~10% higher for APP-GFP expressing cells than for N1 cells at 24h. Cell death did not change with time for vector N1, but increased by about 20% for all APP-GFP expressing cells. In addition, DAPT did not affect cell death for N1 or APP-GFP transfected cells. Since the percentage of cell death is not as high as the decrease in cell density, one can infer that APP also decreases cell proliferation, and that AICD is not the main fragment responsible for those effects. Following, the presence of cuboid, elongated and plastic cells was scored in epifluorescence microphotographs (Figure 18).

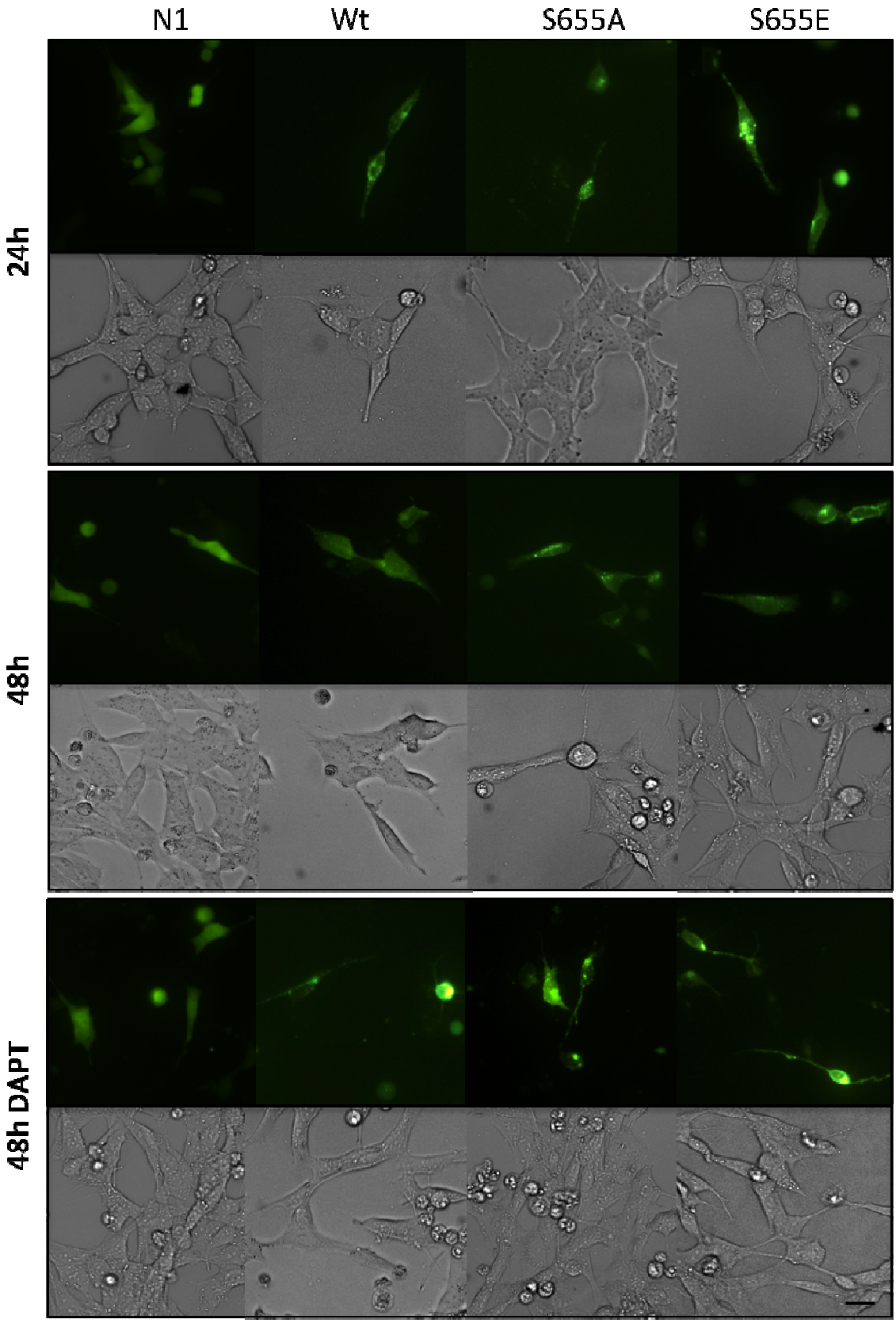

Figure 18. Epifluorescence and phase contrast microphotographs of non-differentiated SH-SY5Y cells transfected with N1 and APP-GFP cDNAs for 24 and 48h, in the presence or absence of DAPT.

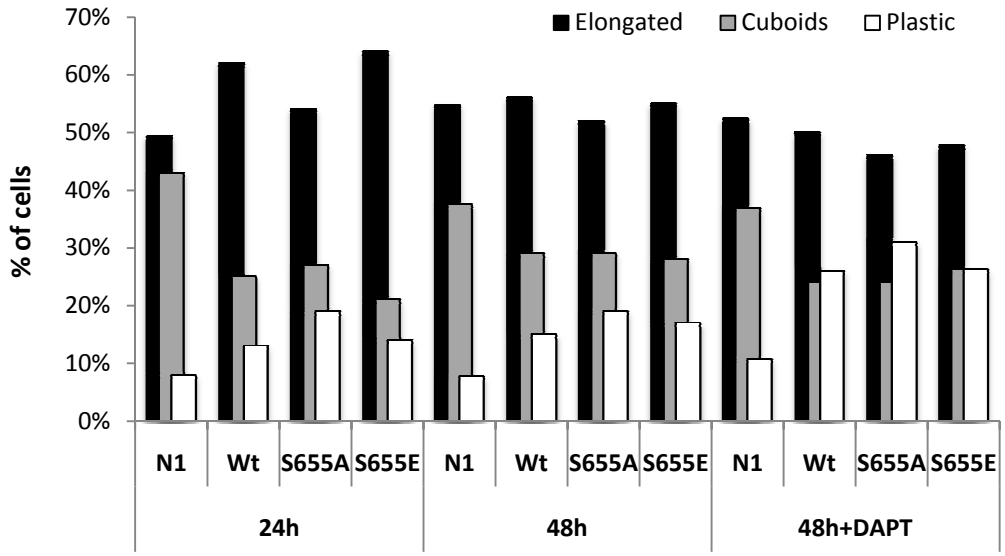

Figure 19. Evaluation of SH-SY5Y cells morphology upon 24 and 48h transfection with N1 vector, Wt, S655A and S655E APP-GFP cDNAs, in the presence or absence of DAPT in the 48h time point. N1: vector EGFP-N1 transfected cells; Wt, S655A, S655E: APP-GFP tranfected cells.

Regarding cell morphology (Figure 18 and Figure 19), at 24h all APP-GFP expressing cells had increased elongated and plastic morphologies over cuboids, comparatively to N1 cells. S655 phosphorylation appears to favour elongation of the cell body, while S655A expression also led to elongated cells but with more rounded cell bodies (Figure 18). With time in culture N1 population tended to elongate to the expense of cuboid morphology. In contrast, APP-GFP expressing cells tended to decrease elongated morphology to more cuboid shapes. Interestingly, DAPT reverted part of this effect, but turned elongated cells more plastic, especially for the S655 mutants (see Figure 18). This also occurred for some N1 elongated cells exposed to DAPT, but S655A and S655E cells were generally more plastic and less symmetric than Wt or N1 expressing cells.

Since morphologic alterations depend on actin cytoskeleton alterations, the presence of lamellipodia was scored as a parameter of actin dynamics (Figure 20).

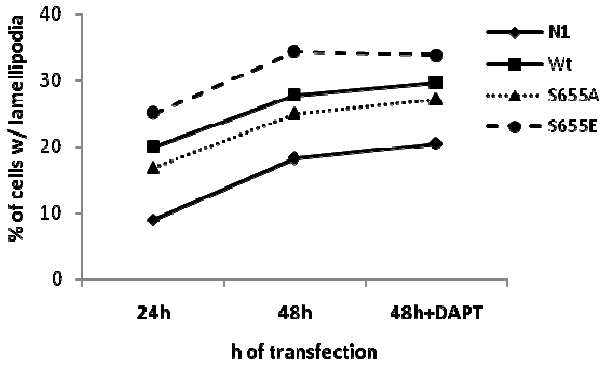

Figure 20. Quantification of the number of cells with lamellipodia features upon 24 and 48h transfection with N1 vector, Wt, and S655A and S655E APP-GFP cDNAs, in the presence or absence of DAPT in the last 24h of the 48h time point. N1: vector EGFP-N1 transfected cells; Wt, S655A, S655E: APP-GFP tranfected cells.

Results obtained show that the percentage of cells with lamellipodia increased with time of transfection. However, expression of all APP-GFP proteins highly increased lamellipodia already at 24h (about 2-fold increase over N1 values), with S655E showing the highest effect. Incubation with DAPT did not affect the increase in the number of lamellipodia (Figure 20).

From the epifluorescence microphotographs it could be denoted that APP-GFP expression was able to increase neuritogenesis in some cells, and actually trigger cellular differentiation in the absence of a morphogene such as RA. Neuritogenesis and neuritic elongation were therefore assayed using several parameters. First, the percentage of cells with pre-neurites, that is neurites in development, > 20 µm, were scored, and their mean length measured (Figure 21-A and B)

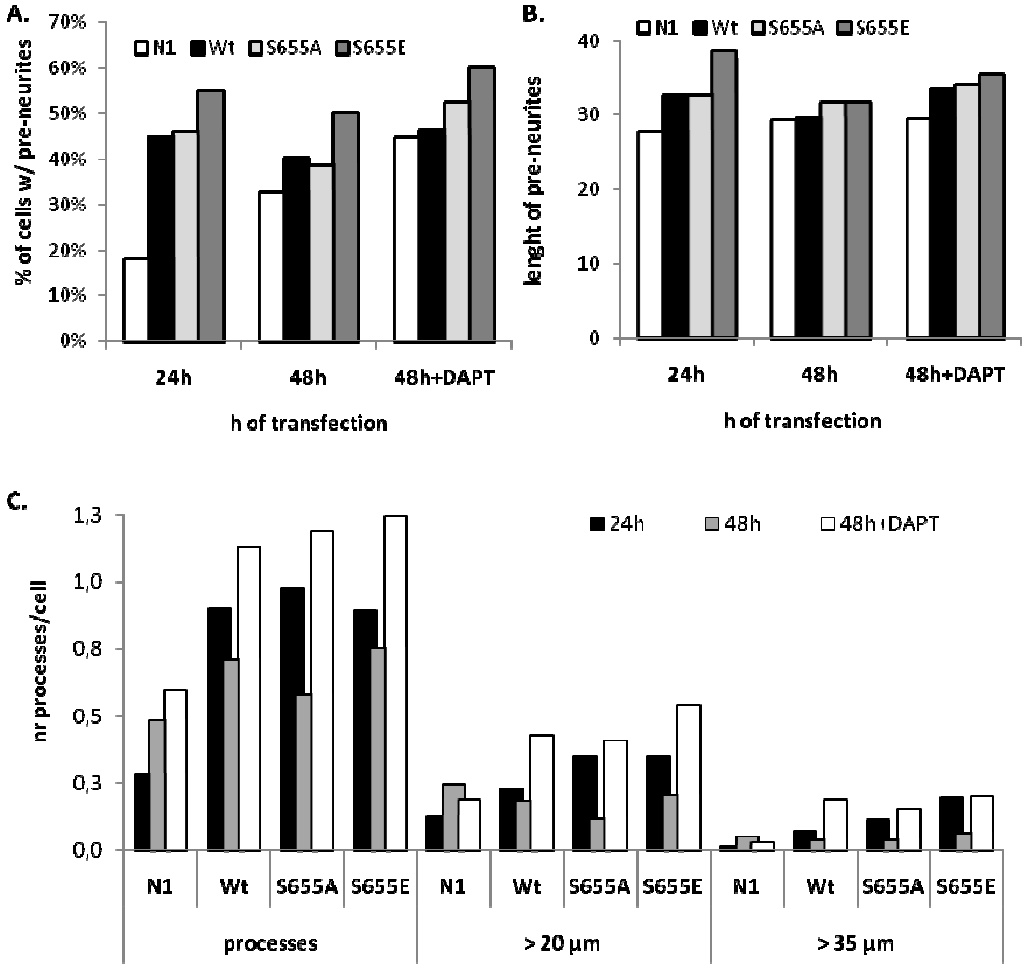

Figure 21. Morphometric analysis of SH-SY5Y cells transfected with the APP-GFP cDNAs for 24 and 48h, in the presence or absence of DAPT. N1: vector EGFP-N1 transfected cells; Wt, S655A, S655E: APP-GFP transfected cells. **A.** Percentage of cells with pre-neurites (processes > 20 µm). The percentage of transfected cells bearing at least one process higher than 20 µm was calculated. **B.** Mean pre-neurites length. The mean length of processes greater than 20 µm was calculated. **C.** Number of processes per cell. All processes arising from a cell ('processes'), processes longer that 20 µm ('> 20 µm') and neurites (processes longer than 35 µm, '>35 µm') were considered.

Concerning the ability of APP cDNAs to trigger SH-SY5Y cell neuritogenesis (Figure 21-C), APP-GFP expression greatly increased the number of cells bearing pre-neurites at 24h, in comparison with the N1 vector alone (Figure 21-A). Further, APP-GFP also increased neuritic length at 24h (Figure 21-B), with S655E being the most efficient in this process and also presenting higher percentage of cells with neurites. Interestingly, while with time in culture (48h) the percentage of N1 expressing cells with pre-neurites increased, this percentage decreased in APP-GFP transfected cells. This effect was completely reverted by DAPT, what was even able to further increase the number of N1 cells with pre-neurites. Regarding neuritic length, a similar effect was observed. After 48 hours of transfection, APP-GFP induced neuritic retraction, apparently in an AICD-dependent manner, since it was greatly reverted by DAPT (Figure 21-B).

The number of all processes and neurites (pre-neurites, and neurites > 35 µm) was also scored, and expressed as number per cell (Figure 21-C). APP-GFP remarkably increased the number of processes and neurites at 24h, with S655A being more efficient in the genesis of protruding processes, while S655E appears more efficient in elongating the processes (high number of pre-neurites and highest number of neurites). Again, while for N1 these numbers increased at 48h, for APP-GFP expressing cells the number of processes decreased with time. AICD appears to be involved in this inhibition of neuritogenesis, since this effect is totally reverted by DAPT incubation, with the number of all processes even surpassing the control ones.

In addition, the number of secondary neurites was also quantified (

Figure 22) and, although very few and almost only present in APP-GFP transfected cells, results showed that APP-GFP was able to induce neuritic ramification, with the S655A phosphomutant being the most efficient. An increase in secondary processes could be further obtained with DAPT incubation (~1.4 fold increase), suggesting that AICD also inhibits the generation of secondary processes.

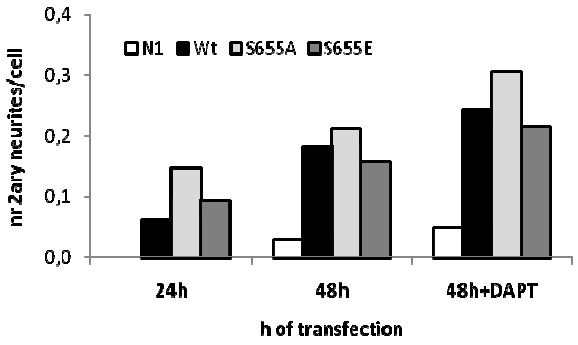

Figure 22. Number of secondary neurites per cell in SH-SY5Y cells transfected with the APP-GFP cDNAs for 24 and 48h, in the presence or absence of DAPT in the last 24h of the 48h time period.

The role potentially played by the APP and its proteolytic products sAPP and AICD was further evaluated in this experiment. Cells treated as above were collected and cells lysates subjected to SDS-PAGE. The rates of APP-GFP transfection and production of CTFs and AICD-GFP were analysed by Western blot, together with the protein expression of putative AICD target genes, and cytoskeleton proteins. In addition, two other samples were ran side-by-side to evaluate the effects of sAPP in these proteins expression. These corresponded to cells transfected with vector N1-EGFP alone but incubated in the last 24h of transfection with sAPP-enriched medium, derived from an extra set of Wt APP-GFP transfected cells.

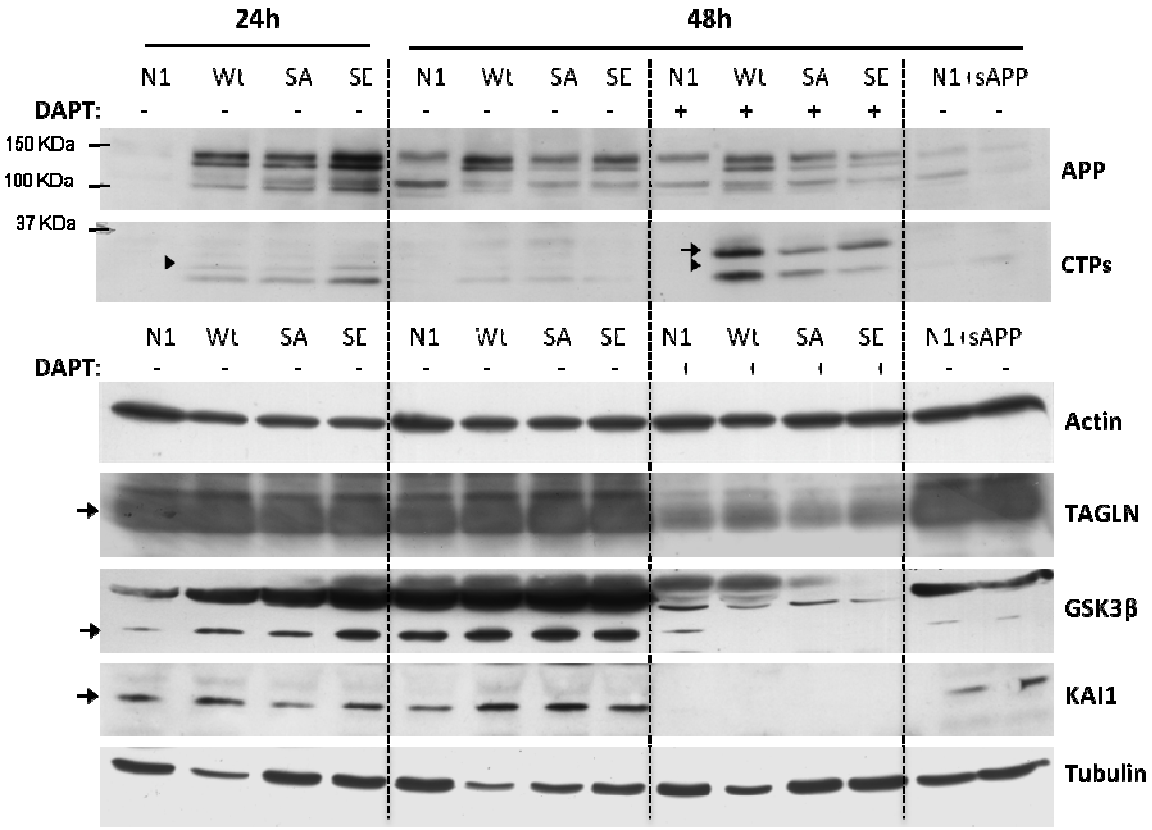

Figure 23. Immunoblot analysis of non-differentiated SH-SY5Y cells transfected with the Wt, S655A and S655E APP-GFP cDNAs and treated or not with 1µM DAPT. 24h, 48h, hours of APP-GFP transfection. Cell lysates were probed with antibodies against APP C-terminus, to evaluate APP-GFP and CTFs-GFP levels, and against actin, transgelin (TAGLN), GSK-3β, KAI-1, and against β-tubulin.

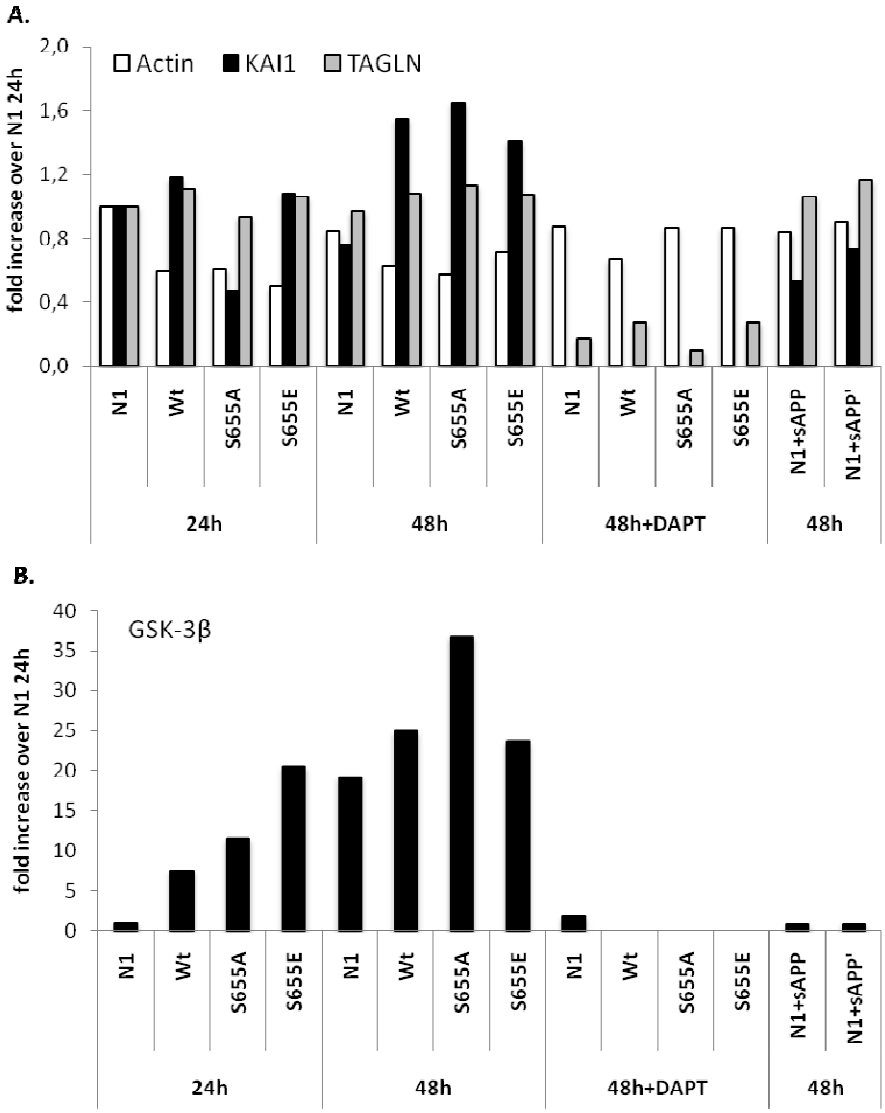

Figure 24. Quantification of the effects of Wt, S655A and S655E APP-GFP transfection on actin, KAI-1 and trangelin (A.) and GSK-3β (B.) protein expression levels. Data are presented as fold-increases over the values of N1 sample at 24h (taken as 1.0), upon correction to the relative transfection of the APP-GFP proteins at 24h.

Figure 23 (upper panel) shows that upon APP-GFP transfection (bands a and b in the anti-APP C-terminus immunoblot), CTF-GFP and AICD-GFP fragments are produced, as expected ('CTPs', bands below 37 KDa, only present in APP-GFP expressing cells). These fragments decreased with time of transfection (as do full-length APP-GFP proteins), and while CTF-GFP bands increased with DAPT incubation (arrow), AICD-GFP disappeared (arrowhead).

In terms of cytoskeleton proteins, Figure 24-A shows that in general actin levels decreased with APP-GFP expression, an effect not mediated by sAPP as actin levels are not altered by sAPP addition, but potentially by AICD, as DAPT incubation partially reverts the decrease. Further, β-tubulin levels were also affected by APP-GFP, as Wt APP-GFP expression decreased tubulin

markedly. Of note, protein levels were corrected for the relative initial transfection levels of the APP-GFP proteins (24h).

Concerning the protein expression of potential AICD-target genes, GSK-3β, KAI-1 and TAGLN appear to be sensitive to AICD production in SH-SY5Y cells. These proteins exhibited an increase in their protein levels in cells producing AICD-GFP (24h, APP-GFP versus N1 expressing cells), reached a plateau with time of transfection (48h), and decreased (or even disappeared) with DAPT incubation (48h+DAPT). GSK-3β is the most sensitive AICD target gene of the ones evaluated, showing higher increases in APP-GFP transfected cells, and TAGLN is the less sensitive that showed lower increases over N1. Additionally, KAI 1 and GSK-3β are sensitive to the S655 phosphorylation state of APP. At 24h the S655A mutant was not able to induce KAI-1, and GSK-3β was highly induced by S655E. However, at 48h the levels of these proteins were higher for S655A. Very interestingly, most of these potentially AICD-induced genes protein products reached a plateau at 48h, while APP-GFP and AICD levels decrease with time. Furthermore, sAPP addition did not increase any of these proteins, and even decreased GSK-3β levels at 48h, what will be addressed in future experiments.

5. Discussion

In the present work we addressed the ability of APP (and its proteolytic fragments sAPP and AICD) to mediate neuronal differentiation, namely morphogenic and neuritogenic alterations, and the role played by APP phosphorylation at S655 in those processes.

We have first concluded that the Turbofect lipid reagent method is a more suitable method for APP cDNAs transfection of SH-SY5Y cells than the Cap-glycerol method. In fact, other authors were able to transfect SH-SY5Y cells using the Lipofectamine reagent, a lipid-mediated method very similar to Turbofect [119], but more expensive. Nonetheless, Ruiz-León and Pascual (2003) efficiently transfected SH-SY5Y using CaP-Glycerol, but used a different transfectant cDNA and a more moderate differentiation condition (1 µM RA)[104].

Furthermore, we also gather evidence that the percentage of differentiated cells is sensitive to the differentiation conditions used and to cell transfection, upon four days of differentiation. The mean neurite length was not affected by the differentiation conditions tested, what may be due to the early time point of differentiation in cause. Based on the percentage of differentiated cells, we established that the best combination of FBS/RA for differentiation of both control and transfected SH-SY5Y cells, requires a percentage of 10% FBS, acting as a protective agent against the prejudice of the combination of higher RA concentrations and APP transfection. As the 10 µM RA/10% FBS combination rendered the most homogeneous results in terms of percentages of cell differentiation, it was our elected combination for subsequent assays. In fact, several authors report the use of 10 µM RA/10% FBS to accomplish SH-SY5Y neuronal-like differentiation [105, 119-121].

Following, we evaluated the effects of APP overexpression in SH-SY5Y cells differentiation, and the role played by APP phosphorylation at S655 in this process. For that, SH-SY5Y cells were incubated in 10 µM RA/10% FBS media for fours days, being transfected at the second day of differentiation with the vector EGFP-N1 or the Wt, S655A and S655E APP-GFP cDNAs. Table 6 resumes the APP-GFP-induced alterations that we have observed, relative to control conditions (cells transfected with the EGFP-N1 vector).

Table 6. Summary of the effects of overexpressing APP with APP-GFP cDNAs, and of mimicking APP phosphorylation in an early SH-SY5Y differentiation period (4 days). APP-GFP cDNAs effects were compared to the N1-EGFP ones.

		APP-GFP		
		Wt	S655A	S655E
sAPP/APP		↓	↓	≈
Differentiation Markers	Acetyl Tub	↓	↓↓	↓↓
	MAP-2	↓	↓	↓
	β-Tubulin	↓	↓	↓
Cell Viability	Living cells	↓	↓	↓
	Dead cells	≈	↑	↑
Morphometrics	% Cells w/ processes	↓	↓	≈
	% Cells w/ pre-neurites	↓	↓	≈
	% Cells Dif.	↓	↓	↑
	Neurite Length	≈	↑	↑
F-actin analysis	Fibers	↓↓	↓↓	↓
	Intermed.	↑↑	≈	≈
	Cortical	↑	↑↑	↑

Symbols used: arrows indicate increases or decreases; ≈ indicates maintenance.

APP-GFPs transfection significantly increased the levels of full-length APP. However, while for the phosphomimicking S655E mutant it resulted in similar sAPP/APP ratios as N1-EGFP transfected cells, this was slightly lower for the Wt APP-GFP protein and decreased to half for S655A APP-GFP. These suggest that the α-secretase enzyme is not highly activated at this time point of differentiation, and when overexpressing its substrate APP this pathway was somehow saturated; the fact that S655E seemed a better substrate for this pathway is not surprising, since this was already observed to occur in COS-7 cells [89-90].

In addition, APP-GFP overexpression decreased all the microtubule-associated differentiation markers analysed (degree of α-tubulin acetylation; levels of the MAP-2 isoforms), with S655E mutant presenting the highest decreases in tubulin acetylation and MAP-2a/b levels. Interestingly, this is the same mutant that was able to raise the percentage of differentiated cells and to markedly increase the neurite length. In contrast, Wt and S655A mainly decreased the morphometric parameters. Further, all APP-GFP proteins led to different F-actin rearrangements. While Wt and S655A resulted in higher destabilization of the basal F-actin fibres, S655E APP-GFP transfected cells decreased less the number of cells with F-actin stress fibers and led to more moderated increases in the intermediate and cortical phenotypes.

In synthesis, Wt APP overexpression resulted in lower degree of cell differentiation, what maybe related to its lower sAPP/APP ratio and higher degree of destabilization of the microtubules and actin cytoskeletons. Mimicking S655 phosphorylation through the use of the S655E mutant lessens this detrimental effect and is even able to surpass it, enhancing the number of differentiated cells and neurite length, while the dephosphomimicking S655A mutant did not enhance the number of differentiated transfected cells.

The positive effects of S655E in neurite length are most probably related to its higher sAPP/APP ratio, since sAPP is described to be neuritogenic, and S655E transfection was able to enhance differentiation in non-transfected neighbour cells. Furthermore, they may also be related to its ability to lead to more moderated F-actin fibers destabilization. Apparently, in this initial time period of differentiation general microtubule instability and moderated F-actin instability direct neurite elongation modulated by APP phosphorylation. However, apparently in disagreement with the established models of neurite differentiation describing the requirement of microtubule stability and actin instability for neuritogenesis to occur, the present results are not totally contradictory to the models of cytoskeleton dynamics in neuronal differentiation. In fact, taking a closer look to the results, we can correlate the decreased levels of acetylated tubulin to necessary local microtubule instability at neuronal tips in order to enable neurite elongation. Furthermore, S655E transfection resulted in similar levels of the low molecular weight MAP-2c/d isoforms to N1-EGFP transfected cells, and the MAP-2c isoform was associated to the linkage of microtubules with actin cytoskeleton. Regarding F-actin, a certain degree of actin instability is necessary for the protruding of processes and for exiting a quiescence state, but our results point that a certain degree of stability is necessary during or at the end of neurites elongation.

By its turn, S655A APP-GFP transfected cells were associated with a statistic significant decrease in the sAPP/APP ratio, concordant with the already reported delayed sAPPα secretion

[89-90]. The decreased percentage of S655A differentiated cells may be also related to its marked increase in a cortical F-actin phenotype, indicative of increased actin fibers disorganization within the cell body and clumping of actin fibers at the periphery, as seen by Müller et al (2003), following AICD and FE65 cell overexpression [118]. As typical neurites are very dynamic, elongating in a saltatory manner, with periods of abrupt advances alternating with periods of retraction and pausing[115], the S655A enhanced F-actin instability may alters these balance and led to a higher level of retraction and shorter periods of quiescence. Further experiments on the mechanisms underlying APP-GFP-induced actin dynamics will be conducted, in order to better understand the results.

The observed inhibitory net effects of Wt APP-GFP in differentiation could be morphogen-dependent, time-dependent, and AICD-dependent. Indeed, the APP fragment AICD may mediate part of the inhibitory effects, since it has been related with actin dynamics and cortical F-actin phenotype[118]. Further, in this experiment, APP-GFP transfection was let to occur for 48h, a period long enough for AICD-induced gene transactivation to occur and render visible effects, and AICD was recently correlated with low degree of PC12 differentiation and stem cells neurogenesis [107-108].

Thus, we have further analyzed in detail which morphologic alterations, related to neuronal-like differentiation, could be induced by APP in a time-dependent manner, and the influence of APP S655 phosphorylation and AICD generation in these effects. For these, non-differentiated SH-SY5Y cells were transfected with Wt, S655A, and S655E APP-GFP cDNAs for 24 and 48h, the later in the presence or not of DAPT, a drug that inhibits CTF cleavage to AICD.

First, APP-GFP proteins were again observed to decrease cell number, as in the RA-induced differentiation assays, probably by its observed increase in cell death, and potentially by blocking proliferation[122]; we also observed that the AICD appears not to be the main fragment involved, contrary to what was reported for RA-induced P19 differentiated cells [123]. Nonetheless, APP CTFs may also induce cell death [124], and thus DAPT incubation renders no net effect since it inhibits one fragment (AICD) but favors the other (CTF).

Following, several morphologic alterations and the levels of putative AICD-dependent genes were monitored in these conditions, and

Table 7 summarizes the results obtained. For a easier interpretation, data obtained from APP-GFP transfection at 24h was compared to EGFP-N1 data also at 24h; 48h data was compared to 24h data (eg increase or not over the same conditions at 24h); 48h + DAPT data was compared to 48h data (eg decrease over the same basal DAPT minus conditions at 48h).

Table 7. Summary of the S655 phosphorylation-dependent effects of APP and AICD in cells morphology and in the expression of relevant proteins.

		APP-GFPs 24h (over N1 data)			APP-GFPs 48h (over 24h data)			APP-GFPs 48h + DAPT (over 48h data)		
		Wt	S655A	S655E	Wt	S655A	S655E	Wt	S655A	S655E
Cell Viability	Living cells	↓↓	↓↓	↓↓	≈	≈	≈	≈	≈	≈
	Dead cells	≈	↑	↑	↑	↑	↑	≈	≈	≈
Morphology	Plastic	↑	↑	↑	≈	≈	↑	↑	↑	↑
	Elongated	↑	↑	↑	↓	↓	↓	≈*	≈*	≈*
	Cuboids	↓↓	↓↓	↓↓	↑	↑	↑	↓	↓	↓
Morphometry	% Cells w/ pre-neurites	↑	↑	↑↑	↓	↓	↓	↑	↑	↑
	Pre-neurites length	↑	↑	↑↑	↓	↓	↓↓	↑	↑	↑
	Nr Processes	↑↑	↑↑	↑↑	↓	↓↓	↓	↑↑	↑↑	↑↑
	Nr 2ary neurites	↑	↑	↑	↑↑	↑	↑	↑	↑	↑
Actin Dynamics	% Cells w/ lamellipodia	↑	↑	↑	↑	↑	↑	≈	≈	≈
	Actin levels	↓	↓	↓	≈	≈	≈	≈	↑	↑
AICD-target genes (protein levels)	KAI-1	↑	≈	↑	↑	↑	↑	Ø	Ø	Ø
	TAGLN	↑	↓	≈	↑	↑	↑	↓↓	↓↓	↓↓
	GSK-3β	↑	↑	↑↑	↑	↑↑	↑	Ø	Ø	Ø

* cells become more elongated, but as these cells are also more plastic, they were scored as 'plastic'. Symbols used: arrows indicate increases or decreases; ≈ indicates maintenance; Ø indicates complete inhibition (absence).

APP-GFP 24h transfection was observed to increase cell elongation and plasticity. Very importantly, APP phosphorylation at S655 favours even more elongated morphologies. However, 48h of APP-GFP transfection led to less elongated morphologies and generally appeared to lead to some undifferentiation. This could be reverted by DAPT incubation that was able to further increase cell elongation and plasticity in comparison to the 24h time point. Such patterns suggest

that AICD inhibits to some extent cell plasticity and elongation, favouring the regular cuboid phenotype.

Moreover, initial APP-GFP transfection was able to positively influence all the morphometric parameters, mainly the number of processes per cell, but also the percentage of cells with pre-neurites and neurites, pre-neuritic lenght, and the number of pre-neurites and neurites per cell. Indeed, at 24h, APP-GFP transfection itself was able to induce differentiation (cells with neurites). Very interestingly, 48h of APP-GFP transfection had a negative influence on neuritogenesis, leading to a decrease in such parameters (as in the first experiment, with RA incubation). Remarkably, if cells were treated with DAPT in the last 24h, this drug was able to totally reverse these APP transfection time-dependent decreases, connecting the AICD with APP negative modulation of neurite formation, as already suggested by other authors [107-108].

Regarding actin dynamics, APP-GFP transfections both resulted in decreased actin levels and increased percentages of lamellipodia. So it appears that APP cDNAs transfection is sufficient to alter actin dynamics in order to promote lamellipodia advance. Again, it is important to note that the S655E rendered higher percentage of cells with lamellipodia, which can be associated with its ability to less perturb F-actin stability and potentially to its elongated phenotypes. Although AICD is being related with destabilization of actin fibers, this APP-GFP-induced lamellipodia effect appears to be AICD-independent (since DAPT did not inhibit this effect).

In synthesis, APP-GFP overexpression initially induces morphologic alterations leading to higher cellular differentiation, but with time of transfection these effects are reverted, cells tend to be less differentiated in morphology and neurites tend to retract. This appears to involve AICD-dependent mechanisms since DAPT incubation partially retained APP-GFP-induced cell body elongation, and completely reverted neuritogenesis inhibition. Of note, S655 phosphorylation enhances APP-GFP-induced differentiation but was not able to block time-dependent inhibitions.

Hence, we went on to analyze the levels of putative AICD-dependent protein products, to see if any of these proteins profile could correspond to the pattern of alterations monitored. When transfecting SH-SY5Y cells with APP-GFP, the levels of AICD increased, and the protein expression of the AICD-target genes monitored altered in a fashion consistent with increased AICD signaling. In addition, the levels of GSK-3β, TAGLN and KAI-1 further increased upon 48h of transfection and decreased after incubation with the γ-secretase inhibitor DAPT, what correlates well with the 48h inhibition and with the recovery of the morphometric parameters upon AICD inhibition. Moreover, DAPT incubation led to even lower protein levels that the ones presented in the 24h condition, what may explain the exacerbated processes outgrowth presented by these

cells. Mechanistically, the decrease in GSK-3β is most possible accompanied by a concomitant decrease in its activity, which may lead to reduced MAPs phosphorylation, microtubule stability, and thus alter neuritic morphology. Transgelin levels were also implicated in the organization of actin fibers, and may therefore influence neuritogenesis[118]. In contrast, KAI-1 is a metastasic inhibitor, anti-proliferative, and so it should potentially have positive influences in differentiation, by inducing a block in proliferation. However, as the γ-secretase has other substrates, further studies are required to establish which AICD-induced mechanism(s) and gene target(s) are responsible for the neurite outgrowth retraction.

6. Conclusion

The experiments performed in this work indicate that a more sustained (48h) overexpression of APP cDNAs can be detrimental to neuronal-like differentiation, inducing an overall inhibition of differentiation parameters. We gathered evidence that the APP proteolytic fragment AICD may mediate such retraction on SH-SY5Y neuritogenic output. In contrast, more immediate (24h) increases in the levels of APP may be beneficial for neurite outgrowth and APP alone is, indeed, able to trigger neuronal-like morphological alteration in SH-SY5Y cells. Moreover, such positive effects seem to be dependent on S655 APP phosphorylation. In fact the S655E mutant was in general able to more markedly induce the differentiation process, most likely due to its higher sAPP/APP ratio and less moderate F-actin instability. Further, as 48h of S655E expression was able to increase differentiation over N1 control only in RA-differentiated cells, one can speculate that RA, a natural morphogen, is able to attenuate in some extent the APP-GFP detrimental effects. The nature of the AICD-induced inhibitory signalling mechanisms will be evaluated in future experiments.

7. References

1. Gilbert SF. Developmental Biology. Sinauer Associates Inc.; 2006.

2. Alberts B, Bray D, Lewis J, Raff M, Roberts K, Watson JD. Molecular Biology of the Cell. New York and London: Garland Science; 2002.

3. Fukata Y, Kimura T, Kaibuchi K. Axon specification in hippocampal neurons. Neuroscience Research 2002; 43:305-315.

4. Dotti C, Sullivan C, Banker G. The establishment of polarity by hippocampal neurons in culture. J. Neurosci. 1988; 8:1454-1468.

5. Standring S. Gray's Anatomy: The Anatomical Basis of Clinical Practice. Spain: Elsevier Churchill Livingstone; 2005.

6. Siegel G, Agranoff B, Albers R. Basic Neurochemistry: Molecular, Cellular and Medical Aspects. Philadelphia: Lippincott-Raven; 1999.

7. Mattson MP. Establishment and plasticity of neuronal polarity. Journal of Neuroscience Research 1999; 57:577-589.

8. Polleux F, Snider W. Initiating and Growing an axon. Cold Spring Harbor Perspectives in Biology 2010; 2:1-15.

9. Barnes AP, Polleux F. Establishment of Axon-Dendrite Polarity in Developing Neurons. Annual Review of Neuroscience 2009; 32:347-381.

10. Bradke F, Dotti CG. Changes in membrane trafficking and actin dynamics during axon formation in cultured hippocampal neurons. Microscopy Research and Technique 2000; 48:3-11.

11. Craig AM, Banker G. Neuronal Polarity. Annual Review of Neuroscience 1994; 17:267-310.

12. Witte H, Bradke F. The role of the cytoskeleton during neuronal polarization. Current Opinion in Neurobiology 2008; 18:479-487.

13. Tahirovic S, Bradke F. Neuronal Polarity. Cold Spring Harbor Perspectives in Biology 2009; 1.

14. Dehmelt L, Halpain S. The MAP2/Tau family of microtubule-associated proteins. Genome Biology 2004; 6:204.

15. Hall A, Lalli G. Rho and Ras GTPases in Axon Growth, Guidance, and Branching. Cold Spring Harbor Perspectives in Biology 2010; 2.

16. Yuen EC, Li Y, Mischel RE, Howe CL, Holtzman DM, Mobley WC. Neurotrophins and the Neurotrophic Factor Hypothesis. Neural Notes 1996; 1:3-7.

17. Kaplan DR, Miller FD. Neurotrophin signal transduction in the nervous system. Current Opinion in Neurobiology 2000; 10:381-391.

18. Whitford KL, Dijkhuizen P, Polleux F, Ghosh A. MOLECULAR CONTROL OF CORTICAL DENDRITE DEVELOPMENT. Annual Review of Neuroscience 2002; 25:127-149.

19. Horton AC, Ehlers MD. Neuronal Polarity and Trafficking. Neuron 2003; 40:277-295.

20. Peter M, Ursula CD. Regulation of retinoic acid signaling in the embryonic nervous system: a master differentiation factor. Cytokine & growth factor reviews 2000; 11:233-249.

21. Ross SA, McCaffery PJ, Drager UC, De Luca LM. Retinoids in Embryonal Development. Physiological Reviews 2000; 80:1021-1054.

22. Guo W, Jiang H, Gray V, Dedhar S, Rao Y. Role of the integrin-linked kinase (ILK) in determining neuronal polarity. Developmental Biology 2007; 306:457-468.

23. Yoshimura T, Arimura N, Kaibuchi K. Signaling Networks in Neuronal Polarization. J. Neurosci. 2006; 26:10626-10630.

24. Bradke F, Dotti CG. The Role of Local Actin Instability in Axon Formation. Science 1999; 283:1931-1934.

25. Bito H, Furuyashiki T, Ishihara H, Shibasaki Y, Ohashi K, Mizuno K, Maekawa M, Ishizaki T, Narumiya S. A Critical Role for a Rho-Associated Kinase, p160ROCK, in Determining Axon Outgrowth in Mammalian CNS Neurons. Neuron 2000; 26:431-441.

26. Schwamborn JC, Puschel AW. The sequential activity of the GTPases Rap1B and Cdc42 determines neuronal polarity. Nat Neurosci 2004; 7:923-929.

27. Koh CG. Rho GTPases and Their Regulators in Neuronal Functions and Development. Neurosignals 2006; 15:228-237.

28. Luo L, Hensch TK, Ackerman L, Barbel S, Jan LY, Nung Jan Y. Differential effects of the Rac GTPase on Purkinje cell axons and dendritic trunks and spines. Nature 1996; 379:837-840.

29. Hakeda-Suzuki S, Ng J, Tzu J, Dietzl G, Sun Y, Harms M, Nardine T, Luo L, Dickson BJ. Rac function and regulation during Drosophila development. Nature 2002; 416:438-442.

30. Ng J, Nardine T, Harms M, Tzu J, Goldstein A, Sun Y, Dietzl G, Dickson BJ, Luo L. Rac GTPases control axon growth, guidance and branching. Nature 2002; 416:442-447.

31. Ng J, Luo L. Rho GTPases Regulate Axon Growth through Convergent and Divergent Signaling Pathways. Neuron 2004; 44:779-793.

32. Chen L, Liao G, Waclaw RR, Burns KA, Linquist D, Campbell K, Zheng Y, Kuan C-Y. Rac1 Controls the Formation of Midline Commissures and the Competency of Tangential Migration in Ventral Telencephalic Neurons. J. Neurosci. 2007; 27:3884-3893.

33. Kassai H, Terashima T, Fukaya M, Nakao K, Sakahara M, Watanabe M, Aiba A. Rac1 in cortical projection neurons is selectively required for midline crossing of commissural axonal formation. European Journal of Neuroscience 2008; 28:257-267.

34. Gualdoni S, Albertinazzi C, Corbetta S, Valtorta F, de curtis I. Normal levels of Rac1 are important for dendritic but not axonal development in hippocampal neurons. Biology of the Cell 2007; 099:455-464.

35. Kimura K, Ito M, Amano M, Chihara K, Fukata Y, Nakafuku M, Yamamori B, Feng J, Nakano T, Okawa K, Iwamatsu A, Kaibuchi K. Regulation of Myosin Phosphatase by Rho and Rho-Associated Kinase (Rho-Kinase). Science 1996; 273:245-248.

36. Banzai Y, Miki H, Yamaguchi H, Takenawa T. Essential Role of Neural Wiskott-Aldrich Syndrome Protein in Neurite Extension in PC12 Cells and Rat Hippocampal Primary Culture Cells. Journal of Biological Chemistry 2000; 275:11987-11992.

37. Kunda P, Paglini G, Quiroga S, Kosik K, Caceres A. Evidence for the Involvement of Tiam1 in Axon Formation. J. Neurosci. 2001; 21:2361-2372.

38. Jiang H, Guo W, Liang X, Rao Y. Both the Establishment and the Maintenance of Neuronal Polarity Require Active Mechanisms: Critical Roles of GSK-3² and Its Upstream Regulators. Cell 2005; 120:123-135.

39. Shi S-H, Jan LY, Jan Y-N. Hippocampal Neuronal Polarity Specified by Spatially Localized mPar3/mPar6 and PI 3-Kinase Activity. Cell 2003; 112:63-75.

40. Ménager C, Arimura N, Fukata Y, Kaibuchi K. PIP3 is involved in neuronal polarization and axon formation. Journal of Neurochemistry 2004; 89:109-118.

41. Yoshimura T, Arimura N, Kawano Y, Kawabata S, Wang S, Kaibuchi K. Ras regulates neuronal polarity via the PI3-kinase/Akt/GSK-3[beta]/CRMP-2 pathway. Biochemical and Biophysical Research Communications 2006; 340:62-68.

42. Yoshimura T, Kawano Y, Arimura N, Kawabata S, Kikuchi A, Kaibuchi K. GSK-3² Regulates Phosphorylation of CRMP-2 and Neuronal Polarity. Cell 2005; 120:137-149.

43. Gartner A, Huang X, Hall A. Neuronal polarity is regulated by glycogen synthase kinase-3 (GSK-3{beta}) independently of Akt/PKB serine phosphorylation. J Cell Sci 2006; 119:3927-3934.

44. Garrido JJ, Simón D, Varea O, Wandosell F. GSK3 alpha and GSK3 beta are necessary for axon formation. FEBS Letters 2007; 581:1579-1586.

45. Inagaki N, Chihara K, Arimura N, Menager C, Kawano Y, Matsuo N, Nishimura T, Amano M, Kaibuchi K. CRMP-2 induces axons in cultured hippocampal neurons. Nat Neurosci 2001; 4:781-782.

46. Shi S-H, Cheng T, Jan LY, Jan Y-N. APC and GSK-3² Are Involved in mPar3 Targeting to the Nascent Axon and Establishment of Neuronal Polarity. Current biology : CB 2004; 14:2025-2032.

47. Zhou F-Q, Zhou J, Dedhar S, Wu Y-H, Snider WD. NGF-Induced Axon Growth Is Mediated by Localized Inactivation of GSK-3² and Functions of the Microtubule Plus End Binding Protein APC. Neuron 2004; 42:897-912.

48. Asada N, Sanada K, Fukada Y. LKB1 Regulates Neuronal Migration and Neuronal Differentiation in the Developing Neocortex through Centrosomal Positioning. J. Neurosci. 2007; 27:11769-11775.

49. Barnes AP, Lilley BN, Pan YA, Plummer LJ, Powell AW, Raines AN, Sanes JR, Polleux F. LKB1 and SAD Kinases Define a Pathway Required for the Polarization of Cortical Neurons. Cell 2007; 129:549-563.

50. Shelly M, Cancedda L, Heilshorn S, Sumbre G, Poo M-m. LKB1/STRAD Promotes Axon Initiation During Neuronal Polarization. Cell 2007; 129:565-577.

51. Kishi M, Pan YA, Crump JG, Sanes JR. Mammalian SAD Kinases Are Required for Neuronal Polarization. Science 2005; 307:929-932.

52. Choi Y-J, Di Nardo A, Kramvis I, Meikle L, Kwiatkowski DJ, Sahin M, He X. Tuberous sclerosis complex proteins control axon formation. Genes & Development 2008; 22:2485-2495.

53. Chen YM, Wang QJ, Hu HS, Yu PC, Zhu J, Drewes G, Piwnica-Worms H, Luo ZG. Microtubule affinity-regulating kinase 2 functions downstream of the PAR-3/PAR-6/atypical PKC complex in regulating hippocampal neuronal polarity. Proceedings of the National Academy of Sciences 2006; 103:8534-8539.

54. Zhou F, Snider W. Cell biology. GSK-3beta and microtubule assembly in axons. Science 2005; 308:211-214.

55. Markus A, Zhong J, Snider WD. Raf and Akt Mediate Distinct Aspects of Sensory Axon Growth. Neuron 2002; 35:65-76.

56. Mattson M, Murain M, Guthrie P. Localized calcium influx orients axon formation in embryonic hippocampal pyramidal neurons. Brain Res Dev Brain Res 1990; 52:201-209.

57. Tanzi R, Gusella J, Watkins P, Bruns G, St George-Hyslop P, Van Keuren M, Patterson D, Pagan S, Kurnit D, Neve R. Amyloid beta protein gene: cDNA, mRNA distribution, and genetic linkage near the Alzheimer locus. Science 1987; 235:880-884.

58. Goldgaber D, Lerman M, McBride O, Saffiotti U, Gajdusek D. Characterization and chromosomal localization of a cDNA encoding brain amyloid of Alzheimer's disease. Science 1987; 235:877-880.

59. Kang J, Lemaire H-G, Unterbeck A, Salbaum JM, Masters CL, Grzeschik K-H, Multhaup G, Beyreuther K, Muller-Hill B. The precursor of Alzheimer's disease amyloid A4 protein resembles a cell-surface receptor. Nature 1987; 325:733-736.

60. Robakis N, Wisniewski H, Jenkins E, Devine-Gage E, Houck G, Yao X, Ramakrishna N, Wolfe G, Silverman W, Brown W. Chromosome 21q21 sublocalisation of gene encoding beta-amyloid peptide in cerebral vessels and neuritic (senile) plaques of people with Alzheimer disease and Down syndrome. Lancet. 1987; 14:384-385.

61. Schmechel D, Goldgaber D, Burkhart D, Gilbert J, Gajdusek D, Roses A. Cellular localization of messenger RNA encoding amyloid-beta-protein in normal tissue and in Alzheimer disease. Alzheimer Dis Assoc Disord. 1988; 2:96-111.

62. Coulson EJ, Paliga K, Beyreuther K, Masters CL. What the evolution of the amyloid protein precursor supergene family tells us about its function. Neurochemistry International 2000; 36:175-184.

63. Ling Y, Morgan K, Kalsheker N. Amyloid precursor protein (APP) and the biology of proteolytic processing: relevance to Alzheimer's disease. The International Journal of Biochemistry & Cell Biology 2003; 35:1505-1535.

64. Selkoe DJ. Alzheimer's Disease: Genes, Proteins, and Therapy. Physiological Reviews 2001; 81:741-766.

65. Tanaka S, Shiojiri S, Takahashi Y, Kitaguchi N, Ito H, Kameyama M, Kimura J, Nakamura S, Ueda K. Tissue-specific expression of three types of [beta]-protein precursor mRNA: Enhancement of protease inhibitor-harboring types in Alzheimer's disease brain. Biochemical and Biophysical Research Communications 1989; 165:1406-1414.

66. Roßner S, Ueberham U, Schliebs R, Regino Perez-Polo J, Bigl V. The regulation of amyloid precursor protein metabolism by cholinergic mechanisms and neurotrophin receptor signaling. Progress in Neurobiology 1998; 56:541-569.

67. De Strooper B, Annaert W. Proteolytic processing and cell biological functions of the amyloid precursor protein. J Cell Sci 2000; 113:1857-1870.

68. Turner PR, O'Connor K, Tate WP, Abraham WC. Roles of amyloid precursor protein and its fragments in regulating neural activity, plasticity and memory. Progress in Neurobiology 2003; 70:1-32.

69. Gralle M, Ferreira ST. Structure and functions of the human amyloid precursor protein: The whole is more than the sum of its parts. Progress in Neurobiology 2007; 82:11-32.

70. Suzuki T, Nakaya T. Regulation of Amyloid β-Protein Precursor by Phosphorylation and Protein Interactions. Journal of Biological Chemistry 2008; 283:29633-29637.

71. Small SA, Gandy S. Sorting through the Cell Biology of Alzheimer's Disease: Intracellular Pathways to Pathogenesis. 2006; 52:15-31.

72. Bayer TA, Wirths O, Majtényi K, Hartmann T, Multhaup G, Beyreuther K, Czech C. Key Factors in Alzheimer's Disease: β-amyloid Precursos Protein Processing, Metabolism and Intraneuronal Transport. Brain Pathology 2001; 11:1-11.

73. Thinakaran G, Koo EH. Amyloid Precursor Protein Trafficking, Processing, and Function. Journal of Biological Chemistry 2008; 283:29615-29619.

74. Zheng H, Koo E. Biology and pathophysiology of the amyloid precursor protein. Molecular Neurodegeneration 2011; 6:27.

75. Kinoshita A, Fukumoto H, Shah T, Whelan CM, Irizarry MC, Hyman BT. Demonstration by FRET of BACE interaction with the amyloid precursor protein at the cell surface and in early endosomes. J Cell Sci 2003; 116:3339-3346.

76. Iwatsubo T. The [gamma]-secretase complex: machinery for intramembrane proteolysis. Current Opinion in Neurobiology 2004; 14:379-383.

77. Zhang Y-w, Thompson R, Zhang H, Xu H. APP processing in Alzheimer's disease. Molecular Brain 2011; 4:3.

78. Luo W-j, Wang H, Li H, Kim BS, Shah S, Lee H-J, Thinakaran G, Kim T-W, Yu G, Xu H. PEN-2 and APH-1 Coordinately Regulate Proteolytic Processing of Presenilin 1. Journal of Biological Chemistry 2003; 278:7850-7854.

79. Tarassishin L, Yin YI, Bassit B, Li Y-M. Processing of Notch and amyloid precursor protein by γ-secretase is spatially distinct. Proceedings of the National Academy of Sciences of the United States of America 2004; 101:17050-17055.

80. Müller T, Meyer HE, Egensperger R, Marcus K. The amyloid precursor protein intracellular domain (AICD) as modulator of gene expression, apoptosis, and cytoskeletal dynamics--Relevance for Alzheimer's disease. Progress in Neurobiology 2008; 85:393-406.

81. Lee M-S, Kao S-C, Lemere CA, Xia W, Tseng H-C, Zhou Y, Neve R, Ahlijanian MK, Tsai L-H. APP processing is regulated by cytoplasmic phosphorylation. The Journal of Cell Biology 2003; 163:83-95.

82. Schettini G, Govoni S, Racchi M, Rodriguez G. Phosphorylation of APP-CTF-AICD domains and interaction with adaptor proteins: signal transduction and/or transcriptional role – relevance for Alzheimer pathology. Journal of Neurochemistry 2010; 115:1299-1308.

83. Lee M, Kao S, Lemere C, Xia W, Tseng H, Zhou Y, Neve R, Ahlijanian M, Tsai L. APP processing is regulated by cytoplasmic phosphorylation. J Cell Biol 2003; 163:83 - 95.

84. Gandy S, Czernik A, Greengard P. Phosphorylation of Alzheimer disease amyloid precursor peptide by protein kinase C and Ca2+/calmodulin-dependent protein kinase II. Proc Natl Acad Sci USA 1988; 85:6218 - 6221.

85. Isohara T, Horiuchi A, Watanabe T, Ando K, Czernik A, Uno I, Greengard P, Nairn A, Suzuki T. Phosphorylation of the cytoplasmic domain of Alzheimer's beta-amyloid precursor protein at Ser655 by a novel protein kinase. Biochem Biophys Res Commun 1999; 258:300 - 305.

86. Ramelot TA, Nicholson LK. Phosphorylation-induced structural changes in the amyloid precursor protein cytoplasmic tail detected by NMR. Journal of Molecular Biology 2001; 307:871-884.

87. Gandy S, Czernik AJ, Greengard P. Phosphorylation of Alzheimer disease amyloid precursor peptide by protein kinase C and Ca2+/calmodulin-dependent protein kinase II. Proceedings of the National Academy of Sciences of the United States of America 1988; 85:6218-6221.

88. Isohara T, Horiuchi A, Watanabe T, Ando K, Czernik AJ, Uno I, Greengard P, Nairn AC, Suzuki T. Phosphorylation of the Cytoplasmic Domain of Alzheimer's [beta]-Amyloid Precursor Protein at Ser655 by a Novel Protein Kinase. Biochemical and Biophysical Research Communications 1999; 258:300-305.

89. Vieira S, Rebelo S, Esselmann H, Wiltfang J, Lah J, Lane R, Small S, Gandy S, da Cruz e Silva E, da Cruz e Silva O. Retrieval of the Alzheimer's amyloid precursor protein from the endosome to the TGN is S655 phosphorylation state-dependent and retromer-mediated. Molecular Neurodegeneration 2010; 5:40.

90. Vieira S, Rebelo S, Domingues S, da Cruz e Silva E, da Cruz e Silva O. S655 phosphorylation enhances APP secretory traffic. Molecular and Cellular Biochemistry 2009; 328:145-154.

91. Turner P, O'Connor K, Tate W, Abraham W. Roles of amyloid precursor protein and its fragments in regulating neural activity, plasticity and memory. Prog Neurobiol 2003; 70:1 - 32.

92. Schubert W, Prior R, Weidemann A, Dircksen H, Multhaup G, Masters CL, Beyreuther K. Localization of Alzheimer [beta]A4 amyloid precursor protein at central and peripheral synaptic sites. Brain Research 1991; 563:184-194.

93. Masliah E, Mallory M, Ge N, Saitoh T. Amyloid precursor protein is localized in growing neurites of neonatal rat brain. Brain Research 1992; 593:323-328.

94. Ferreira A, Caceres A, Kosik K. Intraneuronal compartments of the amyloid precursor protein. J. Neurosci. 1993; 13:3112-3123.

95. Milward EA, Papadopoulos R, Fuller SJ, Moir RD, Small D, Beyreuther K, Masters CL. The amyloid protein precursor of Alzheimer's disease is a mediator of the effects of nerve growth factor on neurite outgrowth. Neuron 1992; 9:129-137.

96. LeBlanc A, Kovacs D, Chen H, Villaré F, Tykocinski M, Autilio-Gambetti L, Gambetti P. Role of amyloid precursor protein (APP): study with antisense transfection of human neuroblastoma cells. J Neurosci Res. 1992; 31:635-645.

97. Hung AY, Koo EH, Haass C, Selkoe DJ. Increased expression of beta-amyloid precursor protein during neuronal differentiation is not accompanied by secretory cleavage. Proceedings of the National Academy of Sciences of the United States of America 1992; 89:9439-9443.

98. Qiu W, Ferreira A, Miller C, Koo E, Selkoe D. Cell-surface beta-amyloid precursor protein stimulates neurite outgrowth of hippocampal neurons in an isoform-dependent manner. J. Neurosci. 1995; 15:2157-2167.

99. Allinquant B, Hantraye P, Mailleux P, Moya K, Bouillot C, Prochiantz A. Downregulation of amyloid precursor protein inhibits neurite outgrowth in vitro. The Journal of Cell Biology 1995; 128:919-927.

100. Small D, Nurcombe V, Reed G, Clarris H, Moir R, Beyreuther K, Masters C. A heparin-binding domain in the amyloid protein precursor of Alzheimer's disease is involved in the regulation of neurite outgrowth. J. Neurosci. 1994; 14:2117-2127.

101. Perez RG, Zheng H, Van der Ploeg LHT, Koo EH. The beta -Amyloid Precursor Protein of Alzheimer's Disease Enhances Neuron Viability and Modulates Neuronal Polarity. J. Neurosci. 1997; 17:9407-9414.

102. Young-Pearse T, Chen A, Chang R, Marquez C, Selkoe D. Secreted APP regulates the function of full-length APP in neurite outgrowth through interaction with integrin beta1. Neural Development 2008; 3:15.

103. Ikin AF, Sabo SL, Lanier LM, Buxbaum JD. A macromolecular complex involving the amyloid precursor protein (APP) and the cytosolic adapter FE65 is a negative regulator of axon branching. Molecular and Cellular Neuroscience 2007; 35:57-63.

104. Ruiz-León Y, Pascual A. Induction of tyrosine kinase receptor b by retinoic acid allows brain-derived neurotrophic factor-induced amyloid precursor protein gene expression in human sh-sy5y neuroblastoma cells. Neuroscience 2003; 120:1019-1026.

105. Holback S, Adlerz L, Iverfeldt K. Increased processing of APLP2 and APP with concomitant formation of APP intracellular domains in BDNF and retinoic acid-differentiated human neuroblastoma cells. Journal of Neurochemistry 2005; 95:1059-1068.

106. Ando K, Oishi M, Takeda S, Iijima K-i, Isohara T, Nairn AC, Kirino Y, Greengard P, Suzuki T. Role of Phosphorylation of Alzheimer's Amyloid Precursor Protein during Neuronal Differentiation. J. Neurosci. 1999; 19:4421-4427.

107. Sim P-L, Heese K. Ligand-Dependent Activation of the Chimeric Tumor Necrosis Factor Receptor-Amyloid Precursor Protein (APP) Reveals Increased APP processing and Suppressed Neuronal Differentiation. Neurosignals 2010; 18:9-23.

108. Ma Q-H, Futagawa T, Yang W-L, Jiang X-D, Zeng L, Takeda Y, Xu R-X, Bagnard D, Schachner M, Furley AJ, Karagogeos D, Watanabe K, et al. A TAG1-APP signalling pathway through Fe65 negatively modulates neurogenesis. Nat Cell Biol 2008; 10:283-294.

109. Sabo SL, Ikin AF, Buxbaum JD, Greengard P. The Amyloid Precursor Protein and Its Regulatory Protein, FE65, in Growth Cones and Synapses In Vitro and In Vivo. The Journal of Neuroscience 2003; 23:5407-5415.

110. König G, Masters CL, Beyreuther K. Retinoic acid induced differentiated neuroblastoma cells show increased expression of the [beta]A4 amyloid gene of Alzheimer's disease and an altered splicing pattern. FEBS Letters 1990; 269:305-310.

111. Beckman M, Iverfeldt K. Increased gene expression of [beta]-amyloid precursor protein and its homologues APLP1 and APLP2 in human neuroblastoma cells in response to retinoic acid. Neuroscience Letters 1997; 221:73-76.

112. Murray JN, Igwe OJ. Regulation of [beta]-amyloid precursor protein and inositol 1,4,5-trisphosphate receptor gene expression during differentiation of a human neuronal cell line. Progress in Neuro-Psychopharmacology and Biological Psychiatry 2003; 27:351-363.

113. da Cruz e Silva OAB, Iverfeldt K, Oltersdorf T, Sinha S, Lieberburg I, Ramabhadran TV, Suzuki T, Sisodia SS, Gandy S, Greengard P. Regulated cleavage of alzheimer [beta]-amyloid precursor protein in the absence of the cytoplasmic tail. Neuroscience 1993; 57:873-877.

114. von Rotz RC, Kohli BM, Bosset J, Meier M, Suzuki T, Nitsch RM, Konietzko U. The APP intracellular domain forms nuclear multiprotein complexes and regulates the transcription of its own precursor. Journal of Cell Science 2004; 117:4435-4448.

115. Dehmelt L, Halpain S. Actin and microtubules in neurite initiation: Are MAPs the missing link? Journal of Neurobiology 2004; 58:18-33.

116. Dehmelt L, Smart FM, Ozer RS, Halpain S. The Role of Microtubule-Associated Protein 2c in the Reorganization of Microtubules and Lamellipodia during Neurite Initiation. The Journal of Neuroscience 2003; 23:9479-9490.

117. Harada A, Teng J, Takei Y, Oguchi K, Hirokawa N. MAP2 is required for dendrite elongation, PKA anchoring in dendrites, and proper PKA signal transduction. The Journal of Cell Biology 2002; 158:541-549.

118. Muller T, Concannon CG, Ward MW, Walsh CM, Tirniceriu AL, Tribl F, Kogel D, Prehn JHM, Egensperger R. Modulation of Gene Expression and Cytoskeletal Dynamics by the Amyloid Precursor Protein Intracellular Domain (AICD). Mol. Biol. Cell 2007; 18:201-210.

119. Cuende J, Moreno S, Bolanos JP, Almeida A. Retinoic acid downregulates Rae1 leading to APCCdh1 activation and neuroblastoma SH-SY5Y differentiation. Oncogene 2008; 27:3339-3344.

120. Biton S, Gropp M, Itsykson P, Pereg Y, Mittelman L, Johe K, Reubinoff B, Shiloh Y. ATM-mediated response to DNA double strand breaks in human neurons derived from stem cells. DNA Repair 2007; 6:128-134.

121. Miloso M, Villa D, Crimi M, Galbiati S, Donzelli E, Nicolini G, Tredici G. Retinoic acid-induced neuritogenesis of human neuroblastoma SH-SY5Y cells is ERK independent and PKC dependent. Journal of Neuroscience Research 2004; 75:241-252.

122. Zhang Y-w, Wang R, Liu Q, Zhang H, Liao F-F, Xu H. Presenilin/γ-secretase-dependent processing of β-amyloid precursor protein regulates EGF receptor expression. Proceedings of the National Academy of Sciences 2007; 104:10613-10618.

123. Nakayama K, Ohkawara T, Hiratochi M, Koh C-S, Nagase H. The intracellular domain of amyloid precursor protein induces neuron-specific apoptosis. Neuroscience Letters 2008; 444:127-131.

124. Lee J-P, Chang K-A, Kim H-S, Kim S-S, Jeong S-J, Suh Y-H. APP carboxyl-terminal fragment without or with Aβ domain equally induces cytotoxicity in differentiated PC12 cells and cortical neurons. Journal of Neuroscience Research 2000; 60:565-570.

Appendix

Cell Culture Solutions

- **PBS (1x)**

For a final volume of 500 ml, dissolve one pack of BupH Modified Dulbecco's Phosphate Buffered Saline Pack (Pierce) in deionised H_2O. Final composition:

- 8 mM Sodium Phosphate
- 2 mM Potassium Phosphate
- 140 mM Sodium Chloride
- 10 mM Potassim Chloride

Sterilize by filtering through a 0.2 µm filter and store at 4°C.

- **10 mg/ml Poly-D-lysine stock (100x)**

To a final volume of 10 ml, dissolve in deionised H_2O 100 mg of poly-D-lysine (Sigma-Aldrich).

- **Poly-D-lysine solution**

To a final volume of 100 ml, dilute 1 ml of the 10 mg/ml poly-D-lysine stock solution in borate buffer.

- **10% FBS MEM:F12 (1:1)**

- MEM (Gibco, Invitrogen)	4,805 g
- F12 (Gibco, Invitrogen)	5,315 g
- $NaHCO_3$ (Sigma)	1,5 g
- Sodium pyruvate (Sigma)	0,055 g
- Streptomycin/Penicillin/Amphotericin solution (Gibco, Invitrogen)	10 mL
- 10% FBS (Gibco, Invitrogen)	100 mL
- L-glutamine (200 mM stock solution)	2,5 mL

→ Dissolve in distilled (d) H_2O;

→ Adjust the pH to 7.2/ 7.3;

→ Adjust the volume to 1000 mL with dH_2O.

- **Freezing medium**

- Growth medium (MEM:F12)	7 mL
- FBS (10-20%)	2 mL
- Glycerol (10-15%) or DMSO (5-20%)	1 mL

Calcium-phosphate-mediated Transfection Solutions

- **2x HEPES-buffered saline (HBS)** **100 mL**

- NaCl	280 mM	1,6 g
- KCl	10 mM	0,074 g
- $Na_2HPO_4.2H_2O$	1,5 mM	0,0213 g
- Dextrose	12 mM	0,2 g
- HEPES	50 mM	1 g

→ Dissolve in a total volume of 90 mL of distilled (d)H_2O;

→ Adjust the pH to 7.05 (with 0.5N NaHO);

→ Adjust the volume to 100 mL with dH_2O;

→ Sterilize the solution by passing it through a 0.22-µm filter;

→ Store the filtrate in 5 mL aliquots at -20ºC.

- **CaCl2 2M solution**

- $CaCl_2.6H_2O$	10,8 g	or
- $CaCl_2.2H_2O$	5,88 g	

→ Dissolve in a final volume of 20 mL of dH_2O;

→ Sterilize the solution by passing it through a 0.22-µm filter;

→ Store in 1 mL aliquots at 4ºC.

- **0,1x TE solution (pH 8.0)** **40 mL**

- Tris.Cl solution (pH 8.0)	1 mM	40 µL

- EDTA solution (pH 8.0) 0,1 mM 8 µL

→ Sterilize the solution by passing it through a 0.22-µm filter

→ Store in aliquots at 4ºC.

- **Glycerol (15% v/v) in 1x HBS 20 mL**

- 10 mL 2x HBS

- 3 mL glycerol

- 7 mL dH_2O

→ Add the 15% autoclaved glycerol to filter-sterilized HBS solution just before use.

SDS-PAGE and Immunoblotting Solutions

- **LGB (Lower gel buffer) (4x)**

To 900 ml of deionised H_2O add:

- Tris 181.65 g
- SDS 4 g

Mix until the solutes have dissolved. Adjust the pH to 8.9 and adjust the volume to 1L with deionised H_2O.

- **UGB (Upper gel buffer) (5x)**

To 900 ml of deionised H_2O add:

- Tris 75.69 g

Mix until the solute has dissolved. Adjust the pH to 6.8 and adjust the volume to 1 L with deionised H_2O.

- **30% Acrylamide/0.8% Bisacrylamide**

To 70 ml of deionised H_2O add:

- Acrylamide 29.2 g
- Bisacrylamide 0.8 g

Mix until the solute has dissolved. Adjust the volume to 100 ml with deionised water. Filter through a 0.2 µm filter and store at 4^oC.

- **10% APS (ammonium persulfate)**

In 10 ml of deionised H_2O dissolve 1 g of APS. Note: prepare fresh before use.

- **10% SDS (sodium dodecilsulfate)**

In 10 ml of deionised H_2O dissolve 1 g of SDS.

- **Loading Gel Buffer (4x)**

- 1 M Tris solution (pH 6.8) 2.5 mL (250 mM)
- SDS 0.8 g (8%)
- Glicerol 4 ml (40%)
- β-Mercaptoetanol 2 ml (2%)
- Bromofenol blue 1 mg (0.01%)

Adjust the volume to 10 ml with deionised H_2O. Store in darkness at room temperature.

- **1 M Tris (pH 6.8) solution**

To 150 ml of deionised H_2O add:
- Tris base 30.3 g

Adjust the pH to 6.8 and adjust the final volume to 250 ml.

- **10x Running Buffer**

- Tris 30.3 g (250 mM)
- Glycine 144.2 g (2.5 M)
- SDS 10 g (1%)

Dissolve in deionised H_2O, adjust the pH to 8.3 and adjust the volume to 1 L.

- **Resolving (lower) gel solution** (60 ml)

	7.5%	or	**10%**
- H_2O	29,25 ml		25,2 ml
- 30% Acryl/0.8% Bisacryl solution	15 ml		19,8 ml
- LGB (4x)	15 ml		15 ml
- 10% APS	300 µL		300 µL
- TEMED	30 µL		30 µL

- **<u>Resolving (lower) gel solution for gradient gels</u>** (60 ml)

	5% and **20%**
- H_2O	17.4 ml / 2.2 ml
- 30% Acryl/0.8% Bisacryl solution	5 ml / 20 ml
- LGB (4x)	7.5 ml / 7.5 ml
- 10% APS	150 µL / 150 µL
- TEMED	15 µL / 15 µL

- **<u>Stacking (upper) gel solution</u>** (20 ml)

	3.5%
- H_2O	13.2 ml
- 30% Acryl/0.8% Bisacryl solution	2.4 ml
- UGB (5x)	4.0 ml
- 10% APS	200 µL
- 10% SDS	200 µL
- TEMED	20 µL

- **<u>1x Transfer Buffer</u>**

- Tris 3.03 g (25 mM)
- Glycine 14.41 g (192 mM)

Mix until solutes dissolution. Adjust the pH to 8.3 with HCl and adjust the volume to 800 ml with deionised H_2O. Just prior to use add 200 ml of methanol (20%).

- **<u>10x TBS (Tris buffered saline)</u>**

- Tris 12.11 g (10 mM)
- NaCl 87.66 g (150 mM)

Adjust the pH to 8.0 with HCl and adjust the volume to 1L with deionised H_2O.

- **<u>10x TBST (TBS+Tween)</u>**

- Tris 12.11 g (10 mM)
- NaCl 87.66 g (150 mM)
- Tween 20 5 ml (0.05%)

Adjust the pH to 8.0 with HCl and adjust the volume to 1L with deionised H_2O.

- **Membranes Stripping Solution** (500 ml)

- Tris-HCl (pH 6.7) 3.76 g (62.5 mM)
- SDS 10 g (2%)
- β-mercaptoetanol 3.5 ml (100 mM)

Dissolve Tris and SDS in deionised H_2O and adjust with HCl to pH 6.7. Add the mercaptoethanol and adjust volume to 500 ml.